Laser diagnostics and minor species detection in combustion using resonant four-wave mixing: a review

Johannes Kiefer[1,2] and Paul Ewart[3]

[1] School of Engineering, University of Aberdeen, Aberdeen, UK

[2] Erlangen Graduate School in Advanced Optical Technologies (SAOT), University Erlangen-Nuremberg, Erlangen, Germany

[3] Department of Physics, Clarendon Laboratory, University of Oxford, Oxford, UK

Corresponding author: Johannes Kiefer

School of Engineering

University of Aberdeen

Fraser Noble Building

Aberdeen AB24 3UE

United Kingdom

Tel: +44 1224 272495

Email: j.kiefer@abdn.ac.uk

Abstract

Laser-based methods have transformed combustion diagnostics in the past few decades. The high intensity, coherence, high spectral resolution and frequency tunability available from laser radiation has provided powerful tools for studying microscopic processes and macroscopic phenomena in combustion by linear and nonlinear optical processes. This review focuses on nonlinear optical techniques based on resonant four-wave mixing for non-intrusive measurements of minor species in combustion. The importance of minor species such as reaction intermediates is outlined together with the challenges they present for detection and measurement in the hostile environments of flames, technical combustors, and engines. The limitations of conventional optical methods for such measurements are described and the particular advantages of coherent methods using nonlinear optical techniques are discussed. The basic physics underlying four-wave wave mixing processes and theoretical models for signal calculation are then presented together with a discussion of how combustion parameters may be derived from analysis of signals generated in various four-wave mixing processes. The most important four-wave mixing processes, in this context, are then reviewed: Degenerate Four-Wave Mixing (DFWM), Coherent Anti-Stokes Raman Scattering (CARS), Laser Induced Grating Spectroscopy (LIGS) and Polarization Spectroscopy (PS). In each case the fundamental physics is outlined to explain the particular properties and diagnostic advantages of each technique. The application of the methods mentioned to molecular physics studies of combustion species is then reviewed along with their application in measurement of concentration, temperature and other combustion parameters. Related nonlinear techniques and recent extensions to the ultra-fast regime are briefly reviewed. Finally practical considerations relevant to multi-dimensional and multi-species measurements, as well as applications in technical combustion systems are discussed.

Keywords: nonlinear optical spectroscopy, four-wave mixing, combustion diagnostics, minor species detection, laser-induced gratings, polarization spectroscopy

Article Outline

1 Introduction

Energy from renewable sources such as solar and wind power is the goal of much current research and technological development. Combustion, however, is and is likely to remain for the foreseeable future, the most important energy source for heat, electrical power and especially for transportation. In technical combustion systems the chemical energy of fossil fuels such as coal, crude oil and natural gas is converted into heat through oxidation with oxygen from air. However, fossil fuel resources are limited and alternatives like biofuels [1] or novel technologies such as fuel cells [2] are not yet able to meet the demand. Consequently, for a sustainable use of fossil fuels it is desirable to further improve the efficiency, maintainability and reliability of existing combustion devices. Achieving such improvements depends upon an improved understanding of the fundamental combustion chemistry as well as optimized engineering design. Further motivation for improved understanding of combustion and increased device efficiency is the need to reduce the environmental impact of emissions from fossil fuel combustion. Apart from "greenhouse gases" such as carbon dioxide these emissions include nitric oxides (NO_x), sulphuric oxides (SO_x), harmful organic compounds (e.g. aromatic hydrocarbons) and particulate matter or soot which have harmful effects on human health.

In general, combustion is a rather complex phenomenon where chemical reactions, fluid dynamics as well as heat and mass transfer processes are involved and, moreover, interact with each other. In combustion chemistry it is usually not sufficient just to consider a global chemical reaction equation involving only the reactants (i.e. fuel and oxidizer), and the products, (e.g. carbon dioxide and water). To achieve deeper understanding, the entire reaction mechanism involving numerous reaction paths and a large number of intermediate trace species, as well as the local gas temperature and pressure, must be taken into account [3, 4].

Knowledge of the spatially and temporally resolved concentration of different flame intermediate species together with their temperature is of great value and allows insight into the individual chemical processes taking place. Several molecules are typically utilized as indicators for different flame regions. For instance, formaldehyde (HCHO) is formed and subsequently consumed again in an early stage of the chemical conversion of hydrocarbons [5]. Therefore, the presence of HCHO indicates the region in a flame where the temperature is relatively low and the fuel molecules are decomposing [6]. In contrast, the formyl radical (HCO) is generated in a reaction where a major part of the chemical energy is released as heat [7]. Therefore HCO indicates the location of the actual flame front in hydrocarbon combustion [8, 9]. A further interesting intermediate species is hydroxyl (OH) which is formed in the high temperature region. Since it has a relatively long lifetime OH exists in a wide flame area and to a certain extent in the exhaust gas as well [10]. It is therefore commonly employed to study flame structures and to determine flame surface density [11]. The CH radical, like HCO is present in a thin layer of the reaction zone, is often employed as a flame front marker as well, because it exhibits advantageous properties for spectroscopic detection [12] in comparison with HCO [8]. Moreover, by detecting several intermediate species such as CH plus OH, that are characteristic for different flame regions, additional information on the combustion and flow processes in a flame can be obtained [11, 13]. Other flame intermediates exert influence on the formation of pollutants. For instance, CH, CN and HCN are strongly involved in the formation of nitric oxides through the prompt NO mechanism [14]. C_2, acetylene and polycyclic aromatic hydrocarbons (PAH) are believed to be intermediates in the generation of soot particles and aggregates [15].

The molecules mentioned are typically present at an extremely low number density. For the experimentalist this presents the challenge to develop highly sensitive diagnostic tools to measure concentration and temperature with high spatial and temporal resolution. In particular, challenges arise from experimental conditions and limitations imposed by the

hostile environments of combusting media. Measurements in flames need to be non-intrusive in order to avoid disturbing the system. Optical methods are inherently non-intrusive and nowadays laser-based techniques are commonly employed [16]. The use of optical emissions however may be influenced by chemiluminescence or thermal radiation from soot particles. Further interferences may arise from elastically scattered laser light by Rayleigh and Mie scattering. Such scattering interferences are not species specific and can have a several orders of magnitude higher intensity than the actual signal of interest [16]. Moreover, inside a flame strong gradients of temperature and density lead to local changes of the refractive index which may influence the propagation of laser beams (beam steering) and signal photons [17]. Finally, the experimental environment itself can also be challenging. In particular, technical combustion systems and devices such as gas turbine combustors and internal combustion engines provide limited optical access to the flame region [18, 19] and, as a consequence, optical arrangements with low numerical aperture must be employed.

A wide variety of diagnostic techniques have been developed to detect flame intermediates. In this article we review the development and use of nonlinear optical spectroscopic techniques for this purpose. Conventional optical diagnostic methods using linear optical processes such as fluorescence or Raman scattering usually involve detection of an incoherent emission of light that radiates into all directions. Nonlinear optical processes, on the other hand, can provide signals in the form of coherent, laser-like beams. Such signal beams have particular advantages in combustion diagnostics where the region to be investigated is usually highly luminous and may offer very limited optical access for signal collection. Nonlinear methods offer signals with high directionality giving better discrimination against background flame emission, high spatial resolution and high selectivity of species and quantum state together with suppression of molecular interferences.

The paper is arranged as follows: Firstly, a brief overview of conventional methods for trace species detection is given together with a discussion of their limitations. Secondly, in section

3, the fundamentals of nonlinear optics are introduced, specifically the general class of processes known as four-wave mixing. In section 4 an outline of the theoretical basis of third-order nonlinear optical processes illustrated by the case of DFWM is presented. The mathematical subsections may be skipped by the non-expert but the introductory section is useful to give a general idea of the underlying physics of FWM processes. The properties of signals generated by these FWM processes are highlighted with their implications for experimental combustion diagnostics. This is followed by detailed reviews of the commonly employed techniques of degenerate four-wave mixing (DFWM), coherent anti-Stokes Raman scattering (CARS), laser-induced grating spectroscopy (LIGS) and polarization spectroscopy (PS). Further related methods are then outlined together with a brief review of practical considerations and fields currently under development.

2 Conventional detection methods for intermediate species

Flame intermediates play a crucial role in combustion chemistry. Therefore a detailed understanding of combustion requires knowledge of their production, location, influence and also their destruction with good time and space resolution. Consequently many approaches to their detection and measurement have been devised. For the sake of completeness a brief overview over the conventional methods will be given in the following but not discussed in detail.

In general, all techniques can be classified into two groups – those that do not use lasers and those that do.

2.1 Techniques without lasers

The oldest, but still common, method to study combustion intermediates is the spectroscopy of natural flame emissions often referred to as chemiluminescence. Such emissions mainly occur from molecular radicals in excited electronic states and the first experiments were reported as early as 1857 by Swan who investigated and identified chemiluminescence of C_2 in a candle flame [20]. Today this method is a standard in almost every combustion laboratory because of its experimental simplicity. Its main drawback is that it is a line-of-sight method and so inherently lacks spatial resolution. Employing appropriate signal collection optics [21], however, or by using tomography methods [22] a limited degree of spatial resolution can be obtained. In addition, the passive nature of the technique limits the number of detectable species to those emitting light in some part of the optically detectable spectrum. Furthermore, the emission from different species can overlap spectrally making detailed analysis difficult.

Many of the non-laser methods involve sampling with physical probes. For this reason these techniques are intrusive and may influence the local combustion by disturbing the fluid flow, by local cooling or by catalytic surface effects etc. Nevertheless they have contributed significantly to a fundamental understanding of flame chemistry. Electron spin resonance

(ESR) spectrometry has mainly been used for measurements of atomic species like N, O and H [23]. Molecular-beam mass spectrometry (MBMS), another sampling method of great importance, has been employed for many years to study flames and the progress in this area has been reviewed in detail by Biordi in 1977 [24] and more recently by Hansen et al. [25]. The third method to be mentioned is gas chromatography (GC) [26]. The techniques based on flame-sampling are typically employed to investigate stationary laminar flames at low pressure. A detailed discussion can be found in reference [25] and the references therein.

2.2 Techniques employing lasers

Laser-based methods have been developed and used since the 1960s and they are nowadays the most common tools for detecting flame intermediates and determination of their concentration and flame temperature. One of the most simple and direct methods is absorption of laser light. (For the sake of completeness it should be mentioned that absorption of light from incoherent sources is also an option). Absorption techniques are comparatively easy to apply and allow a straightforward data evaluation using the Beer-Lambert law which relates the transmittance or absorbance of the sample to the concentration of the absorbing species (The transmittance or absorbance is found simply from the ratio of the transmitted to incident intensity of the light at a wavelength corresponding to a known transition in the absorbing species.). When temporal resolution is not an issue the use of tuneable diode laser absorption spectroscopy (TDLAS) can be an option [27]. This technique uses light from a continuous wave diode laser which is passed through the flame. The transmittance is monitored while the laser wavelength is scanned over a certain spectral range. Diode lasers are available for limited ranges of wavelengths in the near- and mid-infrared region where most of the intermediate species of interest have “fingerprint” spectra arising from ro-vibrational transitions or their overtone and combination bands. On the one hand this represents a clear opportunity to exploit these absorption features for detection, but, on the other hand, the

multitude of absorption lines from carbon dioxide and water leads to interferences that complicate the signal analysis. The most readily available and reliable diode lasers also tend to emit in the overtone regions where the absorption cross-sections are typically several orders of magnitude weaker than in the fundamental bands in the mid-infrared. Future progress in new devices such as room temperature quantum cascade lasers, which operate in the mid- to far-infrared, may address this issue.

The main limitation of TDLAS and related techniques is the lack of temporal and spatial resolution. When high temporal resolution is required techniques employing pulsed laser sources are the methods of choice. However, for trace species detection, in particular when the species of interest have short lifetimes and so exist only in a thin layer of the reaction zone, the use of conventional laser absorption spectroscopy may not provide sufficient sensitivity. For this reason an enhancement of the sensitivity is required. This is often done using multi-pass arrangements, which means that the laser beam is reflected into the flame many times. This approach however leads to a loss of spatial resolution. For these reasons TDLAS has limitations in combustion diagnostics. Nonetheless even in some technical systems useful information can be obtained by exploiting strong absorption transitions in selected species for combustion relevant measurements. Multiplexing of multiple diode lasers and tomographic methods to achieve spatial resolution can provide multiple species and multiple parameter measurements [28]. In this context, the development of hyperspectral sources for absorption spectroscopy is providing a further tool for diagnostics of combustion environments [29-31].

In order to overcome the limitation of weak absorption several practical approaches have been developed to increase the effective absorption path using cavity enhancement. In this context intra-cavity laser absorption spectroscopy (ICLAS) has been used to enhance weak absorption signals. In an ICLAS experiment the absorber (e.g. a gas cell) is positioned inside the cavity of a broad-band laser. The principle of ICLAS is based on the strong sensitivity of the laser emission to the presence of a spectrally selective absorber in the cavity. By recording the

spectrally resolved laser emission the absorption spectrum can be obtained and quantitative information can be extracted. This approach has been developed in the early 1970s and a number of review articles have summarized theoretical aspects and experimental studies, see e.g. refs [32, 33] and the references therein. Analysis of ICLAS signals is complicated by the non-linearity of the signal dependence on the combined effect of an absorber and an amplifier in the laser cavity. A powerful method that avoids this complication is cavity ringdown spectroscopy (CRDS) in which the absorbing species is placed in a passive cavity external to the laser [34]. In CRDS a small fraction of the beam of a pulsed laser is coupled into an optical cavity built from two highly reflecting mirrors. The intensity of light emerging from the cavity decays exponentially as a fraction of the re-circulating light pulse leaks through one of the mirrors. The decay time of the signal decreases in the presence of an absorber in the cavity. Thus the variation in decay time as the laser light wavelength is tuned provides a spectral signature of the absorbing species. The details have been discussed in the literature [34].

One of the most severe drawbacks of absorption techniques arises from their being line-of-sight methods which lack spatial resolution along the propagation direction. Therefore the applicability of such diagnostics is limited especially in technical combustion systems where heterogeneous density and absorber concentration conditions typically apply. Furthermore the presence of soot particles may significantly affect the measurement of the light transmittance. Particulates such as soot act as a black-body absorber and so absorption occurs over a wide spectral range. In addition, particles scatter light by Mie and Rayleigh scattering, depending on the particle size which leads to attenuation in a non-species specific way.

A number of other methods are based on absorption of laser radiation but utilize different measurement strategies to achieve spatially resolved detection. Examples of such techniques are photo-thermal and photo-acoustic spectroscopy. When laser radiation is absorbed by the

species of interest the energy from the excited molecules is subsequently dissipated by collisions. As a consequence the local temperature increases, and the local density and complex refractive index change accordingly. The local deviation from equilibrium conditions eventually results in an acoustic wave which may be detected with a microphone. The spatial resolution of such techniques is again limited. To provide some spatial resolution optical detection is used by crossing a second laser beam with the excitation laser at the position of interest. The deflection of the probe laser beam can be monitored by a position-sensitive detector yielding an estimate for the released energy and thereby for the concentration of the absorbing species [35].

The most common method for minor species detection in flames is laser-induced fluorescence (LIF) [36]. LIF can be understood as an absorption process followed by spontaneous emission of radiation (fluorescence) during the transition back to a lower electronic state, i.e. usually the electronic ground state. The intensity of the emitted fluorescence is used as a measure of the population density of the absorbing species. Species selectivity is provided by tuning the incident laser to resonances in the molecular absorber. Molecular and atomic flame radicals or pollutant species at the parts-per-million (ppm) or sub-ppm level can be probed by single photon absorption processes, e.g., OH, CH, NH, NO or CN. Species such as O, H, N, or CO may be detected using two-photon absorption (two-photon LIF). Quantitative concentration measurements are feasible but rendered difficult by collisionally induced inter- or intra-molecular energy transfer processes. These quenching processes modify the fluorescence intensity by depopulating the excited molecular states. Since the quenching occurs often at rates that are unknown, or that vary spatially according to the (usually unknown) local gas composition and temperature, the LIF intensity cannot be interpreted unambiguously in terms of species concentration.

A LIF spectrum obtained by frequency scanning the laser across numerous absorption features yields a measure of the initial quantum state population for each transition. Using Boltzmann statistics the relative intensities of the lines may be used to infer the equilibrium temperature. The fundamentals and applications of LIF in the field of combustion research have been reviewed in numerous books and articles [16, 36-38].

One strong feature of LIF is that, by forming the exciting laser beam into a sheet, it can easily be used to obtain the 2D distribution of the species of interest [16]. The fluorescence intensity in the plane of the sheet – planar laser induced fluorescence, PLIF – can potentially be interpreted in terms of the species distribution. Moreover, combining PLIF with another method simultaneously can provide a large amount of information (for example: PLIF of another species or other methods such as laser Rayleigh scattering for thermometry or particle imaging velocimetry for the flow field) [11].

A very similar method to LIF from the experimental viewpoint is ultraviolet resonance Raman scattering. In this case the naturally weak Raman scattering effect utilizing an inelastic interaction between the molecules and laser light [39] is enhanced by tuning the excitation laser to a resonance transition of the molecule of interest. This has been demonstrated, for example, for vibrational spectroscopy of allyl radicals [40]. Geier et al. utilized combined signals from laser-induced fluorescence and near-resonance enhanced Raman scattering to detect silicon monoxide in a silica-generating flame [41]. Getty et al. demonstrated detection of benzene and trichloroethylene in methane/air flames using resonance Raman spectroscopy [42].

Finally the technique of resonantly enhanced multi-photon ionization (REMPI) deserves to be mentioned owing to its high sensitivity. In the first step of the REMPI process the molecule of interest is excited by single or multi-photon absorption. A further photon leads to ionization directly from the excited state. By introducing an anode into the flame the electrons ejected

from the molecule can be detected [43]. REMPI is a good alternative to detect species that can absorb radiation but do not fluoresce and hence are poor candidates for LIF measurements. However, since it uses a physical probe in the flame it can not be considered a non-intrusive technique and therefore its application is limited.

To summarize this section, there are many techniques available for the detection of combustion intermediate species. All of them however have drawbacks that make their application under certain circumstances or in special environments difficult or even impossible. The methods that require probe sampling (e.g., mass spectrometry or gas chromatography) or inserting a physical detector (REMPI) may affect the flame significantly and hence they are not non-intrusive. Chemiluminescence as a passive process is limited to species that are present in excited states and emit radiation. Absorption methods (including TDLAS, ICLAS and CRDS) are line-of-sight techniques and provide limited spatial resolution. In contrast, the linear laser techniques of LIF and PLIF are relatively easy to implement and can deliver species-specific, spatially- and temporally-resolved information. Limitations arise from the spontaneous nature of the emitted radiation. The fluorescence signal is emitted into a 4π solid angle and so signal collection requires good optical access and large numerical apertures. This is a particular problem in technically relevant combustion systems where only limited optical access to the measurement volume may be available. Most seriously for quantitative measurements the LIF or PLIF signal is compromised by unknown local quenching effects that are particularly deleterious at high pressures. In conclusion, there is a strong need for further diagnostic techniques that overcome the limitations that afflict conventional and linear laser techniques. In this paper the particular properties of nonlinear optical processes are presented as potential and actual solutions to some of these problems.

3 Nonlinear optical spectroscopy

3.1 Nonlinear optical methods

Diagnostic methods that use the light scattered or absorbed by the gases undergoing combustion have the great advantage that they can be sensitive to trace quantities of the species being detected. Furthermore the chemical processes involved in the combustion are not disturbed by the measurement of the light signal. There are however some major disadvantages. For the conventional methods outlined in the previous section these include lack of spatial resolution in absorption methods and processes that interfere with, obscure or modify the intensity of the signal in emission or scattering methods so that it becomes difficult to relate the recorded intensity to the combustion parameter being measured. In particular, the natural light emitted by flames or scattering of the incident laser light by soot particles can mask the weak signals arising from laser induced fluorescence or Rayleigh and Raman scattering. Perhaps the most difficult problem facing LIF methods is the effect of molecular collisions that quench the fluorescence in a way that is often difficult or impossible to quantify. All of these methods can be categorised as “linear optical methods” since the intensity of the signals are linearly proportional to the intensity of the input light. In order to overcome some of these problems “non-linear optical methods” have been developed. The signal intensities in such methods are proportional to the second, third or higher power of the incident laser intensity – hence the signal is non-linearly proportional to the input intensity. Resonant four-wave mixing is, from the viewpoint of optical diagnostics, an important sub-set of nonlinear optical methods.

The important aspect however is not the nonlinearity but the *coherence* property of the generated light forming the signal. In the case of linear scattering methods such as LIF the signal is the result of a spontaneous emission by excited molecules leading to *incoherent* light i.e. the phase of the emitted light is random and the direction of the emission is also randomly

distributed over a 4π solid angle. In contrast the signals emitted by nonlinear optical processes such as resonant four-wave mixing are *coherent,* the phase of the light is not random but linked to that of the incoming coherent laser light. Consequently the emitted light is directional and propagates as a laser-like beam with low divergence. This coherent property of the signal gives these methods an immediate advantage over the linear optical methods that spread the signal over a sphere so that the intensity decays with distance according to the inverse square law. Practically all of the laser-like nonlinear signal can be detected and at a long distance away from the region of generation by which point the background luminosity or scattering from particles may be reduced to negligible proportions. In addition resonant four-wave mixing signals are sensitive to even trace quantities of the species being detected. The problem of collisional quenching can also be considerably reduced or eliminated in some circumstances. This can be done if the nonlinear signal is generated faster than the collisions can dephase the driven oscillations or by using ultra-short laser pulses in which the interaction is completed before any collisions occur.

The list of advantages provided by resonant four-wave mixing methods include: coherent (laser-like) signal leading to high signal-to-noise ratios, reduced sensitivity to collisional quenching, time and space resolution, sensitivity to trace quantities, species and state selectivity using high spectral resolution afforded by narrow linewidth lasers and reduction of Doppler broadening. The nonlinear interactions probe molecular excitations giving microscopic information that may be used to derive thermodynamic parameters such as species concentrations and temperatures. In addition the interaction of the excited molecules with the surrounding gas leads to changes in the bulk behaviour of the medium giving information on the macroscopic properties such as pressure, gas velocity and mass flow as well as temperature.

Although resonant four-wave mixing methods can address some of the problems encountered by linear techniques they also have their own peculiar disadvantages. The nonlinear optical

process is inherently more complicated and, in general, requires more complex analysis. In addition the signals are sometimes affected by interference from other nonlinear processes occurring simultaneously. Practical disadvantages include the need for high power lasers, more complex optical arrangements and alignment involving difficulties of optical access for the multiple beams required. Strategies have been and are being developed to mitigate these disadvantages both theoretically and practically e.g. provision of easy-to-run analysis software and reliable optical design to ease alignment problems.

In order to understand how the particular advantages and disadvantages of resonant four-wave mixing techniques arise we need to understand the underlying physical mechanisms involved. This is the subject of the following section.

3.2 The physics of four-wave mixing

A comprehensive treatment of the fundamental principles of four-wave mixing can be found in a number of textbooks [16, 44, 45]. In particular the excellent texts by Boyd [44] and Eckbreth [16] respectively provide detailed treatments of the fundamental nonlinear optics and a more simplified introduction in the context of applications in combustion. In this section we outline the underlying physics and how the signal strengths may be calculated to form the basis for measurements in diagnostic applications. We begin by reminding ourselves of the basic physics of linear optics. In this case the interaction of light with matter is described by the simple equation:

$$P(\omega) = \varepsilon_o \chi(\omega) E(\omega) \tag{3.1}$$

Physically this represents the generation of a polarization i.e. a distribution of electric dipoles, $P(\omega)$, whose magnitude is proportional to the amplitude of the incoming electric field of the light wave, $E(\omega)$. The constant of proportionality $\chi(\omega)$ is the susceptibility and ε_o is the permittivity of free space. The susceptibility $\chi(\omega)$ is a function of the light wave frequency,

ω, and becomes large when this corresponds to a natural resonance frequency in the atoms or molecules of the medium i.e. the frequency at which the atom or molecule will make a transition from the ground to an excited state. $\chi(\omega)$ is a complex function such that the imaginary part describes the absorption of the light by the atom and the real part describes the dispersion i.e. the change in phase velocity suffered by the light as it passes through the medium. The susceptibility $\chi(\omega)$ thus defines the (complex) refractive index of the medium. The oscillating dipole represented by $P(\omega)$ radiates electromagnetic energy i.e. some of the incoming light is scattered by the atoms or molecules. The polarization thus acts like a source term in Maxwell's equations describing the propagation of the light in the medium. The propagation of the light – its growth or decay – is therefore described by the wave equation derived from Maxwell's equations for the fields.

$$\nabla^2 E(\omega) = \frac{1}{c^2}\frac{\partial^2 E(\omega)}{\partial t^2} + \mu_o \frac{\partial^2 P(\omega)}{\partial t^2} \tag{3.2}$$

The wave arising from $P(\omega)$ is, according to equation 3.1, linearly proportional to the amplitude of the incoming wave $E(\omega)$ – hence this describes linear optics.

Exactly the same physics is involved in a nonlinear optical process. The expression for the polarization induced by an incoming field given in equation 3.1 may be generalized to include more than one field – or the same field more than once i.e. higher powers of the field amplitudes $E_i(\omega_i)$:

$$P(\omega) = \varepsilon_o \chi^{(1)}(\omega_1)E_1(\omega_1) + \varepsilon_o \chi^{(2)}(\omega)E_1(\omega_1)E_2(\omega_2) + \varepsilon_o \chi^{(3)}(\omega\ )E_1(\omega_1)E_2(\omega_2)E_3(\omega_3) + \ldots \tag{3.3}$$

The total induced polarization now has a nonlinear dependence on the incoming field amplitudes e.g. in the simple case where there is only one incident field, $\omega_1 = \omega_2$, including

only the second term in the expansion gives a nonlinear polarization that has a component depending quadratically as well as one depending linearly on the incoming field amplitude. The coefficients of the higher order terms $\chi^{(i)}(\omega)$ decrease by many orders of magnitude from one order to the next. Therefore the higher order terms giving the nonlinearity are usually negligibly small and most optical phenomena are very accurately linear. The situation changes however if either the field amplitudes $E_i(\omega_i)$ become much larger than usual or the susceptibility coefficients $\chi^{(i)}(\omega_i)$ become large. The electric field in bright sunlight is about 600 Vm^{-1} whereas the field in a laser may be many orders of magnitude larger e.g. the field in a laser beam of intensity ~1 $MWcm^{-2}$ is ~10^6 Vm^{-1}. So nonlinear effects are often found when intense laser light passes through a medium. The susceptibility coefficients, which vary with frequency, are also orders of magnitude larger than usual at frequencies corresponding to resonance transitions in the molecules of the medium. It is this frequency dependence that allows nonlinear optical processes to be used for spectroscopy. Thus nonlinear laser spectroscopy uses both means of enhancing a nonlinear signal by using intense electric fields and tuning the frequency to resonance in some molecular species in the medium.

For reasons of symmetry the second order term in $\chi^{(2)}(\omega)$ is zero in isotropic media such as gases and so the first nonlinear term that can contribute to the nonlinear polarization in such media is $\chi^{(3)}(\omega)$, the third order susceptibility. We can now consider how this term leads to the phenomenon of four-wave mixing.

Considering only the third order term the nonlinear polarization is:

$$P_{NL}(\omega_l) = \varepsilon_o \chi_{ijkl}{}^{(3)}(\omega) E_i(\omega_i) E_j(\omega_j) E_k(\omega_k) \tag{3.4}$$

This general expression shows that a polarization may be created oscillating at frequency ω_l in response to driving fields at three different frequencies ω_i, ω_j and ω_k. One way of thinking about this is to think of the field $E_k(\omega_k)$ acting on a medium whose refractive index is being modified by the action of the other two fields $E_i(\omega_i)$ and $E_j(\omega_j)$:

$$P_{NL}(\omega_l) = \varepsilon_o[\chi_{ijkl}{}^{(3)}(\omega)E_i(\omega_i)E_j(\omega_j)]E_k(\omega_k) \tag{3.5}$$

The action of the first two fields is to cause the refractive index to vary in time at the optical frequencies ω_i and ω_j. This leads to a beating of the three fields involved. Since the three terms can be taken in any sequence the polarization frequency ω_l can take a range of values given by the sums and differences of the incoming frequencies:

$$\omega_l = \omega_i \pm \omega_j \pm \omega_k \tag{3.6}$$

Thus three waves incident on a medium which responds nonlinearly produce a fourth wave radiated by the induced nonlinear polarization. This is the origin of four-wave mixing. The condition represented by equation 3.6 is simply the conservation of energy of the incoming and generated photons.

Once the fourth, or signal, wave is generated by the radiating polarization it can take part in the general mixing process so we do have *four* waves mixing. How much of this fourth wave is produced and measured will depend on the intensity of the incident three waves, the value of the nonlinear susceptibility at the relevant frequency, and, importantly, the geometry of the propagating waves defined by the respective wave vectors $\vec{k}_i(\omega)$. The geometry is important because the induced molecular dipoles will have to form a phased array if they are to generate a propagating wave i.e. they radiate a propagating wave only in a direction where the phase of

the dipoles is such that their radiation constructively interferes with the travelling signal wave. The wave vectors must satisfy the following condition to achieve this *phase matching*:

$$\vec{k}_l = \vec{k}_i \pm \vec{k}_j \pm \vec{k}_k \tag{3.7}$$

Equation 3.7 then represents the conservation of momentum of the photons. It can be seen from equation 3.6 that four-wave mixing encompasses a wide range of possible signal generating processes. The particular process that is observed will depend on the choice of the three input frequencies and the geometrical arrangement i.e. phase matching of the beams. The most important processes for our purposes are the following:

$\omega_4 = \omega_1 - \omega_1 + \omega_1 = \omega_1$ Degenerate Four Wave Mixing, DFWM

$\omega_4 = \omega_1 - \omega_2 + \omega_1$ Coherent Anti-Stokes Raman Scattering, CARS

Variations on these basic processes include Two-Colour Four Wave Mixing, TC-FWM, where $\omega_4 = \omega_1 - \omega_1 + \omega_2 = \omega_2$, and Electronically Resonantly Enhanced CARS or ERE-CARS where $\omega_4 = \omega_1 - \omega_2 + \omega_3$. In addition Laser Induced Grating Spectroscopy, LIGS, and also Polarization Spectroscopy, PS, can be treated as four-wave mixing processes. The molecular transitions involved in all these processes described by equation 3.6 are shown schematically in figure 3.1. The allowed quantum states in the molecules are represented by solid lines whereas the dashed lines represent virtual states. The transitions induced by the interacting photons are represented by vertical arrows and show schematically the energy conservation represented by equation 3.6.

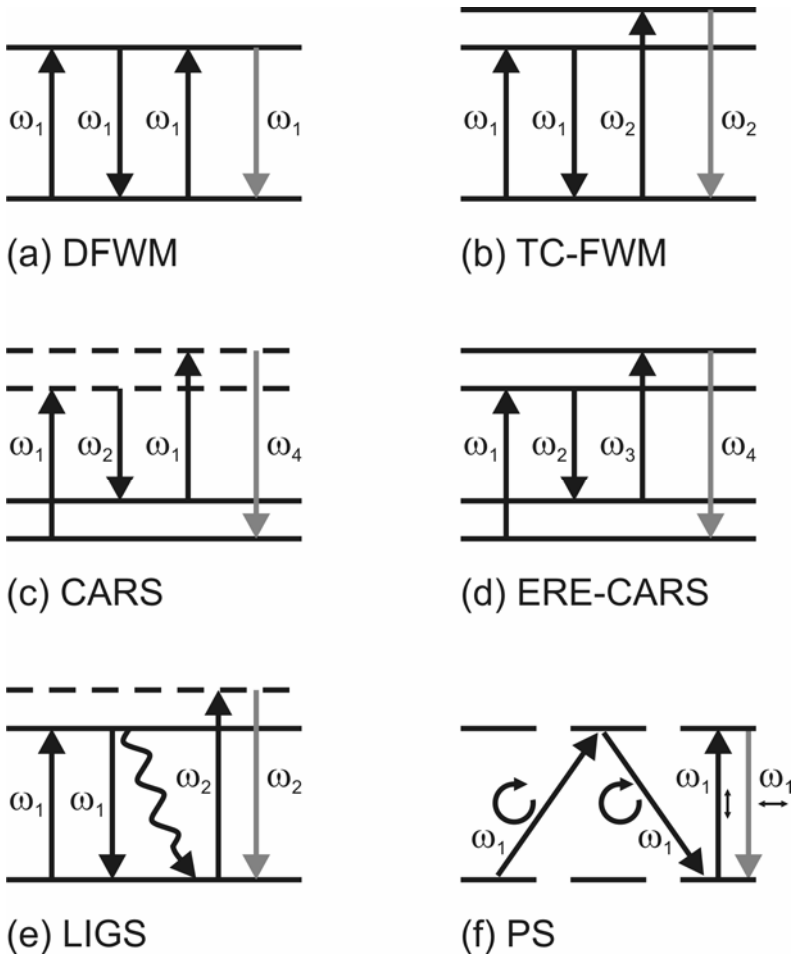

Figure 3.1: Transitions between allowed molecular states involved in resonant four-wave mixing processes. The lower solid line represents the ground state and upper solid lines and dashed lines represent allowed excited and virtual states respectively. The transitions induced by the interacting photons are represented by vertical or diagonal arrows. The wavy arrow in (e) represents a non-radiative or quenching transition. The circulating symbols in (f) indicate circular polarization of the incident photons and the double headed arrows indicate two orthogonal linear polarization states of the photons. In this example σ^+ light induces $\Delta m = +1$ transitions leading to depopulation of the lower degenerate m_J substates. In each diagram the three arrows on the left represent input photons and the right hand arrow (grey) represents the signal photon.

The geometrical arrangements that satisfy the momentum conservation represented by equation 3.7 are shown in figure 3.2 for the processes in which phase matching is a critical aspect viz. DFWM, TC-FWM, LIGS, CARS and ERE-CARS. In these processes the physical interaction can be represented by the generation of a grating structure and subsequent scattering of one of the waves off this structure to yield the signal. Two of the input beams are designated as “pump beams” and the other is designated the “probe beam”. In the cases of DFWM and TC-FWM two of the degenerate frequency beams interfere to produce a spatially varying intensity pattern or grating which is “written” into the medium by the nonlinear

response of the molecules. This provides a spatially varying refractive index grating that scatters some of the radiation from the third input beam to give the signal beam. Since the interfering beams have the same frequency the induced grating is stationary in space.

Two geometrical arrangements are possible to achieve the phase matching condition as shown for the case of DFWM. The first case consists of two counter-propagating pump beams and the probe of wavelength λ intersecting at some arbitrary angle θ. The spacing of the interference pattern, Λ, and hence of the grating will be:

$$\Lambda = \frac{\lambda}{2\sin(\theta/2)} \tag{3.8}$$

In this arrangement the momentum of the pump beams sums to zero so the momentum of the probe and signal must then also sum to zero to conserve momentum. The result is that in this "Backward Pump Geometry", BPG, the signal is emitted counter-propagating to the probe and is automatically phase matched. The angle θ therefore can have any value. In practice however θ is kept small otherwise the grating spacing Λ is so small that thermal motion of the molecules washes out the grating so rapidly that the scattering efficiency is dramatically reduced. When the incident laser linewidth is narrower than the Doppler width of the enhancing molecular transition only those molecules that have no velocity component along the input laser beams can interact with all three beams. Moving molecules "see" the incident laser light Doppler shifted out of resonance and so they do not contribute to the signal. This property can be very useful for spectroscopy in flames where Doppler broadening is the main limitation to spectral resolution.

The second possible geometry has the two pumps and probe beam propagating all in the forward direction but at a small angle to each other. Phase matching again is easily achieved by ensuring the angles between the beams are equal for the degenerate frequency case or have the required value to ensure the transverse momentum adds to zero in the case of TC-FWM.

This “Forward Pump Geometry”, FPG, has the advantage that all the molecules can contribute to the signal, not just those with zero velocity relative to the beams as in the BPG resulting in stronger signals.

Since the grating in the case of DFWM and TC-FWM is composed of a spatial variation of population of excited molecular states it will decay rapidly owing to spontaneous emission or collision effects which may both dephase the dipoles or de-excite them by inelastic scattering i.e. quenching. The FWM interaction returns the molecules to the ground state. Thus energy is simply redistributed from the three input fields to the signal field and the outgoing pump and probe fields. If quenching collisions occur, however, some of the energy is prevented from being re-coupled to the fields. This energy deficit appears as heat in the medium – inelastic collisions transfer energy to translational (kinetic) and internal energy of the colliding molecules. The result is that the same grating pattern is produced as a local variation in temperature and density. This is a bulk property of the gas and decays much more slowly than the molecular population grating. This thermal grating persists after the exciting lasers have disappeared and so signals can be produced by scattering also after the excitation has ceased. The strength of the scattered signal may be used to probe the dynamics of the thermal grating decay. This laser induced grating scattering requires that the probe beam is incident on the grating at the Bragg angle to produce the diffracted signal beam. The angle of incidence must therefore be chosen to match the probe wavelength to the grating spacing.

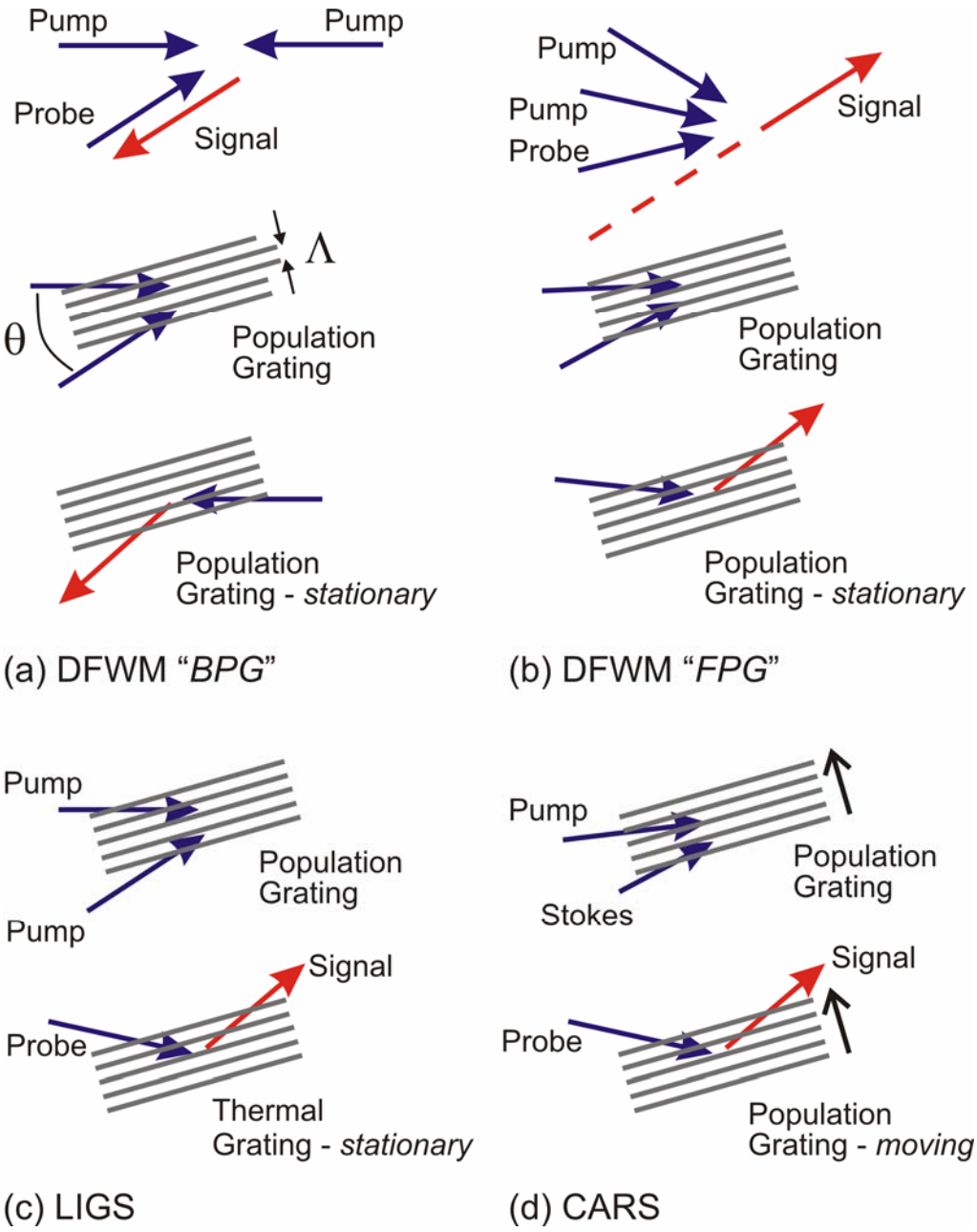

Figure 3.2: Grating structures induced in four-wave mixing processes: (a) DFWM with Backward Pump Geometry, BPG, (b) DFWM with Forward Pump Geometry, FPG, (c) LIGS and (d) CARS. In ERE-CARS the pump and probe waves will have different frequency. The arrangements of arrows indicate approximately the geometry of the interacting beams to achieve phase matching.

In the case of CARS, a grating is produced by interference of one pump beam and a second beam often referred to as Stokes beam, so called because it is shifted in frequency by the "Stokes shift" corresponding to a molecular vibration or rotation frequency observed in the normal Raman effect. The interference pattern produced by two beams of different frequency is not stationary in space and moves at a speed determined by the frequency difference

between the pump and Stokes beam. Consequently the grating associated with the interference pattern is moving and so the beam that is scattered off the moving grating will be Doppler shifted. In CARS the "probe" beam is usually at the same frequency as the pump and the scattered beam is Doppler shifted upwards by an amount equal to the Stokes shift. Thus the signal beam is increased in frequency to that of the Anti-Stokes wave in Raman scattering. The signal is coherent owing to the phase imposed by the coherent excitation beams and so the overall process is termed Coherent Anti-Stokes Raman Scattering, CARS. As can be seen in figure 3.1(c) the interaction involves two successive two-photon transitions via virtual states. The process is therefore inherently weak since two-photon transitions have much lower probability than single photon resonant transitions. This problem is addressed by using two pumps of different frequency chosen to coincide with resonant single photon electronic transitions. Each of the photon interactions is therefore resonantly enhanced leading to Electronically Resonantly Enhanced CARS or ERE-CARS.

The remaining technique, Polarization Spectroscopy, PS, can be thought of as a four-wave mixing process in the following way. A probe beam is linearly polarized by passing through a polarizer prism and then through a medium and is then blocked by an orthogonally aligned linear polarizer i.e. an analyzer. In the absence of any other beams the medium presents a linear isotropic refractive index to the probe. As a consequence the crossed polarizer and analyzer result in a zero intensity reaching the detector. When, however, a strong, circularly polarized, pump beam interacts with the medium optical pumping creates an unequal population in the degenerate magnetic sub-states of the molecules making the medium optically active i.e. it presents a different refractive index value to right and left circularly polarized light. So when the pump is present the plane of polarization of the probe beam is rotated resulting in some transmission through the analyzer. The optical pumping arises from interaction with two waves from the pump beam. The probe provides the third wave that interacts with the optically pumped molecules to create a phased array of dipoles with

polarization rotated relative to that of the probe. This phased array, set up by the propagating probe, radiates the signal – the fourth wave – that is transmitted by the analyzer. Owing to the vector properties of the pump and probe fields the effect is reduced if the crossing angle increases and falls to zero at 90^{o}. As can be seen in figure 3.3 the pump can propagate either in the forward or backward direction relative to the probe and since the molecules must interact with both beams the backward geometry provides a "Doppler-free" signal in a similar way to DFWM with BPG. In practice different combinations of circular and linear polarizations for pump and probe can be chosen that will interact with the molecules in different ways according to the transition selection rules governing the resonant transition being excited.

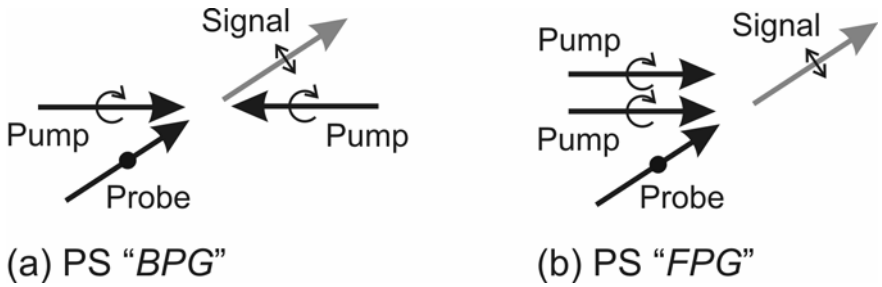

Figure 3.3: Polarization Spectroscopy (a) Backward Pump Geometry, BPG and (b) Forward Pump Geometry, FPG. In both cases the pump beams are shown circularly polarized in the same sense. The component of the signal beam that is orthogonal to the probe polarization is shown.

3.3 The properties of four-wave mixing

Having outlined the basic physics underlying four-wave mixing we are now in a position to understand how the advantageous properties of these nonlinear processes arise. Firstly, with the exception of LIGS, the coherent nature of the signals arises from the polarization that is driven by the three input waves: two pumps and one probe. The induced polarization creates a phased array of oscillators that radiates a wave that grows in amplitude along a direction determined by the phase matching geometry, or the direction of the probe beam in PS. The signal wave is therefore emitted as a coherent laser-like beam. Such a signal beam is then

easily spatially filtered from isotropically scattered laser light or flame luminescence leading to high signal-to-noise ratios. In the case of LIGS the coherence of the signal arises from Bragg scattering off a macroscopic grating structure created by interference of two coherent beams.

The phase matching geometry also allows the interaction to be generated from a small volume defined by the intersection of the pump and probe beams. This crossed-beam arrangement automatically provides good spatial resolution. Although PS does not require phase matching it shares the property of having good spatial resolution by virtue of using crossed pump and probe beams. The volume of the interaction region can be typically tens to hundreds of microns in transverse extent by about one millimeter in length. Time resolution is determined by the duration of the incident laser pulses which can range from tens of nanoseconds to a few femtoseconds using Q-switched and mode-locked lasers respectively. In principle, pulses of the order of microseconds in duration can also be used (provided that the intensity is sufficient for generating nonlinear optical signals) and these are still fast on the time scale of many combustion phenomena of interest.

The strength of the signal is determined by the population of the initial quantum state, N_J, and the value of the molecular third order susceptibility $\chi^{(3)}(\omega)$. The *amplitude* of the induced polarization and hence of the radiated signal wave will therefore also be proportional to the population. The signal *intensity* therefore scales with the square of the population density, N_J and so the signal intensity gives a measure of the concentration of the resonantly interacting species.

The frequency dependence of $\chi^{(3)}(\omega)$ is responsible for the enhancement of the interaction when the input frequencies correspond to resonant transitions in the molecules. The signal strength will be many orders of magnitude larger on-resonance than off-resonance and this then gives the process spectroscopic selectivity. Particular species and specific quantum states

can be excited selectively by choosing the input frequencies and using narrow-bandwidth lasers. Thus species present at trace levels of the order of ppm can be readily detected against a background of other majority species. This is important in detecting transient or radical species involved in combustion chemistry and the spatial resolution allows them to be detected even within narrow reaction zones of flames. Further properties such as the reduced sensitivity to molecular collision effects and the derivation of thermodynamic parameters of interest in combustion depend on the specific form of $\chi^{(3)}(\omega)$ for each process and will be considered in the following sections.

3.4 Experimental considerations and data analysis

The need for high power in the input beams has been noted but "How high does the power need to be?" The normal refractive index responsible for linear optics arises because all the molecules are in their ground state. So an approximate guide as to what power is needed is given by the power needed to significantly perturb this population. A quantitative guide to the degree to which the population is changed is known as "saturation". The medium is said to be saturated when the populations of the ground and excited states are equal. The intensity of light needed to drive the populations into this condition is known as the "saturation intensity". In practice it is possible to detect nonlinear effects even when the degree of excitation is several orders of magnitude smaller than this level. Since excited molecules will relax to the ground state in a time τ, the fluorescence lifetime, we require a photon of the appropriate energy, $\hbar\omega$, to fall into the cross-sectional area of the molecule, σ, at a rate given by $1/\tau$. This power will also have to be contained in a spectral width determined approximately by the linewidth, $\Delta\omega$, of the resonance transition. The required spectral power density, or saturation intensity, I_{sat}, is then given by:

$$I_{sat} \approx \frac{\hbar\omega}{\sigma\tau\Delta\omega} \tag{3.9}$$

Typical values for a molecular transition in the optical region of the spectrum lead to a saturation intensity of the order of 1 $MWcm^{-2}cm^{-1}$. This can be readily obtained from a pulsed laser providing around 0.1 mJ in a 10 ns pulse in a beam of cross-section 0.1 cm^2 and a linewidth of around 0.1 cm^{-1}. In practice pulse energies down to a few microjoules can be used with focused beams of good quality i.e. single transverse mode or approximately Gaussian profiles. In many cases it is desirable to focus the input pump and probe beams to diameters of order 10 - 100 μm in order to obtain maximum spatial resolution. In other cases, however, a small interaction volume may limit the precision of the measurement. Specifically in the case of Laser Induced Thermal Gratings diffusion of the thermal energy out of the interaction region leads to a more rapid decay of the signal and limits the precision of parameters derived from the time behaviour of the signal.

The linewidth of most high power pulsed lasers is usually of the order 0.01 – 0.1 cm^{-1} which is well-matched to the transition linewidths. If higher spectral resolution is required then a single longitudinal mode laser will be needed with a linewidth of the order of 0.001 cm^{-1} that will be limited by the Fourier transform of the temporal pulse envelope. For broadband or multiplex spectroscopy, of course, a wide laser bandwidth will be used but in this case it is still important to maintain the required spectral power density.

Resonant enhancement of the four-wave mixing signal is achieved usually by scanning the frequency (or wavelength) of a narrow-bandwidth laser on to the molecular transitions. In this case the signal is usually detected using a photo-multiplier or photodiode. An example of a high resolution spectrum obtained by scanning a narrow-linewidth laser is shown in figure 3.4. This spectrum of OH was recorded in a methane air flame using the BPG to reduce the Doppler width of the lines. Since most pulsed lasers have a repetition rate of the order of

10Hz the signals may be detected and stored digitally or using a Boxcar averager to improve the signal-to-noise ratio. Alternatively signals may be detected simultaneously on multiple transitions if a broad bandwidth laser is used. All of the signals emitted co-propagate as a single beam i.e they are multiplexed, and so spectral dispersion is required in this case to derive relative intensities of the individual resonantly enhanced signals. Multiplex spectra are recorded on a one- or two-dimensional array detector such as a diode array or CCD.

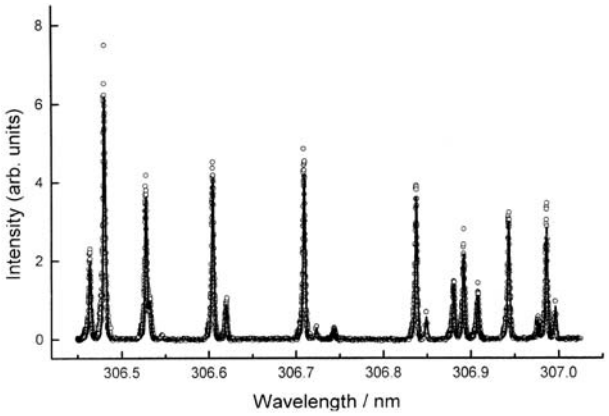

Figure 3.4: A DFWM spectrum of OH in a methane/air flame at atmospheric pressure. The solid line is the theoretical fit to the data calculated using the analytical result of reference [46]. (Figure reproduced with permission from reference [47]).

Apart from ensuring that the laser intensity and linewidth are suitable for generating FWM signals the spatial profile of the beams is also found to be important. In practice it is often found that having a Gaussian profile or TEM_{00} spatial mode will allow good signal-to-noise data to be obtained even when the intensity is several orders of magnitude less than the saturation level. Typically, good signals can be obtained with a smooth beam profile on strong molecular transitions such as the A-X (0,0) band of OH in atmospheric pressure methane/air flames with ~10μJ in a linewidth of ~0.1 cm^{-1}. Alignment of the three incident beams is also clearly important. Retro-reflection of one pump beam to provide spatially overlapping beams is easily achieved using a simple aperture system. A further aperture at the interaction volume is also useful to ensure that the probe beam overlaps the two pumps. Alignment of the signal

beam is made easy by retro-reflecting the probe beam in the BPG to provide a guide beam to align the signal onto the detector. The retro-reflecting mirror is then blocked or removed when recording the DFWM signal. In the case of FPG a system of masks containing apertures to guide the beams to cross at a given angle can be made. The direction of the signal beam is then determined by the path through a suitably arranged set of two apertures at the appropriate phase-matching angle. In the case of DFWM a symmetric set of four apertures in two masks is sufficient to define the directions of the three input beams and the signal beam. Typically a crossing angle of between 2°-10° provides strong signals but these will decrease rapidly as the crossing angle is increased. Finally it is important to ensure temporal overlap of all pulses, at least to within the coherence time of the lasers determined by the inverse of the frequency bandwith.

Species concentrations and temperature are the two most important combustion parameters that are routinely measured using optical diagnostics. Other parameters such as bulk gas velocity, flame speed, pressure and mass flow may also be derived from optical measurements. As noted above the signal intensity in coherent scattering processes is usually proportional to the square of the species concentration or number density, N. (In some cases there may be deviations from this behaviour and these will be noted where relevant.) Thus relative or absolute concentrations can be derived in principle from the measured intensities. In order to derive absolute concentrations it is usually necessary to perform a calibration measurement since some important experimental parameters may be difficult or impossible to measure accurately.

The properties of the spectrum such as the relative intensities of different transitions may be used to derive temperatures by use of a Boltzmann plot which relates the relative population of energy levels N_J e.g. rotational energy levels of quantum number J, to the excitation energy ΔE_J of the levels which depends on the equilibrium temperature, T. In equilibrium the population N_J is,

$$N_J \propto (2J+1)e^{(-\Delta E_J hc/kT)} \tag{3.10}$$

where the factor (*2J+1*) represents the degeneracy of the state, *h* is Planck's constant, *c* the speed of light and *k* is Boltzmann's constant. A plot of ln{population} vs. energy should yield a straight line with slope proportional to *1/T* from which the temperature can be derived. Since the signal intensity is proportional to N_J^2 and the line strength B_{ij} the quantity:

$$\ell n\left\{\frac{\sqrt{I_{signal}}}{[(2J+1)]B_{ij}}\right\} \tag{3.11}$$

represents ℓn {population} and is plotted against the energy term ΔE_J. An example is displayed in figure 3.5 utilizing the spectral data from figure 3.4.

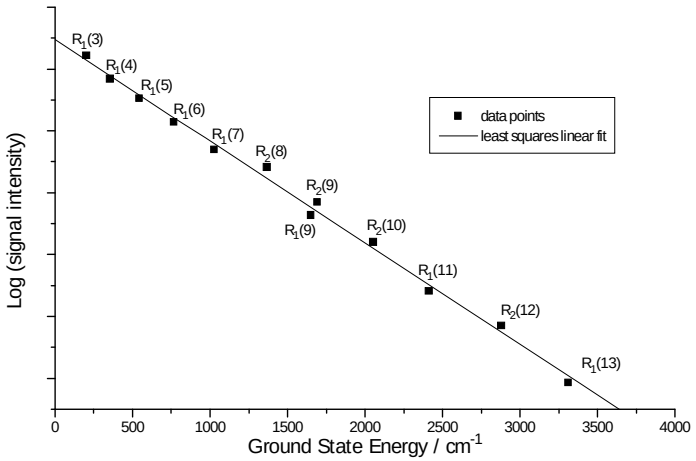

Figure 3.5: Boltzmann plot using the signal intensities from the OH spectrum shown in figure 3.4. The temperature of the flame derived from this data is 1754 $\pm$ 38 K. (Figure reproduced with permission from reference [47].)

Alternatively a broad bandwidth laser source may be used to generate signals simultaneously on multiple transitions. Temperatures are then usually derived from the multiplex spectra by fitting a temperature-dependent modelled spectrum to the experimental data. In this case it is

often necessary to have an accurate theoretical model not only of the relative intensities but also of the resonant lineshapes and their dependence on temperature and pressure. Multiplexed spectral methods provide single-shot data and so are useful in transient combustion situations such as engines, shock tubes or explosions. Scanning methods however can be used advantageously in stable flames.

4 Degenerate and non-degenerate four-wave mixing

The basic optical layout for generating DFWM signals is shown in figure 4.1 for the BPG phase matching arrangement. The essential items are a high power (usually pulsed) laser that is frequency tuneable in the region of the resonant transitions of the species being used. An arrangement of beam splitters is used to generate two pump beams and a single probe beam. A second beam splitter is often used to pick off the reflected signal beam in BPG. An alternative geometry where the forward and backward pumps are at a small angle can be used which leads, by phase matching considerations, to the signal beam being generated at the same small angle to the probe. Pump and probe beams can be made orthogonally polarized so that the signal is also orthogonal to the pumps and hence scattered pump light can be filtered out by a crossed polarizer in the signal path to the detector. The signal is typically detected by a photo-detector placed several metres from the interaction region and spatially filtered by apertures to reduce background interference.

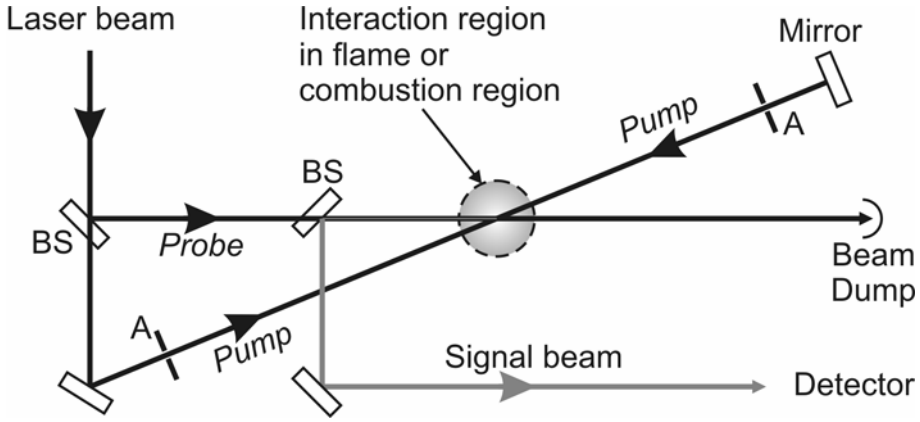

Figure 4.1: Basic optical layout for DFWM using BPG. BS, beam splitter, A, apertures.

Degenerate four-wave mixing was first proposed as a diagnostic method for combustion in 1982 when it was recognised that the resonance enhancement on transitions between excited states allowed signals to be generated by the small excited state populations comparable to

radical species densities in flames [48]. DFWM in a flame was observed in experiments where atomic sodium vapour in a flame was used as a medium for phase conjugate reflection [49]. The first detection of a combustion species using DFWM was that of OH in a flame [50]. In this section we present the fundamental theory of DFWM and how it may be extended and applied to quantitative measurements of combustion parameters.

4.1 Fundamentals

The basic physics of four-wave mixing outlined in the previous section highlights the crucial role of the third order susceptibility $\chi^{(3)}(\omega)$ in determining the strength and spectral properties of the signal. The form of $\chi^{(3)}(\omega)$ itself is determined by the details of the interaction between the input fields and the molecular response. A wide range of physical interactions can contribute to $\chi^{(3)}(\omega)$ such as saturated absorption, two-photon absorption, Raman pumping etc ... depending on the nature of the input fields and their geometrical arrangement. The physics common to all the third order interactions will be illustrated here by deriving $\chi^{(3)}(\omega)$ in the straightforward case of degenerate fields interacting with a two-level atom. The Hamiltonian for the system is:

$$\hat{H} = \hat{H}_o + \hat{V}(t) \tag{4.1}$$

where $\hat{H}_o$ is the unperturbed atomic Hamiltonian i.e. the operator associated with the ground state energy of the atom. $\hat{V}(t)$ is the perturbation energy arising from the atomic dipole interaction with an oscillating electromagnetic field *E(t)*.

$$V_{21}(t) = V_{12}^*(t) = -\mu_{12} E(t) \tag{4.2}$$

where μ_{12} is the atomic dipole moment involved in the transition from the ground state 1 to the excited state 2. The statistically averaged response of the medium is described by the

density matrix composed of the population terms of these two states, ρ_{11} and ρ_{22}, respectively and the associated coherence terms representing the dipole, ρ_{12} and ρ_{21}. The time evolution of the atomic ensemble is described by the master equations:

$$\dot{\rho}_{11} = \frac{i}{\hbar}\left[V_{21}\rho_{12} - V_{12}\rho_{21}\right] + \frac{\rho_{22}}{T_1} \tag{4.3}$$

$$\dot{\rho}_{22} = \frac{i}{\hbar}\left[V_{12}\rho_{21} - V_{21}\rho_{12}\right] - \frac{\rho_{22}}{T_1} \tag{4.4}$$

$$\dot{\rho}_{21} = -\rho_{21}\left(i\omega_o + \frac{1}{T_2}\right) + \frac{i}{\hbar}V_{21}(\rho_{22} - \rho_{11}) \tag{4.5}$$

Here $\hbar\omega_o$ is the energy of the transition between states 1 and 2 and the off-diagonal matrix elements representing the coherences satisfy $\rho_{21} = -\rho_{12}^{*}$. In these equations T_1 is the decay time of the population excitation i.e. the longitudinal relaxation time and is usually determined by the spontaneous or radiative lifetime of the excited state. T_2 is the decay time of the coherence, the transverse relaxation time, determined by the rate of dephasing of the dipole oscillations and usually determined by the atomic collision rate. The equations 4.3, 4.4 and 4.5 are solved in the steady state using the rotating wave approximation RWA [51, 52]. Since we are principally concerned with how the atomic or molecular populations evolve in time as they interact with the radiation we may neglect terms that oscillate at optical frequencies and concentrate only on slowly varying terms. This may be done mathematically by treating the interaction in the frame of reference that rotates with the electric field of the incoming photon – which is fundamentally circularly polarized. In this rotating frame the interaction has a very slow term describing the evolution of the populations and a term at essentially twice the optical frequency which is neglected on the timescales of interest. In this

rotating wave approximation the population difference between excited and ground states are given by:

$$\rho_{22}-\rho_{11}=\frac{-\hbar^2\left(1+T_2^2(\omega-\omega_o)^2\right)}{\hbar^2\left(1+T_2^2(\omega-\omega_o)^2\right)+T_1T_2\left|\mu_{21}\right|^2\left|E\right|^2} \tag{4.6}$$

$$\rho_{21}=\widetilde{\rho}_{21}e^{-i\omega t}=\frac{-\mu_{21}E^*e^{-i\omega t}(\rho_{22}-\rho_{11})}{2\hbar\left(\omega-\omega_o+i/T_2\right)} \tag{4.7}$$

where $\widetilde{\rho}_{21}e^{-i\omega t}$ represents the slowly varying part of the dipole in the RWA.

We have now found the elements of the density matrix we need and so we use them to find the Trace of the matrix which gives us the time-dependent polarization *P(t)* of the medium from:

$$P(t)=N\mathrm{Tr}\left(\rho\mu\right)=N\left(\mu_{12}\rho_{21}+\mu_{21}\rho_{12}\right) \tag{4.8}$$

Writing the polarization as

$$P(t)=\frac{Pe^{i\omega t}}{2}+\frac{P^*e^{-i\omega t}}{2} \tag{4.9}$$

and recalling $P(t)=\varepsilon_o\chi E$, we write,

$$P(t)=\varepsilon_0\left(\frac{\chi Ee^{i\omega t}}{2}+\frac{\chi^*E^*e^{-i\omega t}}{2}\right) \tag{4.10}$$

From these relations we derive:

$$\chi = \frac{-N|\mu_{21}|^2\left(T_2(\omega-\omega_o)+i\right)T_2/\hbar}{1+T_2^2(\omega-\omega_o)^2+T_1T_2|\mu_{21}|^2|E|^2/\hbar^2} \tag{4.11}$$

This expression can be simplified by defining a normalized detuning, $\delta = (\omega - \omega_o)T_2$, and the line centre saturation intensity:

$$I_{sat} = |E_{sat}|^2 = \frac{\hbar^2}{T_1T_2|\mu_{21}|^2} \tag{4.12}$$

and the line centre absorption coefficient: $\alpha_o = N|\mu_{21}|^2 T_2 k/2\hbar$, where k is the wavevector at frequency ω, so that:

$$\chi(E) = \frac{-2\alpha_o(\delta+i)}{k(1+\delta^2+|E/E_{sat}|^2)} \tag{4.13}$$

The form of this expression shows that it represents the susceptibility arising from saturated absorption. We can use it then to describe a four-wave mixing interaction in which the input waves are coupled via the nonlinearity associated with the saturated absorption and dispersion of the medium.

4.1.1 Theory of DFWM

The standard and basic theory of DFWM in absorbing media was presented by Abrams and Lind [53, 54]. We outline briefly here only the salient features of their approach in order to explain the physics. (As with the more complex situations, treated in further theoretical treatments cited below, mathematical details can be found in the original references.) They considered a relatively simple situation in which a monochromatic laser field interacted with a weakly absorbing (i.e. optically thin) medium composed of stationary two-level atoms. The

pump fields in the BPG were assumed to have arbitrary intensity but the probe field was weak – allowing a perturbation theory approach. Thus the total field is written,

$$\begin{aligned} E &= E_0 + \Delta E \\ &= \mathsf{E}_0 e^{i\omega t} + \Delta \mathsf{E} e^{i\omega t} + c.c. \end{aligned} \tag{4.14}$$

where $\mathsf{E}_0 = \mathsf{E}_1 + \mathsf{E}_2$ is the field due to the pumps with spatially varying complex amplitudes E_1 and E_2, and $\Delta\mathsf{E} = \mathsf{E}_3 + \mathsf{E}_4$ is the weak field due to the signal plus probe respectively. The spatially varying amplitudes are written $\mathsf{E}_\mathrm{i} = A_i \exp(-i\vec{k}_i.\vec{r})$. A Taylor expansion of the polarization about E_0 yields to first order in $\Delta\mathsf{E}$ [53],

$$\mathsf{P} = \left(\chi_o \mathsf{E}_\mathrm{o} + \chi_o \Delta\mathsf{E} - \frac{\chi_o}{\left|E_{sat}\right|^2} \frac{(\mathsf{E}_\mathrm{o}^{\,*} \Delta\mathsf{E} + \mathsf{E}_\mathrm{o} \Delta\mathsf{E}^*)\mathsf{E}_\mathrm{o}}{(1+\delta^2 + \left|\mathsf{E}_\mathrm{o}/E_{sat}\right|^2)} \right) e^{i\omega t} + c.c. \tag{4.15}$$

Only the third term in this expansion creates phase matched terms depending on the three input fields. This is then substituted into the wave equation in the slowly varying amplitude approximation given by,

$$\left(\frac{\partial}{\partial z} + \sqrt{\mu_o \varepsilon} \frac{\partial}{\partial t} \right) \mathsf{E} = -i \frac{\omega}{2} \sqrt{\frac{\mu_\mathrm{o}}{\varepsilon}} \mathsf{P} \tag{4.16}$$

Recalling that the complex amplitudes are $\mathsf{E}_\mathrm{i} = A_i \exp(-i\vec{k}_i.\vec{r})$ the phase matched terms in the steady state lead to the coupled amplitude equations,

$$\frac{dA_4}{dz} = \alpha A_4 + i\kappa^* A_3^* \tag{4.17}$$

$$\frac{dA_3^*}{dz} = -\alpha^* A_3^* + i\kappa A_4 \tag{4.18}$$

In these equations A_4 is the amplitude of the signal wave and A_3 the amplitude of the input probe beam. The direction z is taken to be the direction of the probe beam wave vector $\vec{k}_3$. For the case of equal pump intensities $|A_1|^2 = |A_2|^2 = I$ then the coupling coefficients α and κ are given by,

$$\alpha = \frac{\alpha_o}{\varepsilon_o}\frac{(1-i\delta)}{(1+\delta^2)}\frac{1+2I/I_{sat}}{(1+4I/I_{sat})^{3/2}} = \alpha_R - i\alpha_I \tag{4.19}$$

$$\kappa^* = \frac{i\alpha_o}{\varepsilon_o}\frac{(1-i\delta)}{(1+\delta^2)}\frac{2I/I_{sat}}{(1+4I/I_{sat})^{3/2}} \tag{4.20}$$

Here I_{sat} is the frequency dependent saturation intensity $I_{sat} = (1+\delta^2)|E_{sat}|^2$ and α_R and α_I are the real and imaginary parts of the saturated absorption coefficient.

The signal strength is found by integrating the coupled amplitude equations over the interaction length, *L*. In the BPG which we are considering here the probe enters the interaction region at $z = 0$ and so the signal emerges at this point in the opposite direction. The equations may be solved more easily by assuming that the signal is always much weaker than the probe and so the terms in A_4 on the RHS of equation 4.17 and 4.18 can be neglected. We find the signal,

$$A_4(0) = \frac{i\kappa^* A_3^*(0)}{\alpha_R + i\alpha_I}\left(1 - \exp[-L(\alpha_R + i\alpha_I)]\right) \tag{4.21}$$

In the limit of very low absorption the signal intensity is then,

$$I_4 = |\kappa|^2 L^2 I_3 \tag{4.22}$$

Equation 4.21 shows that the amplitude of the signal wave is proportional to the phase conjugate of the probe wave amplitude. This is a consequence of the nonlinear coupling in the BPG which determines that the signal will be a reflection of the probe.

A more general solution for the signal intensity can be found in terms of the atomic or molecular parameters of interest for diagnostic purposes. Two limiting cases are of interest corresponding to weak and strong pump fields i.e. unsaturating and saturating intensities, respectively [16]:

$$I_{sig} \propto \frac{|\mu_{21}|^8 N^2 k^2 T_1^2 T_2^4}{(1+\delta^2)^3} I_{pump}^2 I_{probe} \qquad I_{pump} << I_{sat}(0) \tag{4.23}$$

$$I_{sig} \propto \frac{|\mu_{21}|^2 N^2 k^2 T_2}{T_1} \frac{I_{probe}}{I_{pump}} \qquad I_{pump} >> I_{sat}(0) \tag{4.24}$$

In practice the degree of saturation by the pump varies with detuning across the line so the experiments usually record a signal integrated across the whole resonance line. The spectrally integrated signal is then given in the two intensity limits by:

$$I_{sig}^{\text{int}} = \frac{|\mu_{12}|^8 N^2 k^2 T_1^2 T_2^3}{(1+4I_{pump}/I_{sat})^{5/2}} I_{pump}^2 I_{probe}, \qquad I_{pump} << I_{sat}(0) \tag{4.25}$$

$$I_{sig}^{\text{int}} \propto \left|\mu_{12}\right|^3 N^2 k^2 T_1^{-1/2} T_2^{1/2} . I_{pump}^{-1/2} I_{probe} \qquad I_{pump} >> I_{sat}(0) \tag{4.26}$$

These results allow us to draw some useful conclusions about the behaviour of the DFWM signal. Firstly we note the signal scales with N^2 and so the intensity can be interpreted in terms of the species concentration. Secondly, for weak pump beams ($I / I_{sat} \leq 1$) the signal is strongly affected by pressure or collisional broadening through the dependence on T_2^3. Thirdly, in the case of strong, or saturating, pump beams ($I/I_{sat} \geq 1$) the collisional dependence is considerably weaker. More sophisticated theoretical models have shown specifically that, in the saturated regime, the dependence of the DFWM signal intensity on the relative rate of dephasing collisions and quenching (population transfer) collisions is minimized [55]. Owing to the form of the dependence on T_2 the DFWM signal is sensitive only to the total collision rate rather than separately to quenching and dephasing or other collision effects. This feature gives DFWM an advantage over LIF in situations where the different collision rates are unknown. Fourthly, for pump intensities less than I_{sat} the signal increases quadratically with pump power whereas for intensities exceeding I_{sat} the signal decreases with increasing pump intensity. This means that the signal will reach a maximum for pump intensities in the region of I_{sat} and will also be least sensitive to fluctuations in the pump intensity. It is therefore expedient to operate with pump intensities around I_{sat} both to minimise the sensitivity to collisional and laser fluctuations and to maximise the signal-to-noise ratio. In practice is it usual to plot the signal strength as a function of pump intensity to determine the saturation intensity for a given situation since it depends on factors such as spatial beam profile and lineshape that may not be accurately known. Provided sufficient power is available, a plot will show a deviation from the linear dependence on the square of pump intensity once the saturation level is approached.

4.1.2 Analysis of DFWM signals: Practical considerations

In spite of the considerable simplifications involved in the Abrams and Lind model it has proved to be remarkably successful in predicting the behaviour of DFWM signals in a wide range of applications. For quantitative diagnostics however it becomes necessary to address some of the major approximations made and to develop theoretical approaches that account more accurately for deviations from the simple model encountered in practical applications. In order to improve the Abrams and Lind model the main issues that need to be addressed are:

a) Atomic motion – in media encountered in combustion the thermal motion of high temperature gases leads to considerable Doppler broadening. A further complication is that in the BPG the motion can lead to cross-over resonances since the moving molecules see the pump beam frequency Doppler shifted in opposite senses leading to a non-degenerate interaction. In the FPG the atomic motion has different effects on the resonance and saturation behaviour.

b) Effects of a strong probe field – the grating induced by interference of pump and probe will have highest contrast and greatest scattering efficiency if the pump and probe beams have equal intensity.

c) Non-monochromatic fields – most pulsed laboratory lasers have a finite linewidth that usually exceeds the linewidth of the resonance transitions.

d) Level degeneracy and polarization effects – collisions and orientation of the incident field polarizations will affect the signal behaviour differently from that of a two-level atom when multiple states are degenerate in the energy levels involved.

e) Multiple energy levels – molecular spectra often have closely spaced resonances that will contribute to the signal and so the response will deviate from that of a simple two-level, single resonance interaction.

f) Collisions – with more complex molecular species collision effects modify the lineshape of the response owing to varieties of collisional relaxation effects such as depolarizing collisions and velocity changing collisions.

g) Optical thickness – with high densities of certain species or on strongly allowed transitions the medium may be no longer optically thin leading to spatially varying changes in the field intensities through the interaction region.

We consider first the effects of atomic motion. The most obvious will be to "wash out" the induced grating leading to a reduction in scattering efficiency and lower signals. In the BPG this effect is most serious for the grating formed by the backward pump and the probe since it has a grating spacing Λ of the order of $\lambda/2$. (See equation 3.8 for $\theta \sim \pi$) The grating induced by the forward pump and probe will have a much wider spacing ($\theta \sim 0$, $\Lambda >> \lambda$) and so suffers less from the wash-out effect. The motion also leads to a Doppler shift for the incident laser frequencies and so there will be an effect on the lineshape of the DFWM signal. Atomic motion effects have been treated for the unsaturated regime using perturbation theory [56-59]. These studies show that in the BPG when the Doppler width $\Delta\omega_D$ is smaller than the homogeneous width the result is essentially the same as that of Abrams and Lind. The lineshape will be a Lorentzian cubed. When however the Doppler width exceeds the homogeneous width then the lineshape becomes a simple Lorentzian with a width equal to the homogeneous width. In the FPG all velocity classes contribute to the signal and the lineshape becomes a convolution of the homogeneous line with a Doppler broadened Gaussian. In the limit where the Doppler linewidth is much larger than the homogeneous width the lineshape is a Gaussian squared of width $\Delta\omega_D/\sqrt{2}$.

For the saturated regime the situation is more complicated. The problem was addressed by Attal-Tretout and co-workers who used a non-perturbative approach to treat pump saturation

and atomic motion effects in the FPG which led to modification of the signal lineshapes [60, 61]. Their analytical result however was found to work only for unsaturating probes and provided the pumps were not strongly saturating. A rather complete way of treating the problem was introduced by Lucht and co-workers which proceeds by a direct numerical integration, DNI, of the density matrix equations [55]. They have applied their DNI method to lift almost all of the major restrictions of the Abrams and Lind model and specifically to quantify the effects of atomic motion [62], collisions [63], closely spaced resonances [64], level degeneracy [65], crossed polarization of laser fields [65], as well as the forward phase-matching geometry [66].

The DNI methods have been validated experimentally but are computationally expensive for routine analysis of data. Often the experimental parameter of most interest is the intensity of the signal given by the reflectivity R, – the ratio of signal to probe intensity. Reichardt and Lucht have provided a semi-empirical relationship for R in terms of the relative effects of Doppler and collisional broadening given by [62]

$$R = \frac{R_{\text{hom}}}{1 + (b\Delta\omega_D / \Delta\omega_{\text{C}})^2} \tag{4.27}$$

where R_{hom} is the reflectivity calculated from the A&L model, $\Delta\omega_D$ and $\Delta\omega_{\text{C}}$ are the Doppler and collisional widths respectively. The empirical parameter b is a function of the pump and probe intensity and characterises the saturation level. This result was validated by comparison with the full DNI calculation and experimental data but is qualified by the limitations of the A&L model used to determine R_{hom}, i.e. restriction to a non-degenerate, two-level atom and a non-saturating probe.

The problem of saturation by the probe beam is one of the most important issues from a practical point of view since as noted above the signal will be optimised if the pump and

probe have equal intensities. Therefore if the pump is saturating then so will the probe and so the usual perturbative expansion of the field is no longer valid. The DNI method of Lucht et al. can be adapted to treat this problem also but the computational expense remains an issue. Alternative numerical approaches have also been developed to calculate the DFWM signals but have not found wide application for routine analysis of experimental data [67, 68]. A non-perturbative analytical solution for the DFWM signal intensity and lineshape has been derived by Bratfalean et al. that is valid for monochromatic fields of arbitrary intensity of both pump and probe [46]. The result has been validated against a full numerical solution and also used for rapid simulation of experimental DFWM spectra of molecules such as C_2 and OH [69, 70]. The analytical expression, although complicated, can be calculated on a personal computer in a matter of seconds allowing spectral fitting routines to be applied to experimental data. OH is the most widely used species for flame diagnostics and an example of a DFWM spectrum of this radical in a methane/air flame is shown in figure 3.4. The experimental data show part of the $A^2\Sigma$-$X^2\Pi(0,0)$ band of OH with a fitted theoretical spectrum calculated using the model of [46].

The requirement for high peak power mandates the use of pulsed lasers which, in practice, usually have a finite bandwidth. This invalidates the assumption of monochromatic fields and leads to significant changes to the lineshape and saturation behaviour of the signals. The finite bandwidth is associated with random fluctuations of the field and so the interaction with atoms or molecules will be affected by the precise form of the field statistics. The general problem of finite bandwidth fields of arbitrary intensity may well be intractable but approximate solutions have been derived in some limiting cases. Cooper et al. conducted a theoretical study of the case where the laser bandwidth exceeded all other relaxation rates in the interaction and the results, which involved numerical solutions, were tested experimentally to verify that the predicted saturation behaviour was observed [71, 72]. The

effect of pressure on the integrated signal intensity has also been tested using this theoretical model albeit in an intermediate regime. Nonetheless the decay of the signal induced by broadband lasers with pressure was found to agree with theoretical predictions [73].

A theoretical model for the lineshape of DFWM signals induced by broadband fields was derived by Smith and Ewart and the results verified by measurements on signals generated in flame OH [74]. Their model predicts a Voigt-type profile, dependent on the collision rate Γ, in which the collisional width is 2Γ in the collisionally dominated regime and 4Γ in the limit of dominant Doppler broadening.

A perturbative (weak field limit) method was developed by Vaccaro and co-workers which involved time domain solutions that could be evaluated analytically and therefore efficiently [75]. The non-perturbative analytical method of Bratfalean et al. [46] can be extended to treat finite bandwidth laser interactions by modelling the interaction as an independent spectral response ISR to a set of uncorrelated monochromatic components spanning the laser bandwidth. This method has been used to analyze multiplex FWM spectra induced by very broadband fields [76]. The ISR approach incorporates the contribution of non-degenerate FWM interactions but only in the limit of unsaturating intensities. Such non-degenerate signals are, in principle, inevitable with the use of broad bandwidth fields. Owing to the difficulty in treating such effects under saturation conditions they may be ignored in order to treat the more important effect of saturation which is effectively dominated by degenerate spectral components close to resonance.

Level degeneracies and polarization effects modify the standard Abrams and Lind result and need to be considered when probing molecular species by DFWM. The signal-to-noise ratio is often improved by using crossed laser polarizations in pump and probe beams. The generated signal is then orthogonally polarized to the strong pumps and so use of a crossed polarizer in the detection path leads to improved rejection of noise from scattered pump radiation. The effect on the signal is described by a J-dependent geometrical factor $G(J)$; a function of the

relative polarization and the ΔJ of the transition, which modifies the basic A&L result for both weak and strong pump fields [77, 78].

Absorption by the medium may be a problem when using strong resonance lines to enhance the DFWM signal. In particular the distortion of relative intensities of different molecular lines caused by line-centre absorption will affect values of temperature or concentration derived from the signals [79, 80]. In this case the signal no longer follows the expected quadratic dependence on number density, N. In general the treatment requires numerical calculation appropriate to the particular situation. Absorption will reduce the intensity of the incoming pump and probe leading to reduced signal generation. The effects may be compensated partially by use of saturating laser power [48, 81]. As a general rule it is advisable to use only optically thin media for quantitative measurements using DFWM. In many cases this can be achieved by simply using a transition in the molecule of interest that has a suitably low line strength yet sufficient to provide measurable signals.

Resonant four-wave mixing has found widespread application in a range of molecular physics studies including collision dynamics, kinetics and spectroscopy of jet cooled species. In the present review however we focus on the applications of relevance to combustion. We first note the range of species detected using one- and two-photon resonant processes using laser excitation in spectral ranges from the UV to the mid-IR. Secondly we review the application to measurement of combustion parameters concentration and temperature where measurements have been made in point, line and 2-D configurations. We note the two main approaches that use either narrow linewidth lasers for scanned spectroscopy or broad bandwidth sources for multiplex spectroscopy. Additionally we consider the Two-Colour FWM variant and its particular merits. A review of applications in practical combustion devices will be presented in section 9.

4.2 Molecular physics applications

The first application of resonant FWM to species of combustion interest was the detection of the OH radical in a methane air flame by Ewart and O'Leary using transitions in the A-X (0,0) band around 308 nm [50]. Since then many molecular and radical species have been detected in flames, cells or high temperature arc sources making use of the discrimination afforded by the coherent signal against flame luminescence or scattering. Important diatomic radical species OH, NH [82, 83], CH [84], CN [85] and C_2 [86, 87] were detected and used to evaluate the utility of DFWM as a diagnostic technique in flames. Stable combustion product species such as NO [88] and NO_2 [89] which are major atmospheric pollutants were also detected. Polyatomic species important in combustion such as CH_3 have been detected using DFWM on the UV absorption bands [90, 91] and CH_4, C_2H_2 and C_2H_4 have been detected on the C-H stretching modes in the mid-IR [92-95].

Quantitative analysis of the DFWM spectra required detailed understanding of the various effects outlined in the previous section which modify the behaviour from that predicted by the simple Abrams and Lind model. Such quantitative analysis in turn stimulated the drive towards higher resolution spectra and the use of narrow linewidth lasers to eliminate the effects of laser bandwidth.

Important deviations from the simple theoretical predictions include cross-over resonances that arise in the BPG and the effects of atomic motion. Moving atoms in the BPG see each pump frequency Doppler shifted in opposite directions and so a resonance occurs when the laser frequency is tuned to the mid-point between two transitions that share a common level. The moving absorber is tuned into resonance with one pump going one way and the other pump going in the opposite direction leading to an extra resonance feature in the spectra of NO [96].

Coherent interference effects also arise when two or more closely adjacent transitions contribute to the DFWM signal at a given frequency. Constructive interference leads to

enhanced signal strength above that expected on the basis of the thermal population of the initial rotational state. On the other hand destructive interference leads to dips in the intensity that appear to sharpen the resonances on some spectral features. Such features were observed in DFWM spectra of C_2 in an oxy-acetylene flame [87]. Incorporating such effects leads to better fits of theoretically modelled spectra with experimental data. Using the analytical model of Bratfalean et al. (see figure 4.2) [46] high-resolution DFWM spectra of C_2 in an oxy-acetylene flame were analysed including such coherent interference effects and probe saturation. The data provided improved accuracy in the line positions and also improved values of the molecular parameters of C_2 since high J-value states were detected which probe wider ranges of the inter-atomic potential [69]. Such spectroscopic data is important for the analysis of experimental DFWM spectra and for the accurate derivation from the spectra of combustion parameters such as temperature.

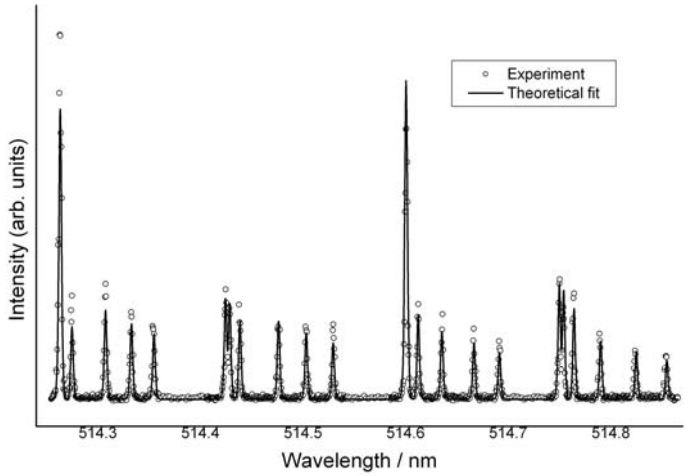

Figure 4.2: High resolution DFWM spectrum of the $d^3\Pi_g - a^3\Pi_u$ (0,0) band of C_2 in an atmospheric pressure oxy-acetylene flame recorded using a scanning narrow-bandwidth pulsed dye laser and the BPG to reduce the Doppler width of the lines. The temperature derived from this spectrum is 3009 K. (Figure reproduced with permission from reference [47].)

Single-photon resonant FWM allows access to electronic transitions in the near UV, visible and IR spectral regions. Two-photon resonant FWM however can provide access to molecular

or atomic transitions of higher energy and has been applied to detection of NH_3 [97] and atomic hydrogen [98] which play important roles in air-fed combustion chemistry. Atomic oxygen has also been detected in flames using two-photon resonant DFWM [99].

4.3 Concentration measurements and thermometry applications

In principle the absolute concentration of the resonantly interacting species in DFWM could be deduced from the measurement of the signal intensity and comparison with the theoretically predicted intensity. Due attention however must be paid to all the effects discussed previously that modify the predictions of the DFWM intensity based on the Abrams and Lind model. In many situations, notably in optically thin media with unsaturating, monochromatic probe beams signal estimates based on the Abrams and Lind model work surprisingly well. The complications encountered in practice and listed in section 4.1.2 can be accounted for in various ways. Effects of atomic motion, saturating probe beams and non-monochromatic fields are accounted for by using the appropriate theoretical model. Relaxation effects arising from de-polarizing collisions on degenerate states may also be accounted for using appropriate theoretical models and simplified by use of parallel polarization of all incident beams. Collisional effects are mitigated by operation with saturating fields and absorption effects may be avoided by using optically thin media or operating with transitions having lower line strengths.

In practice however derivation of the absolute concentration from measured signal intensities is difficult since many of the parameters required for such a direct measurement are not sufficiently well known. Relative concentrations, on the other hand, are much easier to derive from relative intensity measurements. Such relative measurements are often useful since the variation of concentration with some other parameter may provide useful information e.g. spatial distributions of radical species within a flame. Care however needs to be exercised if conditions in the flame or gas being investigated vary spatially or temporally. Variations in

temperature, Doppler and collisional widths for example may lead to differences in relative intensities that do not map the relative state populations. Attal-Tretout and co-workers measured OH concentration profiles in an oxy-acetylene flame and found good agreement between experiment and theory for laser intensities $I \sim I_{sat}$ [61]. Reichardt and Lucht have shown also that measurements in the saturated regime reduce the sensitivity of concentration measurements to the variations in Doppler and collisional width as well as laser intensity fluctuations. By careful choice of an appropriate rotational transition the DFWM reflectivity, given by the relationship in equation 4.27, can be shown to be directly proportional to the square of the concentration over a wide range of temperature [62]. Using saturated DFWM OH concentrations were measured in a well-characterised H_2-air flame for a range of fuel equivalence ratios from 0.5 to 1.5. The flame was stabilized on a Hencken burner that had been shown to produce near-adiabatic temperatures and near-equilibrium H-atom concentrations at the measurement point over a wide range of equivalence ratios. By normalizing the experimental data to calculated values at one equivalence ratio the concentrations were put on an absolute scale [81]. (see figure 4.3)

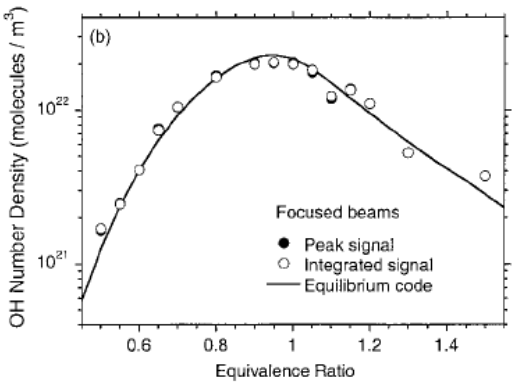

Figure 4.3: Quantitative measurement of OH number density in a H_2-air flame measured by saturated DFWM. The data points represent measurements based on peak signal intensity (solid circles) and line-integrated signals (open circles) i.e. intensity values integrated over the spectral line providing the resonance enhancement. (Figure reproduced with permission from reference [81].)

Simultaneous measurement of the DFWM signal and some other optical signal that has a different dependence on transition moments (or Einstein B-coefficient, B) and concentration, N, has been proposed as a way of eliminating unknown factors for absolute concentration measurements. The combination of DFWM which depends on B^4 and N^2 and linear absorption which depends on B and N allows the unknown parameters to be derived from multiplexed measurements [100]. Radi and co-workers have applied this method and a calibration against a signal from a known concentration to derive absolute concentrations of OH and S_2 in a flame [101, 102].

Combustion diagnostics often demands measurements of relevant parameters such as concentration and temperature over extended regions of space. The challenge is then to extend measurements at a point defined by crossed beams to 1-D (line) and 2-D (surface) measurements. Point-wise measurements were used to map the variation in atomic sodium density over a plane in a flame by moving the flame relative to the crossing point of the pump and probe beams [50]. Two-dimensional maps of relative concentration were then obtained by intersecting a circular profile probe beam with planar sheet pump beams [103]. (Details about multidimensional applications will be discussed in section 9). Concentration imaging was then extended to OH in a flame [104]. Owing to the need to use small crossing angles the images formed by DFWM are severely foreshortened. The dependence on the cube of the intensity also leads to severe variations in image brightness arising from non-uniform laser beams. Some attempt to normalize for inhomogeneous beams was made by recording simultaneously an image generated in a uniform sample in a cell [105]. The practical difficulties in obtaining and analyzing images generated by DFWM have so far limited its application for 2-D imaging of concentrations.

The potential of resonant DFWM for thermometry was demonstrated by Dreier and Rakestraw who recorded DFWM spectra of OH in a flame [106]. The temperature was derived from the relative intensities of rotational lines assumed to be in thermodynamic

equilibrium – a condition that is usually well fulfilled in atmospheric pressure flames. The method relies on the use of a Boltzmann plot as outlined above with equation 3.10 and can be used only for stable flames in which conditions do not change in the time taken to record the spectrum – typically 10 to 30 minutes using pulsed lasers at 10 Hz repetition rate. A common problem that needs to be avoided in using DFWM for thermometry is absorption which will affect stronger lines more than weak ones leading to distortion of the spectral intensity and hence error in the derived temperature. A recursion relation has been introduced to overcome this problem [80]. In practice it is best to avoid this problem by working with optically thin media or using spectral transitions that do not suffer absorption of more than a few percent.

Since temperature is an intensive, rather than an extensive variable it is important to limit the measurement volume so that it does not include regions of different temperature. This problem has been addressed in the context of CARS thermometry where measurements are sometimes biased towards lower values owing to the higher density in colder regions and the quadratic dependence on number density. It is therefore important to limit the size of the measurement volume to dimensions smaller than length scales over which the temperature may be varying. Further discussion on this issue is found in section 5. Problems arise also if temperature gradients and hence refractive index gradients occur that deviate the pump beams and so affect the size and location of the measurement volume. An early attempt to avoid such beam steering problems was made by using a phase conjugate mirror to reflect the forward pump beam in order to generate a distortion-free backward pump to maintain exact overlap of the two pumps [107, 108]. Using this arrangement temperatures were derived from DFWM spectra of OH in a flame [109]. An alternative and more easily implemented strategy that minimizes beam steering effects is to use the FPG since all beams propagate through approximately similar optical paths. Using this method temperatures were measured using DFWM of C_2 by Nyholm et al. [86].

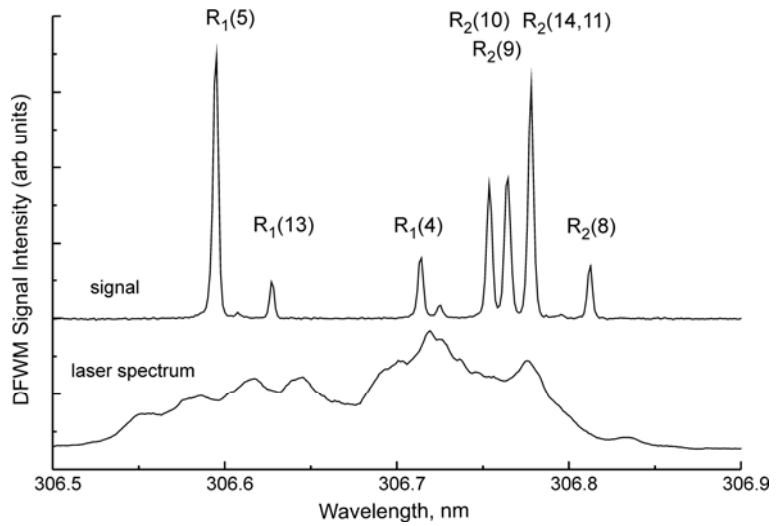

Figure 4.4: Single shot multiplex DFWM spectrum of OH in a methane/oxygen flame at 1 bar pressure. The line assignments are given to the transitions in the R-branch of the A–X (0,0) band of OH. The spectrum was recorded using a broadband modeless laser frequency-doubled by two consecutive doubling crystals. The lower graph shows the simultaneously recorded spectrum of the frequency-doubled modeless laser. (Figure reproduced with permission from reference [47].)

Temporally resolved thermometry requires that the spectral information is obtained within a single laser pulse – a result that is achieved using multiplex or broadband DFWM first demonstrated by Ewart and Snowdon [110]. The first application of broadband DFWM to thermometry used a broadband laser whose spectral width was sufficient to span several lines in OH [79]. A two-line version of the technique used a conventional laser source with a bandwidth sufficient to span two neighbouring but temperature sensitive lines of OH [111]. The accuracy of these initial measurements was limited by the difficulty of producing sufficiently wide spectral coverage of the OH spectrum since the lasers employed had to be frequency doubled to produce the necessary UV radiation. OH has a relatively open spectrum with rotational lines being widely spaced compared to many other molecules and the limited spectral width of frequency doubled broadband lasers thus presents a difficulty. It is the phase-matching requirement that limits the range of wavelengths that can be frequency doubled in a single crystal. One way of overcoming this limitation was to use a broadband modeless laser as the fundamental beam and two crystals oriented separately to double different regions of the broadband spectrum. An example of a single shot broadband OH

spectrum recorded using DFWM with an extended UV laser-spectrum obtained in this way is shown in figure 4.4.

Improved accuracy and precision was achieved by using the fundamental output of a broadband modeless laser operating in the blue spectral region to access transitions in the C_2 molecule by Kaminski et al. [112]. The use of a modeless laser also reduced the spectral noise that is a feature of conventional broadband lasers [113-115]. Accurate and precise temperature measurements of an oxy-acetylene flame were obtained since a large number of transitions were probed simultaneously. The temperature was derived by fitting a modelled multiplex-DFWM spectrum to the experimental data using temperature as the fitting parameter. As part of the fitting procedure the relative intensities of the recorded lines were scaled using the relative intensity of the broadband laser at each spectral location by reference to the simultaneously recorded laser spectrum. The intensity scaling was carried out assuming the relative intensity appropriate to unsaturated FWM signals.

Generally speaking, the larger the number of transitions that are probed the more precise and accurate the derived temperature since averaging reduces the effects of spectral noise on individual spectral components. An example of what is possible is shown in figure 4.5 showing a significant portion of the $d^3\Pi_g - a^3\Pi_u$ (0,0) band of C_2 recorded in a single shot. Care must be taken however to avoid strongly pumping transitions having a common upper or lower level. This can arise in parts of the molecular band where the Fortrat parabola brings such transitions into neighbouring spectral regions. This effect was studied experimentally and theoretically by Lloyd and Ewart who showed that the dephasing effect on the DFWM process arising from pumping by a broadband laser on coupled transitions can lead to errors in the derived temperature [116].

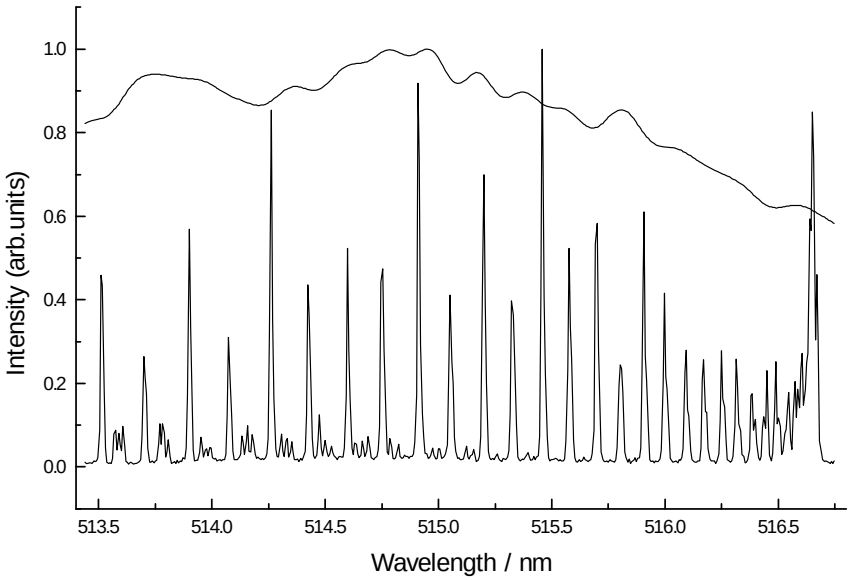

Figure 4.5: Single-shot multiplex FWM spectrum of $d^3\Pi_g - a^3\Pi_u$ (0,0) band of C_2 in an oxy-acetylene flame. The upper line shows the intensity spectrum of the broadband modeless laser used to generate the signal. Note the considerably wider spectral coverage compared to the spectrum of OH in figure 4.4 using the second harmonic of a modeless laser. (Figure reproduced with permission from reference [47]).

A useful variant of DFWM uses one laser to provide the pump and a second laser at a different wavelength to provide the probe beam. This Two-Colour Resonant Four-Wave Mixing, TC-RFWM gains some advantages over DFWM at the expense of having to use two lasers instead of one [117]. The signal is generated when transitions excited by the two different wavelengths share a common level, either upper or lower. The signal is generated only in the presence of both beams and can be used to simplify the signal analysis in spectrally congested regions. Additionally the signal is more easily discriminated using spectral filters from the strong pump beams at a different wavelength. Variations on this theme of two-colour interactions allow different schemes of double-resonance to study molecular excited states and combustion relevant species [118, 119]. Applications of TC-FWM included the detection of OH [120, 121], CH [122], NH [120, 121], C_2 [123], ammonia [124] and atomic hydrogen [98].

A major aim of combustion diagnostics is to develop methods by which relevant parameters can be measured in technical combustion systems such as engines or gas turbines. The

application of resonant FWM techniques to such technical combustors is discussed in section 9.

5 Coherent anti-Stokes Raman scattering

The birth of coherent anti-Stokes Raman scattering, CARS, is usually dated to 1965 and the observation by Maker and Terhune of "three wave mixing" in benzene induced by a pulsed ruby laser [125]. The application of this nonlinear effect to combustion diagnostics was stimulated by the observation of CARS in gases by Taran and co-workers in the early to mid 1970s. The essential features of the optical setup for generating CARS signals are illustrated in figure 5.1. Unlike the degenerate four-wave mixing schemes discussed in the previous section at least two or even three laser sources of different wavelength are required.

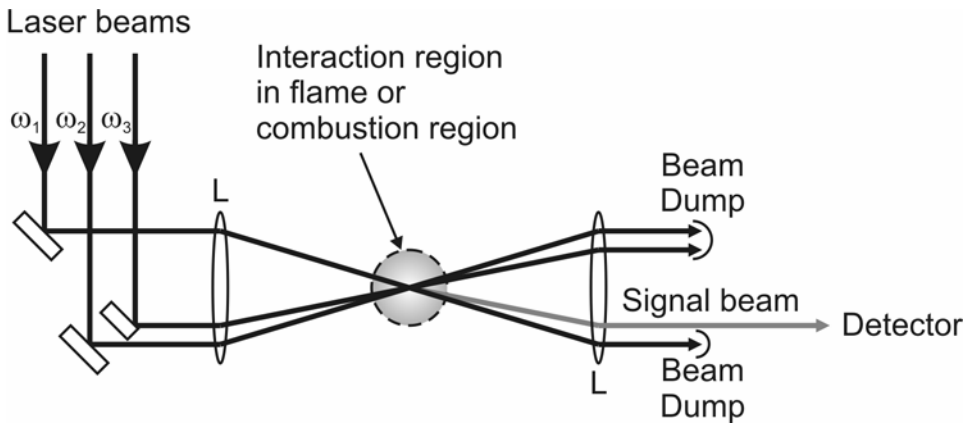

Figure 5.1: Basic optical layout for CARS.

Figure 5.2 shows the energy level diagrams of the principle configurations that are typically used. The most commonly employed form of CARS involves a two-photon resonance mediated by one photon from the pump beam and one from the Stokes beam. Owing to the low probability of such transitions signals are usually observed only from majority species. A greater range of sensitivity however can be achieved using resonant enhancement allowing the detection of minor species. The most common approach is rotational or vibrational CARS where the difference between the frequency of the pump, ω_1, and Stokes, ω_2, lasers matches a rotational or rovibrational Raman transition of the species of interest: $\omega_1 - \omega_2 = \omega_R$.

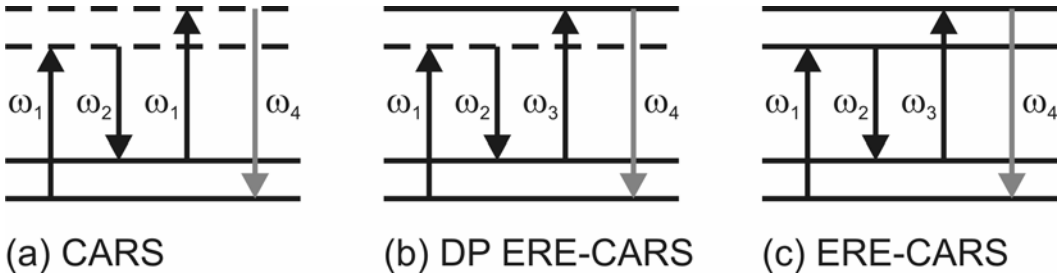

Figure 5.2: Energy level schemes of a) conventional rotational/vibrational CARS, b) electronically resonantly enhanced dual-pump CARS and c) electronically resonantly enhanced CARS.

Rotational and vibrational CARS are established tools for temperature measurements using molecular nitrogen, N_2, which is present in a high concentration in all air-fed combustion environments. In addition the detection of other major species e.g., O_2 [126], CO [127], CO_2 [128], H_2 [129], H_2O [130] and C_2H_2 [131] has been reported. Since neither the pump nor the Stokes frequencies correspond to allowed single photon transitions the excitation is achieved via a two-photon process. As mentioned before, the probability of such two-photon excitation is much lower than one-photon processes and consequently the sensitivity of the Raman process allows only major species to be detected with a minimum concentration of typically ~1%. In order to increase the sensitivity to allow minor species detection (~100 ppm) the probe laser may be tuned to an allowed electronic transition (see figure 5.2b) [132]. By taking this resonance enhancement one step further tuning all laser frequencies to electronic transitions of the molecule of interest, as illustrated in figure 5.2c, detection limits of the order of 1 ppm can be achieved [16].

Since CARS is a parametric process phase matching of the input and signal waves is necessary for efficient signal generation. Phase matching may be effected by one of several arrangements. For combustion diagnostics the most commonly employed geometrical arrangements are the planar and folded crossed beam layouts (often referred to as BOXCARS) and the unstable-resonator spatially enhanced detection (USED-CARS) which

takes advantage of the donut shaped beam from an unstable laser cavity, see figure 5.3. Each of these approaches has its peculiar advantages and disadvantages. With planar BOXCARS (fig. 5.3a) the measurement volume may be considered to be approximately a cylinder with a length typically of a few millimetres and a diameter of order of hundreds of microns. One advantage of this method is the fact that the signal wave is emitted from the intersection region in almost the same direction as one of the pump lasers and so this pump beam can be used to track the signal path to the spectrometer – which, otherwise would be difficult to discern since the weak signal is usually not visible to the naked eye. This simplifies the experiment significantly. The folded BOXCARS (fig. 5.3b) scheme in contrast provides higher spatial resolution owing to the three-dimensional beam overlapping geometry. The experimental application is, however, somewhat more difficult as the signal direction is not indicated by one of the incident laser beams. In practice then a system of apertures in masks is usually constructed to map out the positions of the three input beams (pump and Stokes). The direction of the signal beam is then indicated by apertures to guide a pilot beam (e.g. a HeNe laser) to positions calculated using the known phase matching condition for the wavelengths concerned. The USED-CARS (fig. 5.3c) approach is especially attractive for applications in technical combustion systems. In this case all the laser beams are directed into the measurement volume by the same optical components and as a consequence the alignment is comparatively easy and the setup is very stable. The spatial resolution however is slightly lower than in the BOXCARS arrangements.

Spatial resolution is an important issue in measurements of temperature using non-linear methods such as CARS where the measurement volume may contain regions of significantly different temperature. For example turbulent gases may contain unmixed hot and cold gases on the length scale of a few millimetres or the interaction region may include a flame front with burned (hot) and unburned (cold) gas. Since the CARS signal is proportional to the square of the number density the resulting signal may be dominated by contributions from

cold regions where the density is higher. This was first highlighted by Taran and co-workers [133]. In order to account for this problem Snelling and Parameswaran showed that it is important to simulate the theoretical spectrum by coherent addition of the signals from different temperature regions [134]. The identification and evaluation of such effects in experimentally recorded CARS spectra has been achieved using a weighting procedure by Seeger et al. [135].

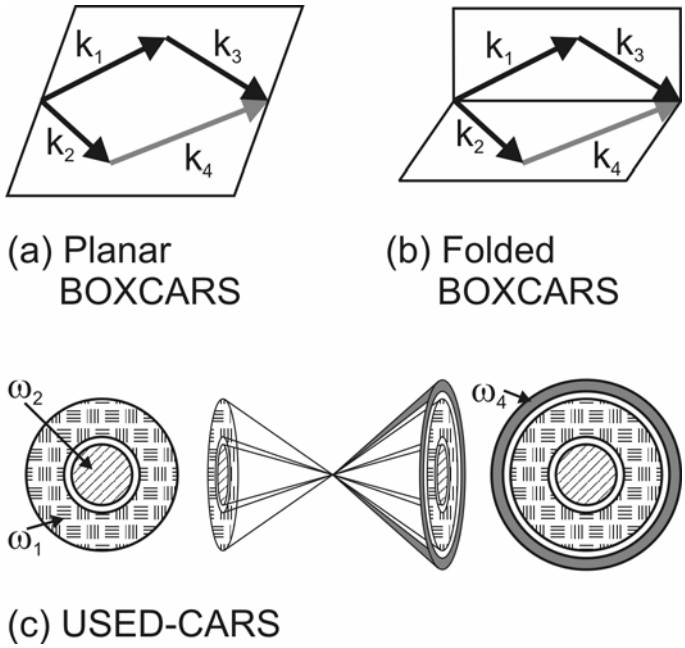

Figure 5.3: Phase matching schemes for CARS (a) planar BOXCARS, (b) folded BOXCARS. k_1 and k_3 are the wave vectors of two photons at the pump frequency ω_1 and k_2 of a photon at the Stokes frequency ω_2. The folded BOXCARS arrangement is obtained by folding the plane in figure (a) along the axis shown in (b) by an angle of 90°. The actual geometry or the arrangement is such that the beams indicated by the k_i-vectors intersect at a point. Folded BOXCARS is symmetric about the folding axis so by rotating diagram (b) through 2π the geometry of USED-CARS is obtained as shown in (c). In practice the donut shaped pump beam at ω_1 is produced by the transverse mode structure of the beam emitted by an unstable resonator.

5.1 Theory of CARS

Although electronic enhancement is necessary for realizing minor species detection using CARS the basic theory will be described for laser frequencies far away from any resonances. This simplifies the theoretical treatment significantly and illustrates the essential physics. In due course some aspects involved in resonance enhancement will be discussed. A more

detailed discussion of the CARS fundamentals can be found in Eckbreth [16] and the references therein.

The basic principles of nonlinear light-matter-interactions have been presented in chapter 3. The essential features involve the wave equation 3.2, the general equation for the polarization induced by an incoming field 3.3 and the expression for the nonlinear polarization induced by three incident monochromatic fields 3.5. Taking this as a starting point and assuming three incoming fields with frequencies ω_1 (pump), ω_2 (Stokes) and ω_3 (probe) the CARS signal is generated at $\omega_4 = \omega_1 - \omega_2 + \omega_3$. The susceptibility tensor of fourth order has, in general, 81 components. For symmetry reasons the resulting CARS polarization $P_{CARS}(\omega_4)$ can be simplified to one containing 27 individual terms. In an isotropic medium, such as a gas, there are 21 non-zero elements of which only three are independent. The relevant components of the susceptibility tensor then have the form:

$$\chi_{xxxx} = \chi_{xxyy} + \chi_{xyxy} + \chi_{xyyx} \tag{5.1}$$

where the subscripts χ_{1234} represent the Cartesian axes indicating the direction of the electric field polarization of input (1,2 and 3) and signal (4) waves with

$$\chi_{xxyy} = \frac{1}{24}(\sigma + 2a + b) \tag{5.2a}$$

$$\chi_{xyxy} = \frac{1}{24}(\sigma + 2a + b) \tag{5.2b}$$

$$\chi_{xyyx} = \frac{1}{24}(\sigma + 2b) \tag{5.2c}$$

where σ is the susceptibility's non-resonant electronic component, and a and b are the isotropic and anisotropic components of the Raman susceptibility, respectively. A detailed derivation has been presented by Owyoung [136]. Considering these equations allows calculation of the polarization state of the CARS wave and its dependence on the incident field polarization states. These relationships have been utilized to find relative orientations of the input beam polarization states to suppress either the elastically scattered laser light [137] or the non-resonant signal contributions which are usually difficult to quantify [138]. In the following however we consider the simplest situation, i.e., when the polarizations of all lasers and as a consequence the signal polarization are parallel.

Writing the electric field of a travelling wave as a harmonic oscillation of frequency ω_i

$$\vec{E}(\omega_i,\vec{r}) = \vec{E}(\omega_i)\cdot e^{i\vec{k}_i\cdot\vec{r}} \tag{5.3}$$

where $\vec{E}(\omega_i)$ is the amplitude and k_i is the wave vector and combining this definition with the wave equation and the equation for the third order polarization the resulting differential equation for the signal wave becomes

$$\frac{\partial^2 E(\omega_4,z)}{\partial z^2} + 2ik_4\cdot\frac{\partial E(\omega_4,z)}{\partial z} = -\frac{\omega_4^2}{c^2}\chi_{CARS}E(\omega_1)E^*(\omega_2)E(\omega_3)\times e^{i\Delta kz} \tag{5.4}$$

The * superscript denotes the complex conjugate, the z coordinate takes into account that the signal is generated only in a single direction due to the phase matching (see section 3) and the parameter Δk is often referred to as phase mismatch defined as (compare eq. 3.7)

$$\Delta k = k_1 - k_2 + k_3 - k_4 \tag{5.5}$$

Assuming that the phase mismatch is small allows the second order differential term in eq. 5.4 to be neglected and so the relation for the CARS signal intensity is given by

$$I_{CARS} \propto \frac{\omega_4^2}{n_1 n_2 n_3 n_4} \cdot \left|\chi_{CARS}\right|^2 \cdot I_1 I_2 I_3 \cdot l^2 \cdot \left\{\frac{\sin(\Delta k l/2)}{(\Delta k l/2)}\right\}^2 \tag{5.6}$$

where n_i are the refractive indices for the frequencies of the individual fields, I_i are the laser intensities and l is the length of the laser beam intersection region. The CARS susceptibility is usually considered as a sum of a resonant and a non-resonant contribution and the resonant one is further divided into a real and an imaginary part

$$\chi_{CARS} = \underbrace{\chi_{CARS,\mathrm{Re}} + i\chi_{CARS,\mathrm{Im}}}_{resonant} + \chi_{CARS,NR} \tag{5.7}$$

The resonant contribution contains the molecule-specific parameters and is given by

$$\chi_{CARS,resonant} \propto \frac{N_a \cdot (N_b - N_a) \cdot \left(\frac{\partial \sigma}{\partial \Omega}\right)_{Raman}}{\omega_2^4 \cdot \left(\omega_{ab}^2 - (\omega_1 - \omega_2)^2 - \frac{i}{2}\Gamma_{ab}\right)} \tag{5.8}$$

where N_a and N_b are the initial populations of the molecular energy levels involved and are related by the Boltzmann distribution, ω_{ab} is the Raman frequency i.e. the frequency difference between the energy levels involved, $\left(\frac{\partial \sigma}{\partial \Omega}\right)_{Raman}$ is the Raman scattering cross section and Γ_{ab} is the spectral width of the Raman transition. Further details of the derivation of the CARS susceptibility and signal intensity are given by Eckbreth [16]. As mentioned above the equations 5.6 and 5.8 are valid only for the case that none of the laser frequencies is in resonance with an electronic transition of a molecule. In the case of electronic resonances the treatment becomes more complicated as additional molecular parameters such as intermediate state populations, transitions strengths, linewidths and saturation effects must be

taken into account. These effects are beyond the scope of the present article and the reader is referred to the literature, see e.g. references [132, 139-141].

From equations 5.6 and 5.8 a number of implications for the practical application of CARS can be seen. Equation 5.6 involves parameters that do not depend on molecular factors. Specifically, for this case of non-resonant interaction, the signal depends linearly on each of the incident laser intensities. When, however, one or more of the lasers is tuned towards electronic transitions nonlinear enhancement and/or saturation effects may occur that alter significantly the intensity dependence. For quantitative temperature and concentration measurements these effects must be taken into account. The signal is also seen to depend quadratically on the length of the intersection region or measurement volume. This quadratic dependence on the length effectively limits the spatial resolution since the signal drops significantly when the measurement volume is reduced in length. The last factor in equation 5.6 describes the influence of the phase mismatch which leads to a sensitivity to the precision of the experimental alignment. This factor is maximal for $(\sin x/x)_{x\rightarrow 0} = 1$ i.e. when Δk tends to zero. This condition of perfect phase matching is achieved by overlapping the laser beams at the exactly correct angles to satisfy the conservation of momentum of the incident photons.
The molecular parameters are included in the resonant part of the CARS susceptibility given in equation 5.8. The numerator contains the population of the initial energy state as well as the population difference of the states involved in the two-photon Raman transition and the cross section for spontaneous Raman scattering. Simply speaking the latter is a molecule-specific quantity describing the Raman transition probability. The first two factors highlight the strong temperature dependence arising from the Boltzmann distribution of the population over the quantum states. The denominator contains the spectral parameters of the Raman transition involved. When the frequency difference of the pump and Stokes laser (ω_1-ω_2) matches the

Raman frequency ω_{ab} within the transition linewidth Γ_{ab} the denominator becomes minimal and consequently the CARS signal is maximised. In electronic resonantly enhanced CARS (ERE-CARS) the signal experiences an enhancement by several orders of magnitude as the transition probabilities for single-photon resonances are much higher compared to fully non-resonant or multiple-photon-resonant processes.

5.2 Molecular physics applications

The resonantly enhanced CARS variant where all lasers are in resonance with electronic single-photon transitions was mainly used from the late 1970s until the mid 1990s. The first application of ERE-CARS to a gas was the detection of iodine by Attal and co-workers in 1978 [142]. In the following years the technique was applied to studying combustion relevant species.

As with other optical diagnostics the OH radical was studied frequently owing to its importance in combustion and its advantageous spectroscopic properties. After first experiments by Verdieck et al. [143] pumping the OH A-X(1,0) transition, Attal-Tretout et al., comparing different experimental arrangements, studied OH produced in a discharge and an atmospheric flat flame by using resonance enhancement via the A-X(0,0) band [141]. In a follow-up work they performed measurements in premixed methane/air flames in a pressure range from 1 to nearly 10 bar [144]. They overlapped the beams of three frequency-doubled tuneable lasers in a folded BOXCARS geometry. The pump and probe lasers were tuned to the A-X(0,0) P_1 7.5 and (1,1) R_1 5.5 transitions, respectively, while the Stokes laser was scanned across the (0,1) O_1 7.5 line. It was found that pressure induced line shifts may be neglected under certain conditions. Moreover, the effects of systematically detuning the individual lasers from the exact resonant frequencies were investigated. This allowed the linewidths and lineshapes of each transition involved to be studied independently and enabled the contributions from stray light and non-resonant four-wave mixing processes to be

modelled. OH radicals were also involved in several works where resonantly enhanced CARS was compared to DFWM [60, 145] and LIF [146] measurements.

Electronic enhancement of CARS allows detection of minor species other than OH including the diatomic species C_2 [147-149], CH [150], and NO [151, 152]. Furthermore polyatomic molecules such as NO_2 [153], NH_2 [154], and C_2H_2 [155] have been investigated using this technique. Initially, CARS spectroscopy was mainly used for nitrogen thermometry and concentration measurements of major species such as reactants and products of combustion. However, more recently, the interest in using CARS for intermediate and minor species detection has experienced a kind of renaissance. In particular the dual-pump CARS approach illustrated in figure 5.2b where the probe laser wavelength is tuned to an electronic transition of the species under investigation was employed to study nitric oxide [132, 156-159] and acetylene [160]. This approach has some advantages compared to the one with three lasers in resonance. As the only requirement for the pump and Stokes laser is that their difference frequency matches a Raman transition, their wavelengths need not be in the ultraviolet (as is typically the case for exciting single-photon electronic resonances). Using visible radiation usually simplifies the experimental arrangement significantly. Moreover, in the visible spectral range broadband dye lasers are available for use as the Stokes source thus allowing single-shot multiple line measurement for time-resolved determination of concentration or temperature [159].

As mentioned above the NO molecule has been extensively studied in recent years. Following proof-of-principle experiments [156] concentration measurements were also demonstrated. A perturbative theory (i.e. for low input laser powers) and a model for calculating ERE-CARS spectra of NO was then developed [132]. In order to validate the model Kuehner et al. conducted experiments in binary mixtures of NO with the buffer gas nitrogen. The pump laser was at a fixed wavelength of 532 nm while either the Stokes or the probe laser respectively was scanned over Raman-active electronic transitions. For both approaches good agreement

was found between experimental measurements and model predictions of line positions and relative line intensities. By finding a detection limit of 100 ppm NO the application of the method to minor species was conclusively demonstrated. Following this work Patnaik et al. [161] studied collisional effects on the molecular dynamics and made a comparison with a previous investigation on quenching of NO in the presence of CO_2, O_2 and N_2 [162]. By using a density-matrix approach to model the evolution of the four-level molecular system it was shown that excited-state electronic quenching does not significantly affect the excited-state population or the ground-state Raman coherence. In addition, Roy et al. [162] showed that this model explained the observations that the ERE-CARS signal is far less sensitive to quenching than LIF under similar conditions.

5.3 Concentration measurements and thermometry applications

Quantitative information can be extracted from CARS spectra in various ways. The most common application of CARS is to measure temperature using the nitrogen molecule. The temperature is derived from fitting of experimental to theoretically calculated spectra using temperature as a fitting parameter. The same procedure can be used to determine concentration. Alternatively a calibration measurement may be made with gas samples of known composition. Such calibration methods however are not feasible for combustion intermediate radicals since they are reactive species and so it is not possible to provide stable, well-defined samples.

In general, the only requirement for performing concentration measurements with CARS is that any characteristic feature of the species of interest can be distinguished in the spectrum. This can in principle be a parameter such as the integrated line intensity, the peak amplitude or the spectral shape as long as they change sufficiently with concentration. In the case of minor species, however, the low concentration results in a resonant signal that is small relative to the non-resonant background which interferes with the spectral signature. In order

to overcome this problem two potential approaches have been developed. Firstly, the tensor nature of the susceptibility allows the dependence of the signal polarization on the polarizations of the incident laser beams to be exploited in order to suppress the non-resonant background [138, 163, 164]. A second possibility is to use short-pulse lasers in the pico-second regime and to delay the probe laser relative to the pump and Stokes pulses. Since the non-resonant contributions occur only when all laser beams are coincident they decay rapidly with increasing probe delay. The Raman coherence in contrast has a certain life-time and so the resonant signal may be generated after a suitable delay to suppress the non-resonant background [165-167]. In this case however the J-dependent collisional dephasing must be taken into account as it affects the temperature derived from time-delayed CARS spectra [168].

Without electronically resonant enhancement CARS has been used to measure concentrations of flame intermediates. This approach however provides only limited sensitivity and detection of trace species such as radicals is not possible. As a consequence, intermediates can be detected only if present in a comparatively high concentration i.e. in the order of about 1% as it is the case for carbon monoxide and hydrogen [129, 169-171]. For minor species detection i.e. when the concentration is far below 1%, the electronically resonant enhancement is necessary. Detection limits have been estimated in some of the previously mentioned work. Attal et al. [148] gave a detection limit of 10^{10} molecules/cm^3 for C_2 and a similar number was found by Doerk et al. [150] for CH radicals. At elevated pressure Attal et al. calculated a detection sensitivity of 6 ppm for OH at atmospheric pressure and 60 ppm at 10 bar [144].

Recent work by Lucht and co-workers has focused on NO and C_2H_2 measurements employing the ERE-CARS approach. Nascent NO concentrations were measured in a hydrogen/air flame and, by using polarization suppression of the non-resonant background, in a sooting acetylene/air flame, both stabilized on a Hencken burner [157]. Quantitative ERE-CARS measurements were made by calibration using NO seeded into the hydrogen/air flame. In

order to obtain sufficient signal levels down to concentrations of 50 ppm the Raman coherence was excited using 12 and 15 mJ of laser pulse energy in the pump (at 532 nm) and Stokes (at 591 nm) beams respectively. The coherence was probed with a electronically resonant UV laser pulse at 236 nm. In a follow-up study a third flame environment - a hydrogen/air counter-flow flame, was investigated in which spatially resolved NO concentrations were measured in good agreement with numerical simulations [158]. These studies used a narrowband Stokes laser necessitating scanning of the laser frequency to obtain the NO spectra. Later work, employing a broadband dye laser as Stokes source, succeeded in recording single-shot measurements which also agreed well with the predicted NO concentrations [159]. The frequency scanning method was used for acetylene detection by ERE-CARS in a nitrogen flow with small amounts of acetylene as well as in a pressure vessel [160]. At ambient conditions a detection limit of some 25 ppm was reported. The result from a calibration measurement at atmospheric pressure is displayed in fig. 5.4 showing the square root of CARS signal intensity plotted against acetylene concentration. Further experiments at elevated pressure revealed that with increasing pressure the spectral data showed increasing deviations from theoretically calculated spectra. The discrepancy may be attributed to the lack of a suitable model for collisional narrowing in the numerical code used to simulate the spectra. In some cases the quadratic dependence on number density may not be strictly observed. When the signal concerned is the integrated signal over the linewidth then pressure broadening or narrowing effects may lead to a deviation from an N^2 dependence [172]. Coherent transient signals such as those generated by shaped ultrashort pulses may also lead to deviations from N^2 behaviour [173].

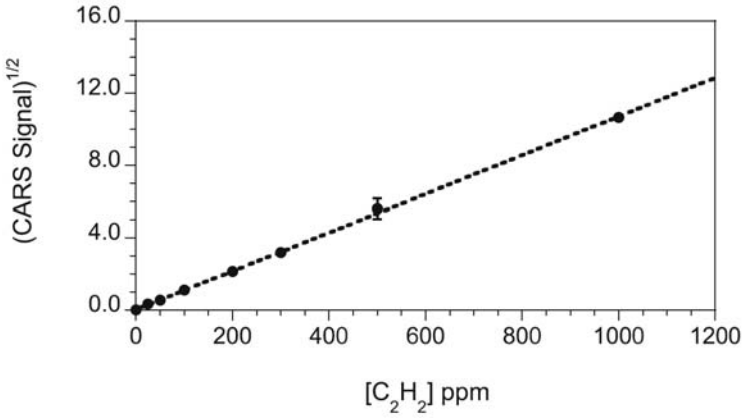

Figure 5.4: Square root of integrated C_2H_2 ERE-CARS signal as a function of C_2H_2 concentration in a jet flow at 1 atm. A typical error bar of 10% is shown at a concentration of 500 ppm. (Figure reproduced with permission from reference [160].)

6 Laser-induced grating spectroscopy

During the DFWM process, as outlined in section 3.2, collisional quenching during molecular excitation can lead to a grating induced in the bulk properties of the medium. This laser-induced grating, LIG, leads to scattering of the probe generating a "parasitic" signal [174-176]. An unsaturated DFWM signal, based on molecular excitation, dramatically decreases with increasing pressure. On the other hand the LIG signal based on quenching of the molecular excited state population increases at higher pressures and so constitutes a growing interference in high pressure situations. This new signal, since it is sensitive to bulk properties such as temperature and pressure, potentially provides a useful diagnostic technique particularly for high pressure applications. Scattering from this laser induced grating is enhanced when the pump beams are resonant with a molecular absorption and so forms the basis of a spectroscopic technique – Laser Induced Grating Spectroscopy, LIGS. The basic physics involves the generation of a grating-like modulation of the medium refractive index as a result of sudden heating and/or compression by pulsed interfering pump beams. The modulation of the density arising from the heating in the high field regions of the interference pattern leads to a thermal grating. This thermal grating consists of two components. On the one hand there is a stationary pattern of density modulation arising from the change in temperature – a "temperature grating". This arises from the heat deposition by absorption of radiation energy at the regions of high intensity in the interference pattern. Secondly, associated with this sudden density modulation an acoustic wave expands from the high field regions i.e. the antinodes of the induced grating pattern. The grating structure of the induced pattern leads to two plane acoustic waves propagating in opposite directions normal to the grating planes. The result is a standing wave oscillation (created by the adiabatic compression) superimposed on the stationary temperature grating (resulting from isobaric heating). Usually the acoustic grating and the temperature grating are of similar amplitude.

The stationary temperature grating decays exponentially owing to thermal diffusion and the acoustic waves decay exponentially by viscous damping effects. [see figure 6.1(a)] The dynamics of the grating can be detected by scattering a probe beam incident at the Bragg angle to the grating planes. Provided the probe beam is essentially constant in intensity during the lifetime of the grating the temporal variation of the scattered signal beam reveals the temporal behaviour of the laser induced grating. Typically the LIGS signal will appear as a rapidly increasing intensity followed by an oscillatory exponential decay as in figure 6.1(b).

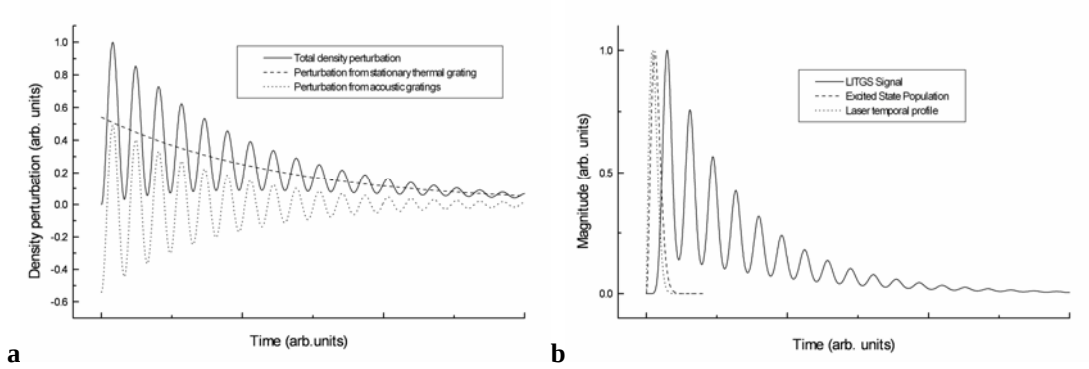

Figure 6.1: (a) Contributions to the induced grating from the stationary temperature grating – a decaying exponential (dashed line) and the perturbation from the acoustic waves (dotted line). The solid line shows the total density perturbation. (b) LIGS excitation by short laser pulse (dotted line) leading to excited molecular state population (dashed line) and the signal generated from the resulting Laser Induced Thermal Grating Scattering, LITGS (solid line).

A LIGS signal can be created even in the absence of a molecular absorption since non-resonant light, of sufficient intensity, may also modulate the refractive index by the phenomenon of electrostriction [177]. In this case acoustic waves are generated by the sudden density modulation arising from electrostriction in the antinodes of the grating pattern. In this case however the stationary temperature grating is very weak [178, 179]. Since the stationary grating is usually negligible compared to the acoustic grating the signal arising from the acoustic oscillations appear on a zero background, rather than an exponentially decaying background of similar amplitude. The result is that these signals oscillate at twice the frequency as those from absorptive or thermal gratings. In this paper we will concentrate on

resonant LIGS since it provides species selectivity as well as diagnostic potential for bulk properties such as temperature, pressure and velocity.

The experimental arrangement to realise LIGS is similar to that used for DFWM in the FPG. Since the readout of the signal arises from scattering off a bulk material property – the gas density modulation – there is no requirement for the probe to be resonant with a molecular transition. The only requirement is that the probe of wavelength λ is incident at the appropriate angle θ to the grating to satisfy the Bragg condition for scattering (see equation 3.8). A typical experimental arrangement is shown in figure 6.2. Usually the pump pulses are provided by nanosecond duration tunable lasers e.g. dye lasers excited by Q-switched Nd:YAG lasers, and a cw laser such as an Argon ion laser is used to provide the probe beam. Other experimental approaches will be detailed below but first the physics underlying the grating dynamics will be outlined to show the potential for LIGS as a quantitative diagnostic technique. It is also important to understand LIGS processes so that steps may be taken to mitigate their interference in DFWM applications. Thermal gratings have also been identified as requiring suppression in some cases of Polarization Spectroscopy [180].

LIGS based on thermal gratings arising from absorption on a molecular resonance is similar to DFWM that also arises from resonant enhancement on molecular transitions. As noted above, in a typical DFWM experiment a signal may also arise from LIGS. The DFWM signal is generated by scattering (or diffraction) off a grating composed of the spatially modulated refractive index caused by changes in the molecular state populations. This modulation in the complex refractive index is tied to the coherently driven molecular oscillations and so decays rapidly once the driving fields are turned off. The coherence decay time is usually set by dephasing collisions and is typically in the picosecond regime in gases. Thus if the third field is delayed by more than the coherence decay time then no signal will be generated. In practice, for nanosecond pump pulses DFWM signals are detectable only when the probe pulse is essentially simultaneous with the pump pulses. In the case of LIGS however the grating

responsible for the scattering or diffraction of the probe is produced in the bulk properties of the medium rather than the molecular quantum states. The decay of the grating in this case is determined by the gas dynamic properties such as thermal diffusivity and viscosity which are many orders of magnitude slower than coherence decay times. Consequently the grating induced by a LIGS process survives for timescales of the order of microseconds after the incident pump laser pulses have disappeared. Thus LIGS signals may be generated by probe beams arriving after the pump pulses up to several microseconds delay. In many applications a cw probe beam is used. A further difference between DFWM and LIGS is that in the former the pump and probe beams are of the same frequency (degenerate) since all three beams use the same molecular resonance enhancement. In the case of LIGS the only constraint on the frequency of the probe is that the wavelength meets the Bragg condition for diffraction from the grating determined by the pump wavelength and crossing angle. The use of a different wavelength probe in LIGS facilitates discrimination against scattered pump light by use of optical filters. There is also a two-colour variant of DFWM where the probe and pump beams share one common level but use resonance enhancement on different transitions. As in DFWM such signals are coherent and require pump and probe to be overlapped in time, or at least delayed by no more than the coherence decay time.

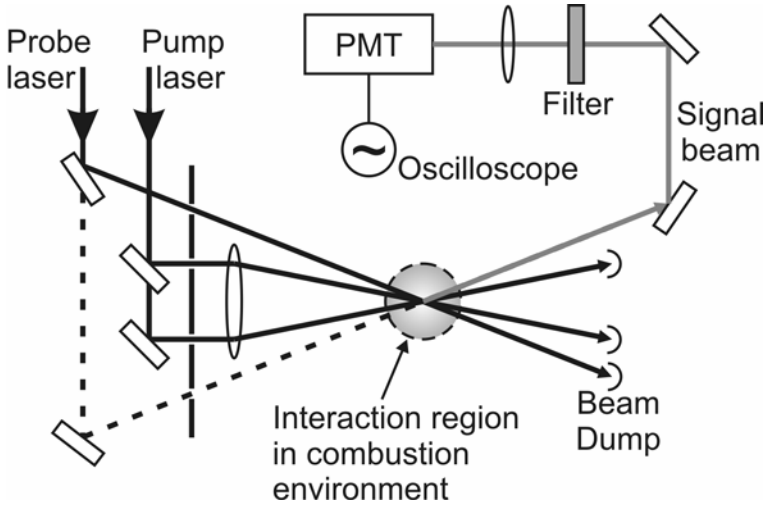

Figure 6.2: Schematic of typical experimental layout for LIGS. Part of the probe laser shown as a dotted line is used as a guide to the direction of the signal on to the photomultiplier detector PMT.

6.1 Fundamentals and theory of LIGS

6.1.1 Basic theory

The time behaviour of LIGS signals is characterised by the growth and decay of the induced gratings. In some cases the grating may be considered to appear instantaneously and so the signal shows a single sided exponential decay with superimposed, decaying, acoustic oscillations. In general however the signal is determined by the rate at which thermal energy is deposited by quenching leading to a growth in signal intensity and simultaneous decay processes which eventually reduce the signal to zero. The dynamics of the grating growth and decay have been treated theoretically by Cummings and coworkers [181, 182], by Paul et al. [175], and Hemmerling and coworkers [179, 183]. A useful introduction to the physics of laser induced gratings is given in the textbook by Eichler et al. [184]. We follow the treatment presented by Paul et al. to outline the essential theoretical method and refer the reader to the original papers for further mathematical details.

We consider the grating to be formed in the *yz*-plane by two parallel polarized plane waves of wavelength λ propagating at a small angle $\pm\theta/2$ to a symmetry axis in the *yz*-plane. The

grating fringe separation Λ is therefore given by equation 3.8. The number density of excited molecules N^* is given, under non-saturating conditions, by a rate equation:

$$\frac{\partial N^*}{\partial t} = E_P BN2[1+\cos(2\pi x/\Lambda)]g(t,\tau_L)\,f(x,d) - (A+Q)N^* + D\frac{\partial^2 N^*}{\partial x^2} \qquad (6.1)$$

where equation E_P is the total energy in each pump pulse, B is the Einstein coefficient and N is the density of absorbing molecules. $g(t,\tau_L)$ and $f(x,d)$ are the normalized temporal and spatial profiles where τ_L is the pump laser pulse duration and d the pump beam spot size in the x-direction. The terms A and Q indicate the rate of loss of excited state population density by spontaneous emission (Einstein A-coefficient) and quenching respectively. Finally, the loss of excited population density by diffusion from the excitation volume in the x-direction is given by the coefficient D. The input of thermal energy to the system from quenching is represented by a fraction ε of the absorbed energy i.e. $\varepsilon\hbar\omega_o QN^*$, where ω_o is the absorption transition frequency.

The subsequent dynamics of the grating evolution are described using a characteristic length and time to provide dimensionless units for the governing equations. The normalized units are: $\zeta(t) = \frac{t}{\tau}$ and $\xi(x) = \frac{x}{\Lambda}$, where τ is the transit time across the grating spacing $\tau = \Lambda/c_o$ for the acoustic waves travelling at the sound speed c_o. The essential physics is described by treating the grating planes as infinite in transverse extent (yz-plane) and, for typical conditions of grating spacing Λ and gas viscosity, the Reynolds number for the flow is large. Thus for such an invicid, one dimensional flow the grating evolution may be described by a set of linearized hydrodynamic equations [44]:

$$\frac{\partial \rho'}{\partial \zeta} + \frac{\partial u'}{\partial \xi} = 0 \tag{6.2}$$

$$\frac{\partial u'}{\partial \zeta} + \frac{1}{\gamma}\frac{\partial P'}{\partial \xi} - \frac{4}{3\,\mathrm{Re}}\frac{\partial^2 u'}{\partial \xi^2} = 0 \tag{6.3}$$

$$\frac{1}{\gamma}\frac{\partial P'}{\partial \zeta} - \frac{\partial \rho'}{\partial \zeta} - \frac{1}{\mathrm{Re}\cdot\mathrm{Pr}}\left(\frac{\partial^2 P'}{\partial \xi^2} - \frac{\partial^2 \rho'}{\partial \xi^2}\right) = \frac{\gamma - 1}{\gamma}\frac{\varepsilon \hbar \omega_o Q \Lambda}{c_o}\frac{N^*(\zeta,\xi)}{P_o} \tag{6.4}$$

These equations describe the evolution of the normalized density perturbation $\rho' = \Delta\rho/\rho_o$, velocity $u' = \Delta u/c_o$ and pressure $P' = \Delta P/P_o$ and involve the fluid dynamic parameters of the Reynolds number $\mathrm{Re} = c_o \Lambda \rho_o/\mu$ and Prandtl number $\mathrm{Pr} = C_p \mu/K$, where μ is the dynamic viscosity and K is the thermal conductivity. These equations are solved using a Laplace transformation under appropriate approximations notably that the problem is treated as irrotational and the source term $N^*(\zeta,\xi)$ is separable, $N^*(\zeta,\xi) = f(\zeta)\, g(\xi)$. The problem can then be reduced to a partial differential equation involving only one unknown variable. With further appropriate approximations a separable solution for the perturbation in density is found of the form $Y(\xi)\, Z(\zeta)$ which leads to a solution for the density perturbation,

$$\rho' = -(2\pi)^2 \frac{\gamma - 1}{\gamma}\frac{\hbar \omega_o B N}{P_o}\frac{8E_P}{\pi d^2} Z(\zeta)\cos(2\pi\xi) \tag{6.5}$$

This has the form of a spatially cosinusoidal modulation in density, which has an overall temporal variation in its magnitude. The temporal variation is given by

$$Z(\zeta) = \varepsilon Q \tau \int_0^{\zeta} W(y) h(\zeta - y) dy \tag{6.6}$$

$W(\zeta)$ is the function which gives the temporal response of the medium to an instantaneous input of thermal energy in the form of a volume grating. The overall temporal response $Z(\zeta)$ is simply the convolution of this instantaneous response $W(\zeta)$ with $h(\zeta)$ which is the temporal profile of the excited state population, and hence the thermal input into the medium. The medium response $W(\zeta)$ can be written as,

$$W(\zeta) = a_1 \exp(s_1 \zeta) - 2a_2 \exp(-u\zeta)\cos(v\zeta + \phi) \tag{6.7}$$

The constants a_1, s_1, a_2, u, v and ϕ are found to depend on γ, Re and Pr. From the form of this solution we see that the medium response and hence the scattered signal will have two terms. The first represents a stationary thermal grating decaying exponentially by heat conduction. The second represents two counter-propagating acoustic waves decaying due to the medium viscosity.

6.1.2 Analysis of LIGS signals, practical considerations

In order to derive values of thermodynamic parameters from experimentally recorded LIGS signals it is necessary to have a quantitative understanding of how the signals depend on the parameter to be measured. A theoretical LIGS signal can then be calculated using the model outlined above and fitted to the experimental data using the value of the unknown parameter as fitting variable. Analytical solutions for the evolution of the laser-induced grating may be found using the methods of Cummings [181] and Paul et al. [175] provided two simplifying assumptions are made. Firstly, the grating must be established in a time much shorter than the acoustic oscillation period, τ_a. Secondly, the medium must have a large Reynolds number,

Re>>1. In practice the condition for Re is usually satisfied but it can be much more difficult to ensure that the grating is produced in a time shorter than τ_a. Typical values of τ_a are in the region of tens of ns but the quenching times that determine the rate of heat deposition in the medium may exceed 100 ns. Furthermore the duration of pump pulses derived from Q-switched lasers are also on the order of τ_a. In general therefore the source function must be evaluated by a convolution of the various contributions. The source function must then be convolved with the grating decay function. When these convolutions involve arbitrary functions a numerical solution is usually required. A further problem arises from the disparate time scales of the different functions ranging over several orders of magnitude. Evaluations of such convolutions constitute a computationally stiff problem. The problem is compounded if the calculation is to be used in a fitting routine that requires rapid evaluation to achieve a best fit in a reasonable time.

One approach to the problem is to use short pulse lasers and contrive to ensure rapid quenching, for example by operating at high pressures with efficient quenching gases. Clearly this approach is not generally applicable. Another approach is to focus only on the acoustic frequency and parameters derivable from this measurement [185]. Approximate analytical solutions to specific problems have been derived by Hemmerling and Kozlov who treated the case of LIGS in pure oxygen arising from quenching of the $B^1\Sigma_g^+$ state following instantaneous excitation [186]. They considered a significant number of quenching mechanisms and channels in a complex analysis involving ~24 non-orthogonal variables related by non-trivial expressions. The results were found to be consistent with experimental observations but were obtained at some cost in analytical complexity. It is not clear that the analysis could be easily generalized. There is therefore a premium for finding a robust and efficient method of data analysis that may be generally applicable even if some compromise must be made in absolute accuracy.

An alternative to analysing LIGS signals in terms of the above theory in the time domain is to transform everything to the frequency or Fourier domain [187]. We have noted that the hydrodynamic equations were solved by Laplace transform methods and in the case of a delta-function excitation in the time domain at $\zeta(t) = 0$ the solutions using Fourier transforms are identical. By suitably redefining the limits of integration the Laplace transforms are changed to Fourier transforms and the analysis is then carried on in the Fourier or frequency domain [188]. The time dependence of the grating or grating impulse function can therefore be expressed in the Fourier domain and convolutions with the source functions involving the quenching and excitation rates can be readily evaluated. Comparison with experimental data can be carried out in the Fourier domain also by transforming the recorded LIGS signal using discrete Fourier transformation. This procedure has the great advantage that efficient FFT programs are available that allow rapid calculation of model LIGS signals and subsequent fitting using well established numerical methods [187].

The theory outlined above shows that the LIGS signal is generated by coherent scattering i.e. diffraction from the grating arising from a density perturbation $\Delta\rho'$ and its associated modulation of the refractive index Δn. The diffraction efficiency of the grating, I_{sig}/I_{probe}, is proportional to Δn^2 and so the detected signal is proportional to $(\rho')^2$ where ρ' is given by equation 6.5. From this we see that the signal is proportional to the square of the lower state population density, *N*. Thus as the pump laser is scanned across the spectrum the relative intensity of the signal will give a measure of the relative quantum state populations and so the temperature could, in principle, be derived from the LIGS spectrum. Care however needs to be exercised. The relative signal strength depends also on the quenching rate and this may vary with rotational quantum number, *J*. Fortunately the LIGS signal contains a wealth of other information from which temperature and other parameters can be derived. We consider now the parameters that may be derived from measurement of LIGS signals.

Accurate and precise temperature measurements may be made using LIGS by analysing the time behaviour of the signal. As noted above, as the acoustic waves traverse the stationary grating at the speed of sound, c_o, the LIGS signal oscillates at a frequency given by the inverse of the fringe transit time $\tau = \Lambda / c_o$. Thus if the grating spacing Λ is known the speed of sound may be derived from the oscillation frequency. Provided the composition of the gas is reasonably accurately known the sound speed may then be used to derive the temperature using the relation $c_o = \sqrt{\gamma RT / M_m}$, where M_m is the mean molecular mass. Since frequencies may be measured with considerably more precision than relative intensities, this provides a more precise measurement of temperature than scanning the LIGS spectrum [189]. The accuracy of the measurement depends on accurate knowledge of the gas composition and the thermodynamic properties of the constituents. In many cases the composition is well known or measurable and the gas dynamic properties may be obtained from the literature. The grating spacing Λ may either be measured directly or derived from a temperature measurement under calibrated conditions.

The temporal evolution and decay of the LIGS signal is described by the response function $W(\zeta)$ in equation 6.7. The exponential decay of the signal is thus determined by gas dynamic properties, γ, Re and Pr, and pressure. Therefore, again provided the gas composition is known and the associated gas dynamic parameters, the pressure may be derived from measurement of the signal decay rate. Thus LIGS provides a remote, non-contact, method to measure gas pressure.

The rate at which thermal energy is deposited in the gas is determined by the quenching rate Q. In principle therefore Q can also be derived from the temporal behaviour of the signal if other gas dynamic parameters are known. Whereas the long-time exponential decay of the

signal is sensitive to pressure it is the initial rise in the signal that is most sensitive to the quenching rate Q.

Finally we note, as mentioned above, the integrated signal intensity will be proportional to the initial molecular state population and so to the absorber concentration. We see therefore that the LIGS signal contains information on temperature, pressure, quenching rates and absorber concentration. Measurements of these parameters may be made using only a single pulse and so high temporal resolution is inherent with this LIGS technique and is set by the duration of the signal pulses. Typically LIGS signals last a few μsec which is usually a short time compared to the time scales involved in combustion. The spatial resolution is determined by the size of the interaction volume. This may not be decreased arbitrarily as the transit of the acoustic waves out of the interaction volume causes faster decay of the acoustic oscillations. Although this effect can be included in the model the reduction in the number of oscillations that can be measured limits the precision of the temperature measurement.

We have noted that the basic assumptions of the LIGS theory are often well satisfied viz. an ideal fluid with high Reynolds number and rapid grating production relative to the acoustic transit time. In general, however, the application of the theory is limited in other respects. It has been tacitly assumed that the medium is isotropic and homogeneous but this may not be the case in turbulent flames where the temperature, pressure, composition and velocity fields may not be uniform in space or time. For example steep temperature or concentration gradients may exist and so the problem may not be reducible to one-dimension nor to have solutions separable in space and time. As with DFWM saturation of the absorbing transition will also have to be considered especially with focussed pump beams. Saturation will lead to a nonlinear response and a distortion of the induced grating from a pure cosinusoidal modulation. Evidence of such distortion can be observed in Fourier transformation of the LIGS signals as higher harmonics on the fundamental acoustic frequency [188]. Other practical issues have been addressed including the effects of opacity of the medium [190],

finite grating extent [182], Gaussian beam profiles [191], and the one dimensional model has been extended to 3-dimensions [192].

6.2 Molecular physics applications

Since the physics of LIGS critically involves the quenching of molecular excited states the technique seems well suited to the study of relaxation dynamics. This was first demonstrated for gas phase studies by Hemmerling and co-workers [193, 194] and the work of this group has been reviewed some years ago [195]. The detailed analysis of the internal relaxation channels in even the relatively simple case of a diatomic molecule such as O_2 proved to be a complex matter as outlined above [186]. Binary mixtures of O_2 and CO_2 have been studied by Hubschmid [196]. Relaxation studies of C_2H_4 and NH_3 have been carried out by comparing experimental LIGS signals obtained in the infra-red using chance coincidences of molecular resonances with certain lines of a CO_2 laser with signals calculated using a simple thermalization model [197]. Similar thermalization studies using LIGS have been done on NO_2 in the visible region of the spectrum [198]. Related LIGS variants have been employed, for example, to study NO [199] and atomic hydrogen [200].

Spectroscopy of overtone transitions is a powerful means of studying the dynamics of molecules in ro-vibrational states containing substantial amounts of internal energy. Such excited states are often involved in chemical reactions and exist as reaction intermediates in combustion processes. Vibrational overtones of O-H in water vapour were studied to understand the contribution of various grating forming mechanisms [201]. Weak overtone and combination bands of methane were detected using LIGS at pressures ranging from 0.2 to 4 bar showing that the technique was capable of detecting transitions with cross-sections as low as 10^{-26} $cm^2 molecule^{-1}$ [202].

The excitation of thermal gratings in molecules has usually been achieved by single photon resonant transitions using lasers in the spectral regions ranging from the UV to the IR. In

cases where molecular excitation cannot be achieved using single photon transitions with existing laser sources two-photon or Raman pumping may be used to populate excited ro-vibrational states. Kozlov and co-workers have demonstrated such an excitation by simultaneously generating spatially overlapping grating patterns using two lasers of wavelength chosen to achieve the stimulated Raman pumping [203, 204]. By exciting transitions in the Q-branches of the $\nu_1/2\nu$ Fermi dyad in CO_2 it was possible to investigate molecular energy transfer processes. The important feature of this technique is that such vibrational excitation is not possible by conventional absorption spectroscopy. Rotational excitation by Raman pumping involves much smaller Stokes frequency differences and so can be achieved using a single broad bandwidth laser. The radiation at the pump and the Stokes frequencies are both present within the broad bandwidth laser output and so the rotational Raman excitation is achieved using only one laser. Such LIGS excitation of rotational Raman pumping has also been demonstrated for N_2, CO_2, and C_3H_8 under stationary conditions in a gas cell at pressures up to 5 bar [205].

6.3 Concentration measurements and thermometry applications

The selective detection of minor molecular species in combustion using LIGS is based on the resonant absorption of energy by tuning the pump laser to accessible electronic and ro-vibrational transitions. A range of stable species and radicals have been detected in this way including NO [118, 182], NO_2 [181, 187, 198, 206, 207], OH [175, 208, 209], H_2O [119, 201, 210, 211], and NH_3. Fuel species such as CH_4 [202], C_2H_4 [197], CH_3OH [176] and C_3H_8 [212, 213] have also been detected but in combustion situations these are usually present in relatively large concentrations. Nonetheless it may be useful to consider LIGS for detection of fuel compounds as they may be present as unburned hydrocarbons in exhaust gases. So far it has not been demonstrated that absolute concentration measurements can be reliably deduced

from measured LIGS signals without some calibration and restriction to conditions not too far removed from those of the calibration measurements.

A major motivation for detection of minor species is the measurement of temperature in flames or post-flame gases. Thermometry using LIGS has the potential for higher precision than is possible using CARS. The precision of CARS thermometry is typically limited by the noise of the recorded spectrum and the ability to accurately fit a theoretical spectrum to the data. Thus the precision is determined by errors in a measurement of *intensity*. The precision of LIGS however is determined by the errors in determining a *frequency*. Frequency measurements are typically more precise than intensity measurements. For example, precisions of single-shot CARS measurements under optimum conditions using a single-mode pump laser and modeless Stokes are of order 2-5% [115]. In comparison a single-shot precision of <0.2% has been reported using LIGS [187]. It is also worth noting that the signal analysis to derive a temperature using LIGS is much simpler than the relatively complex spectral fitting routines required for CARS. In the case of LIGS all that is needed is the measurement of the acoustic oscillation frequency, from which the speed of sound is readily calculated and hence, for known gas composition, the temperature is easily found.

Furthermore, since it is sensitive to minor species, it can also be used in flames or engines where no suitable Raman-active species is present. An early attempt to use laser-induced gratings was based on the rate of decay of a very small spaced grating written by picosecond pump pulses in atomic sodium seeded to a flame [214]. The temperature was derived from the diffusion rate of the atoms based on the Maxwell-Boltzmann distribution. As noted above, however, temperature may be derived more precisely from the measurement of the acoustic oscillation frequency of the LIGS signal provided the gas composition is known [181]. Basing the measurement on a frequency determination makes the technique relatively insensitive to intensity fluctuations. Although the potential for using LIGS for thermometry was recognised at an early stage [175, 181] initial studies focussed on elucidating the dynamics of the grating

evolution and its dependence on gas dynamic parameters. The potential for measurement of temperature and pressure was realized first by Latzel et al. [209] who recorded LIGS signals generated on the $A^2\Pi$-$X^2\Pi(0,0)$ band of OH in a high pressure flame. Values of temperature and pressure were derived from fits of theoretical simulations to the experimental LIGS signals over a range 10 to 40 bar and for different stoichiometric conditions (see figure 6.3). The values obtained were in good agreement with independent temperature measurements using N_2 CARS and predictions from a one-dimensional flame calculation. These and similar experiments by other workers used pulsed excitation by a Nd:YAG pumped dye laser and a cw Argon ion laser as the probe. Use of a cw probe limits the signal since with a total power of typically ~1 W and for gratings lasting of order 10^{-6} s only 1μJ will be available for scattering into the signal. Improved sensitivity was obtained by replacing the cw probe by a long pulse from a flashlamp-pumped dye laser having peak powers in the range of 10^6 W. [187]. Measurements on trace amounts of NO_2 in N_2 at high pressures in static cells achieved a temperature precision of 0.1%. The accuracy and precision of pressure measurement was ~2% limited by uncertainties in the published values of gas dynamic parameters for NO_2 and N_2 mixtures. LIGS thermometry in harsh combustion environments has been demonstrated by Brown and Roberts showing that the technique was feasible even in turbulent and sooting flames [215]. Hart et al. performed LIGS measurements of pressure, temperature and velocity in a supersonic air flow seeding NO_2 as a tracer species for the excitation of thermal gratings [216].

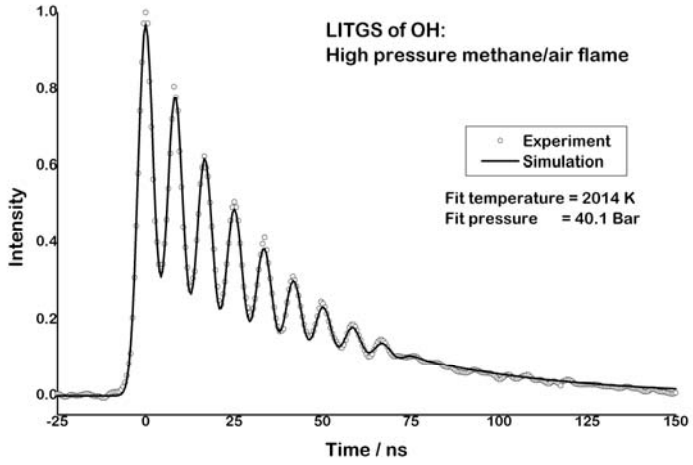

Figure 6.3: LIGS signal from OH in high pressure methane/air flame at 40 bar. The temperature derived from the fit to the data is 2014 K. (Figure reproduced with permission from reference [209].)

All of the LIGS measurements discussed so far were confined to point-like interaction volumes defined by the crossing geometry of the pump beams. Extension of the technique to measurements along a line is discussed in section 9.

To conclude, measurements on minor species using LIGS are possible because of the strong absorption presented by electronic or ro-vibrational transitions in molecules. Analysis of the signals can, in principle, yield several parameters important for combustion such as temperature, pressure as well as species concentration. The main problem in the derivation of such quantities lies in the uncertainty in gas dynamic parameters especially in gas mixtures of unknown composition. Where, however, the unknown species represent only a very small proportion of the mixture, reasonable estimates may be made.

The advantages of LIGS as a probe of minor species lie with the sensitivity arising from strong resonant absorptions. This sensitivity is also dependent on the quenching processes that transfer the energy to the thermal grating and so the signal strength often increases with increasing pressure unlike in the case of DFWM or PS. The technique thus has potential for application in high pressure combustion and engine situations. Since the probe and signal

light is at a different wavelength from the pump radiation discrimination against scattered pump light is facilitated and this provides typically high signal-to-noise ratios. The limitations of using low power cw probe lasers can potentially be overcome by using higher power pulsed lasers having sufficiently long pulse durations to span the lifetime of the induced gratings. Practical matters that need attention include the availability of short pulse lasers with sufficient energy for fast pumping of the thermal grating, intense and stable probe beams with sufficient power and good transverse beam quality to generate reliable and noise-free signals. Future applications of LIGS may involve simultaneous use of DFWM and LIGS to extend measurements over the wide pressure ranges involved in reciprocating engines. Precise and accurate measurements of species concentrations, fuel/air ratios, temperature and pressure on a cycle resolved basis can be envisaged.

7 Polarization spectroscopy

Polarization spectroscopy is similar to DFWM in many respects. The two most common optical layouts for recording PS spectra are shown in fig. 7.1. The essential item is a laser providing a linearly polarized output that is frequency tunable in the region of transitions of the species of interest. A beam splitter is used to generate a strong pump beam and a weak probe beam. Often a simple glass plate with a typical reflectivity of several percent is employed for this purpose. The pump and probe beams are made to intersect thus defining the interaction region or measurement volume. The probe beam passes through a linear polarizer before reaching the interaction region and then through a crossed polarizer, or analyzer, before reaching the detector. Since the analyzer is at 90^o to the polarizer the detector does not see any signal when the pump beam is blocked. When the pump however also passes through the interaction region optical pumping produces an optical anisotropy in the medium. The resulting birefringence and dichroism leads to a polarization rotation and ellipticity of the polarization state of the probe beam. As a result of this polarization change in the probe, part of it can pass the analyzer and reach the photo-detector. In the pump beam a half-wave plate or quarter-wave plate is inserted before it intersects the probe beam. A half-wave plate rotates the linear polarization direction so that the pump and probe are either orthogonally polarized or at 45° angle in order to optimize signal intensity. A quarter-wave plate on the other hand generates a circularly polarized pump beam. In the first case the signal of Q-branch transitions is enhanced according to the appropriate selection rules while in the second case strong signal intensities from R- and P-branches are observed.

Note that polarization spectroscopy is a form of saturation spectroscopy. However, in contrast to saturation spectroscopy, where the modulation of the absorption behaviour is detected against a large background due to the residual transmission of the probe, the signal in PS is detected against an essentially zero background. Since in PS the background is eliminated by

the crossed polarizers a significantly higher signal-to-noise ratio and thereby a much better sensitivity is obtained.

Interestingly, in contrast to the other four-wave mixing techniques, in PS only two beams need to be aligned as two photons are taken from the pump laser beam to drive the four-wave mixing interaction. This simplifies the experiment significantly since phase matching is automatically achieved at any crossing angle owing to the fact that the signal beam follows exactly the direction of the probe beam. The interaction of the pump and probe beams can be done in a forward or backward configuration as illustrated in fig. 7.1 to provide Doppler-broadened or Doppler-free signals, respectively. Depending on the spectral linewidth of the laser the signal intensity can be several orders of magnitude stronger in the forward arrangement. This can be explained by recognizing that the atoms or molecules contribute to the signal only when they "see" the pump and probe laser at the same frequency. When the beams are co-propagating the Doppler shift arising from molecular motion will be the same for both pump and probe beams. Thus all the molecules, independent of the direction they move, see the same frequency and can contribute to the signal generation. In contrast, when the beams are counter-propagating only the molecules that have a zero velocity component along both beams will experience the same light frequency. Thus only those molecules that are stationary or moving perpendicularly to both beams interact to produce a signal. When narrowband single-mode lasers are employed the signal is generated by an extremely small velocity-subgroup and consequently the signal intensity is reduced significantly.

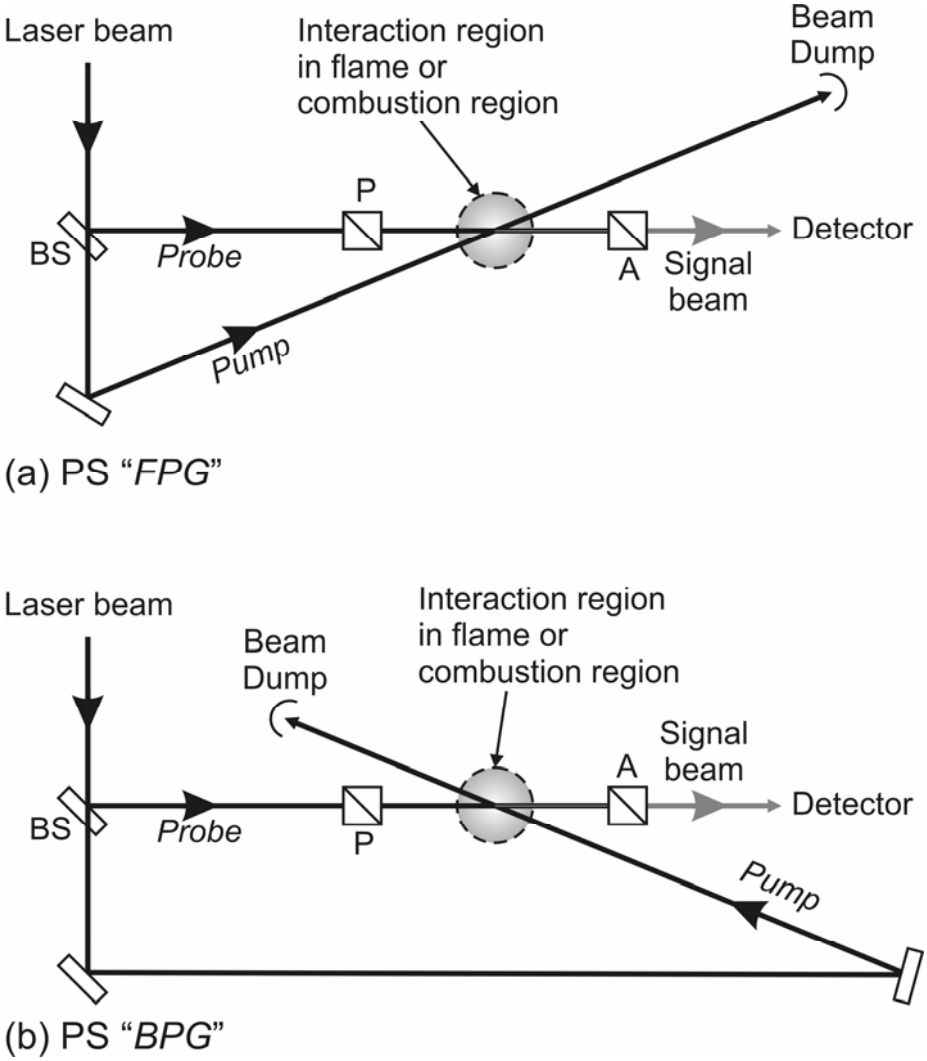

Figure 7.1: Basic optical layout for PS in (a) forward pump geometry and (b) backward pump geometry. P and A indicate the polarizer and analyzer respectively.

Polarization spectroscopy was first introduced in 1976 by Wieman and Hänsch as a sub-Doppler method, related to saturation spectroscopy, but offering a much improved signal-to-background ratio [217]. In their work the Balmer β-line of atomic hydrogen and deuterium was studied by PS in a gas cell. Subsequent studies by Hänsch's group involved Na_2 [218] and NO_2 [219] molecules. The first flame experiments were reported in 1983 by Ernst who detected flame-generated BaO and CaCl using PS [220]. In this section we present the fundamental theory of PS and review its applications for studying molecular physics of flame intermediates as well as quantitative measurements of species concentration and temperature in combustion environments.

7.1 Theory of polarization spectroscopy

The basic theory of PS has been presented in detail in several articles and textbooks, see [16, 219, 221, 222]. Therefore we give here only a brief introduction into the fundamentals in order to provide some further insights into the physics of PS. As mentioned above the pumping induces an optical anisotropy in the medium leading to birefringence and dichroism resulting in changes in the refractive index n and the absorption coefficient α. The optical properties of the anisotropic medium are now different for different polarization states of a propagating electromagnetic wave. Considering the linearly polarized probe beam mathematically as a sum of co-propagating right (superscript +) and left (superscript -) circularly polarized beams of equal intensity, and accordingly introducing the corresponding absorption coefficients α^+ and α^- and refractive indices n^+ and n^- the probe beam components can be written

$$E^+ = E_0^+ \cdot \exp\left\{i\left(\omega t - k^+ z + \tfrac{i}{2}\alpha^+ z\right)\right\} \tag{7.1}$$

and

$$E^- = E_0^- \cdot \exp\left\{i\left(\omega t - k^- z + \tfrac{i}{2}\alpha^- z\right)\right\} \tag{7.2}$$

Propagating through an intersection region with length L results in a phase difference $\Delta\phi$ between the two components

$$\Delta\phi = \left(k^+ - k^-\right)\cdot L = \frac{\omega}{c}\cdot\left(n^+ - n^-\right)\cdot L \tag{7.3}$$

as well as a difference in amplitude

$$\Delta E = \frac{E_0}{2} \cdot \left\{ \exp\left(-\tfrac{1}{2}\alpha^{+}L\right) - \exp\left(-\tfrac{1}{2}\alpha^{-}L\right) \right\} \tag{7.4}$$

For the sake of completeness it should be noted that this description has led to PS also being classified as a modulation technique [16] rather than as a four-wave mixing process.

A straightforward model to determine the PS signal intensity was developed by Teets et al. [219] and Zizak et al. [223] for the case of unsaturated or weakly saturated transitions. This model is based on a number of assumptions and simplifications. For instance, the repopulation of the initial energy state by spontaneous emission (fluorescence) and collisions (quenching) is neglected. In addition, the laser pulse duration is assumed to be shorter than the typical relaxation time of the molecules, and the lifetime of the excited state must also be short in order to not contribute to the optical anisotropy. Introducing the differences in refractive index and absorption coefficient as $\Delta n = n^{+} - n^{-}$ and $\Delta\alpha = \alpha^{+} - \alpha^{-}$, respectively, and assuming that both $\Delta n \ll 1$ and $\Delta\alpha \ll 1$, for a circularly polarized pump beam the signal intensity I_{PS} transmitted by the analyzer can be written [224]:

$$I_{PS}(\omega) = I_{pr}\left[\xi + \theta^2 + b^2 + \frac{\theta\omega L}{c} \cdot \Delta n + \frac{1}{2} bL \cdot \Delta\alpha + \left(\frac{L}{4}\right)^2 \cdot (\Delta\alpha)^2 + \left(\frac{\omega L}{2c}\right)^2 \cdot (\Delta n)^2 \right] \tag{7.5}$$

In equation 7.5 I_{pr} represents the probe laser intensity, ξ is the constant background due to the finite extinction ratio of the polarizers and θ is the angular deviation from the ideal crossing angle of the polarizers. The parameter b accounts for additional birefringence effects that may for example be caused by optical components such as cell windows between the two polarizers. A detailed discussion of such influences is given by Demtröder [222].

In practice the intensity equation can be further simplified. When open flames are investigated, which is typically the case in combustion studies, there are no additional optical components between polarizer and analyzer hence the parameter b can be neglected ($b = 0$). Furthermore,

when the alignment of the polarizers is done carefully the angular deviation θ can also be neglected ($\theta = 0$) and the intensity equation simplifies accordingly. The spectral profile of the difference in absorption coefficient can be considered as Lorentzian [217]

$$\Delta\alpha(\omega) = \frac{\Delta\alpha(\omega_0)}{1 + \left(\frac{\omega_0 - \omega}{\gamma_s/2}\right)^2} = \frac{\Delta\alpha_0}{1 + x^2} \tag{7.6}$$

where ω_0 is the centre frequency of the transition and γ_s its linewidth. The absorption coefficient α and the refractive index n and hence also $\Delta\alpha$ and Δn are related to each other via the Kramers-Kronig relation [222]

$$\Delta n(\omega) = \frac{c}{2\omega_0} \cdot \frac{x \cdot \Delta\alpha_0}{1 + x^2} \tag{7.7}$$

where x represents the term

$$x = \frac{\omega_0 - \omega}{\gamma_s/2} \tag{7.8}$$

Inserting equations 7.6 and 7.7 into the intensity equation 7.5 and neglecting b and θ we get

$$I_{PS}(\omega) \approx I_{pr}\left[\xi + \left(\frac{L \cdot \Delta\alpha_0}{4}\right)^2 \cdot \left(\frac{1}{1 + x^2}\right)^2 + \left(\frac{\omega \cdot L \cdot \Delta\alpha_0}{4\omega_0}\right)^2 \cdot \left(\frac{x}{1 + x^2}\right)^2\right] \tag{7.9}$$

which, considering only frequencies in the close vicinity of the centre transition frequency, can be further simplified to

$$I_{PS}(\omega) \approx I_{pr}\left[\xi + \left(\frac{L \cdot \Delta\alpha_0}{4}\right)^2 \cdot \frac{1}{1+x^2}\right] \tag{7.10}$$

The subscript zero identifies the individual parameters at the centre frequency. The same equation is obtained for the case of linearly polarized pump radiation. The main difference between using linearly and circularly polarized light in the pump beam is manifested in the absorption behaviour. Introducing a polarization independent absorption cross section $\sigma_{J_aJ_b}$ for the transition (J_a, M) → (J_b, M±1) the difference in absorption coefficient can be written

$$\Delta\alpha_0 = \sum_M N_a^M \left(\sigma^+_{J_aJ_b,M} - \sigma^-_{J_aJ_b,M}\right) = -\frac{N_a^J \cdot \sigma_{J_aJ_b} \cdot I_p \cdot \zeta_{J_aJ_b}}{S} \tag{7.11}$$

where $N_a{}^J$ is the population of the initial rotational level and $N_a{}^M$ corresponds to the magnetic sub-level populations. I_p is the pump laser intensity, $\zeta_{J_aJ_b}$ is a geometrical parameter taking into account the angular momenta of the energy states involved and S is a saturation parameter

$$S = \frac{\hbar \cdot \omega}{t \cdot \sigma_{J_aJ_b}} \tag{7.12}$$

where t is the pulse duration of the pump laser. The parameter $\zeta_{J_aJ_b}$ eventually defines which transitions or branches predominantly contribute to the PS signal. This is an interesting and important feature of PS in general. As already mentioned earlier circularly polarized pumping generates high signal intensities from P- and R-branches while Q-branch transitions are weak and *vice versa* for linearly polarized pumping.

In PS molecular or atomic transitions are excited resonantly thus saturation effects play an important role. In practice many experiments are conducted under saturating conditions for

several reasons. High pump pulse energy leads to high signal intensity and the effects of pulse-to-pulse intensity fluctuations are significantly reduced. When the linewidth is dominated by Doppler broadening (e.g. in high temperature flames) Reichardt et al. [221, 225] proposed simplified expressions for the signal intensity in the unsaturated regime

$$I_{PS}^{unsaturated} \propto I_p^2 \cdot I_{pr} \cdot \left(\frac{1}{\Delta\omega_D}\right)^2 \cdot \left(\frac{1}{\Delta\omega_C}\right)^4 \tag{7.13}$$

and the saturated regime

$$I_{PS}^{saturated} \propto I_{pr} \cdot \left(\frac{1}{\Delta\omega_D}\right)^2 \cdot \left(\frac{1}{\Delta\omega_C}\right)^{<1} \tag{7.14}$$

where $\Delta\omega_D$ and $\Delta\omega_C$ are the Doppler width and collisional broadening width respectively. In the saturated regime it is clear that the signal intensity is no longer dependent on the pump laser intensity. However, this approach developed by Reichardt and Lucht [221] is rather complicated as it is based on a direct numerical integration of the density matrix equations. An alternative and less complex approach to describe the saturation behaviour in situations where homogeneous line broadening effects dominate was introduced by Walewski et al. [226] and results in the following phenomenological equation

$$I_{PS} = A \cdot I_{pr} \cdot N^2 \cdot \left(\frac{I_p}{I_p + I_p^{sat}}\right)^2 \tag{7.15}$$

where A is a fitting parameter, N is the number density of the species of interest and I_p^{sat} is the transition specific saturation pump intensity. Note that I_p^{sat} is a different quantity from $I_{PS}^{saturated}$. Whereas I_p^{sat} is a fixed value for a particular spectroscopic line involving a physical

meaning, $I_{PS}^{saturated}$ is the signal intensity under saturated conditions that is detected in an experiment.

7.2 Molecular physics applications

As noted above, the first PS studies were performed in cells with the atomic or molecular gases or vapours of atomic hydrogen and deuterium [217], Na_2 [218] and NO_2 [219]. Flame generated BaO and CaCl were studied *in situ* by Ernst who obtained a remarkably good signal-to-background ratio at low laser intensity and low pressure [220]. These experiments employed continuous wave laser sources. In 1986 Zizak et al. demonstrated the applicability of a pulsed laser [223] by detecting ground-state sodium atoms seeded into a hydrogen flame. The first application of PS to natural flames species was done by Nyholm and co-workers in the 1990s studying OH radicals [224]. Suvernev et al. performed measurements of OH in methane/air and NH in ammonia/oxygen/nitrogen flames [227]. Further PS studies investigating combustion species in the ultraviolet and visible spectrum include detection of C_2 [228, 229], NO [230, 231], CH [232] using resonance enhancement on single photon transitions. Two-photon transitions were used to detect CO [233], NH_3 [233] and N_2 [234] since excitation of electronic states of these molecules requires high energy. In the same way transitions from the ground state of atomic hydrogen would also require two-photon excitation [235]. Under certain circumstances however probing H atoms via two-photon PS between the ground and first excited state may be not practicable. For this reason two groups developed approaches in which the H atoms are initially excited to the first excited electronic state and then polarization spectroscopy is applied involving magnetic sublevels of the first and third excited states [236-238]. At first glance this method is rather complicated. However, as the two-photon transition can be achieved with radiation at 243nm and the subsequent single-photon PS can be performed using a laser at 486nm, the entire six-wave mixing process

can be done employing a single laser source delivering 486nm and frequency-doubling part of the beam to 243nm.

The effect of leakage of light through the analyzing polarizer was studied by Nyholm et al. [228] for C_2 by setting a nonzero crossing angle θ (recall eq. 7.5). While Lorentzian profiles of the R- and P-branch lines under investigation could be recorded with completely crossed polarizers, slightly uncrossing them resulted in a strong contribution of dispersive line shapes hence making an interpretation of the signals difficult or even impossible. In principle, this behaviour is comparable to the interference of resonant and non-resonant signals in CARS which leads to highly non-symmetric line profiles. A more systematic and theoretical study of this phenomenon was performed by Reichardt and Lucht [221] who calculated line profiles employing direct numerical integration of the density matrix equations. Their results reveal that a very small misalignment of the analyzer in the order of 0.1° can exert a strong influence on the line shape (see fig 7.2) and as a consequence affect the measurement.

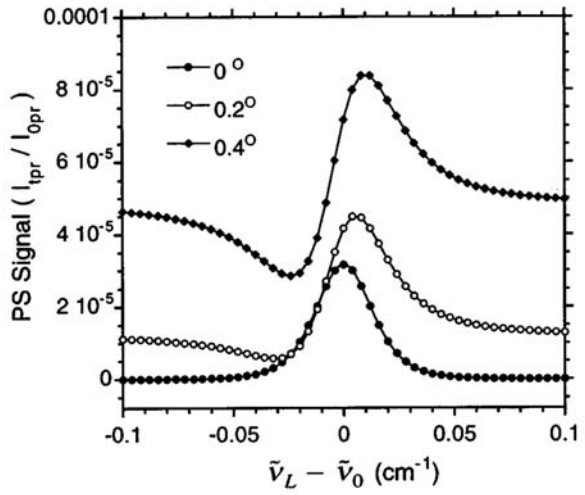

Figure 7.2: Calculated polarization spectroscopy line shapes for the R(4) resonance transition for three different values of the polarizer angle θ and pump beam intensity $I_1 = 10^7$ W/m^2 and homogeneous linewidth $\Delta\tilde{\nu}_H$ = 0.053 cm^{-1}. The number density n^0_1 of the ground level is 2×10^{10} m^{-3} and the spontaneous emission coefficient $A_{21} = 10^6$ s^{-1}. The absorption path length L is 5.0 mm. (Figure reproduced with permission from reference [221].)

Contemplating the above list of species, which have been studied by PS in the ultraviolet and visible spectral region, one might notice that a large number of important flame species is missing. Almost all hydrocarbons as well as the main combustion products water and carbon dioxide do not provide electronic transitions suitable for laser diagnostics at all. Needless to say, knowledge of these species is still of utmost importance for understanding combustion processes. In order to overcome this problem PS was extended to the mid-infrared spectral range, i.e. 1.5-5µm, where rovibrational modes can be probed. This development was made possible by the continuous progress in laser design in this spectral region in recent years. The first application of infrared polarization spectroscopy, IRPS, was demonstrated by Roy et al. in 2002 studying the 2.7µm band of CO_2 [239]. Carbon dioxide was also investigated by Alwahabi et al. [240-243] who studied line-broadening, saturation and vibrational relaxation effects. As an example, the determination of collisional induced line-broadening coefficients of carbon dioxide [242] is illustrated in fig 7.3. To do this, high-resolution PS spectra were recorded in binary CO_2-argon and CO_2-helium mixtures under non-saturating conditions. The radiation at 2µm wavelength was generated by frequency shifting the output from a single-longitudinal mode alexandrite laser yielding an estimated spectral resolution below 300 MHz. Li et al. conducted the first flame experiments in this spectral region by detecting nascent CO_2 and H_2O at atmospheric pressure [244]. Further work on OH and H_2O at high pressure investigated the problem of interferences from these species when detecting minor species in this region of the infra-red spectrum [245].

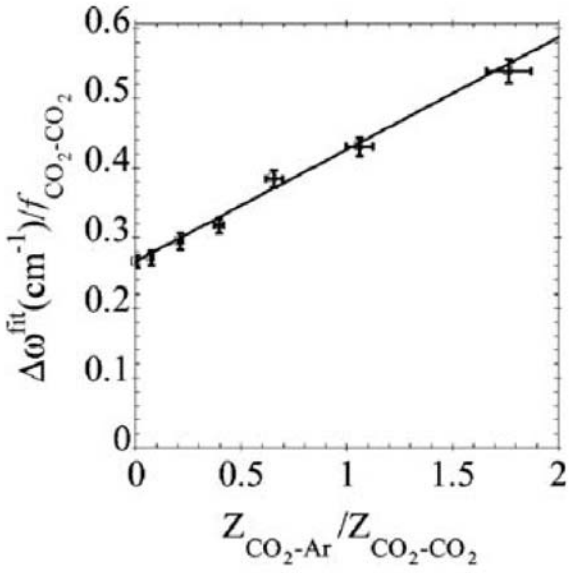

Figure 7.3: Plot of the pressure broadened fitting parameter for CO_2, $\Delta\omega_{CO2\text{-}Ar}$, versus the ratio of $Z_{CO2\text{-}CO2}$ over $Z_{CO2\text{-}Ar}$. The vertical error bars are three times the error values reported by the curve fitting routine. Based on 1% error in the flow meters, the horizontal error bars represent three times the calculated error values of the quantity $Z_{CO2\text{-}Ar}/Z_{CO2\text{-}CO2}$. The weighted least squares linear fitting is presented by the solid line. (Figure reproduced with permission from reference [242].)

In general strong interferences from the thermal emission in flame environments would be expected to hinder the application of optical diagnostics in the infrared. The coherent nature of the four-wave mixing process, however, provides excellent discrimination against such background noise.

IRPS has also been applied to detection of hydrocarbon molecules which are often referred to as dark species since they have no absorption spectra in the visible or UV spectral regions. Such species are however of great interest not only as fuels but as intermediates during the decomposition of fuel molecules as well as the formation of polycyclic aromatic compounds which are precursors of soot. Typically the stretching modes of CH moieties, which occur around 3000cm^{-1} (~3.3μm), are studied. The simplest hydrocarbon methane was investigated by Li et al. [246, 247] and Richard and Ewart [92]. Furthermore, Li et al. performed experiments to study buffer gas influences on the PS signal level of ethane [247] and acetylene [248]. Their results reveal that the quenching rates for different buffer gases are of similar magnitude, which is a big difference to PS in the UV where the quenching cross-

sections can vary orders of magnitude for different species. In a recent letter Li et al. demonstrated the application of IRPS to detect nascent HCl in a $CH_4/O_2/Ar$ flat flame where a small amount of chloroform was seeded into the Ar flow [249].

7.3 Concentration measurements and thermometry applications

Polarization spectroscopy has also been used to determine temperatures and the spatial distribution and concentration of minor species in flames. C_2 was detected in an acetylene/oxygen flame using the Swan band system at 516.5nm with an estimated detection sensitivity of $10^{18}m^{-3}$ [228]. For comparison a detection limit of 25ppm was estimated for OH at flame temperatures [224]. Mid-IR lasers were used by Li and co-workers for probing rovibrational transitions to obtain quantitative measurements of hydrocarbons [247, 248]. They reported detections limits of 50 ppm for ethane and 30 ppm for acetylene at atmospheric pressure. The acetylene calibration measurement is illustrated in fig 7.4 showing also the raw PS signals in the low concentration regime. In a recent work they have demonstrated quantitative acetylene detection in a series of ethylene/air flames after calibration of the experiment in C_2H_2/N_2 mixtures [250].

Most applications of coherent techniques provide only point measurements since the measurement volume is defined by the crossing point of several laser beams. In contrast to other four-wave mixing methods PS and DFWM can be extended to planar measurements allowing the instantaneous visualization of two-dimensional species distributions with reasonable spatial resolution [251]. This has been done by a number of groups for OH [252, 253], C_2 [229] and H [238]. Details will be discussed in section 9.

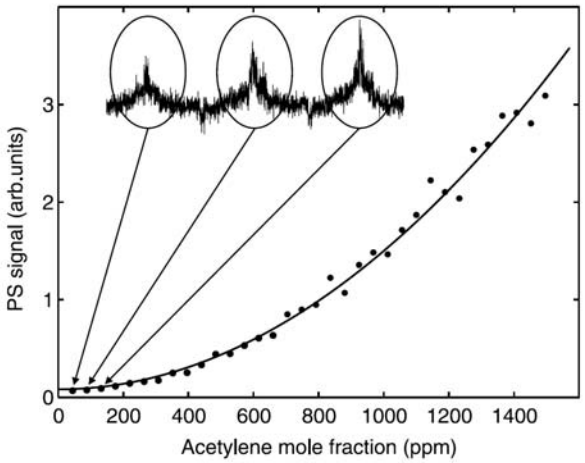

Figure 7.4: IRPS signal intensity as a function of acetylene concentrations obtained at atmospheric pressure. The dots represent the line-integrated signal intensity and the solid curve represents a quadratic dependence fit. The inset shows the raw IRPS excitation scan spectra of the last three data points of the lowest acetylene concentrations adopted in the measurement. (Figure reproduced with permission from reference [248].)

PS thermometry has in most cases been performed utilizing the A-X(0,0) band of OH around 308nm, e.g., by Nyholm et al. [254]. Since OH has a relatively long life-time it can be found in a wide region of most flames hence the OH temperature can be measured in many locations. The usual method of deriving the temperature from a PS spectrum is to use a Boltzmann plot. A logarithmic plot of the relative intensities of different lines, which indicate the initial quantum state populations, are plotted against the energy of the initial state and the slope of the resulting graph delivers the temperature assuming the populations are in Boltzmann equilibrium as previously shown for DFWM in fig. 3.5. A related technique employs the signal intensities of only two lines determining temperature from the intensity ratio [255]. However, a careful selection of the pair of transitions is required in order to obtain reasonable temperature sensitivity. Suvernev and co-workers [227] showed that it is also possible to determine the temperature by fitting theoretically calculated spectra to the experimental ones as it is commonly done in CARS thermometry. Kiefer et al. [255] demonstrated that it is not even necessary to perform theoretical calculations of PS spectra. They utilized the freely available software tool LIFBASE [256] to simulate a library of DFWM spectra which were subsequently compared to the experimental PS spectra of the OH A-X(1,0) band. This rather

pragmatic method yielded temperature data that were found to be in good agreement with results from simultaneous laser-induced fluorescence measurements. In addition, the authors evaluated temperature information using the two-line method in order to get a temperature profile in a laminar slot burner flame, see fig 7.5. A third approach derives the temperature from the spectral shape i.e. from the degree of Doppler broadening. The accuracy of this method is limited however since it is important that the laser linewidth is much narrower than the Doppler width being measured. If the laser linewidth is not sufficiently narrow then it becomes difficult, especially in the presence of noise on the signal, to determine accurately the spectral lineshape which is a convolution of Doppler, collisional and natural lineshapes.

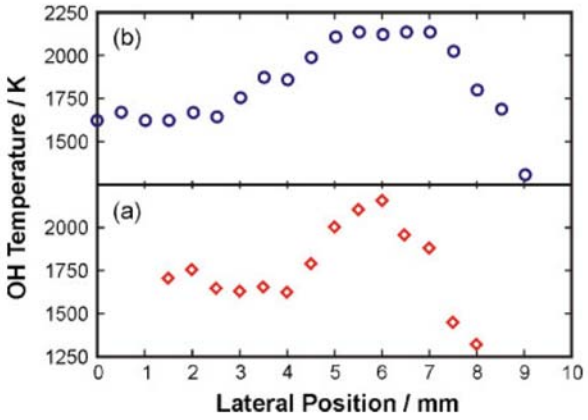

Figure 7.5: OH temperature profiles from the Wolfhard–Parker burner determined by the two-line-method using PS signals: (a) 3-mm height and (b) 12-mm height above the burner exit. (Figure reproduced with permission from reference [255].)

All the thermometry based on PS mentioned above used spectra obtained by frequency-scanning narrowband lasers. Since this procedure takes some time the method is applicable only in steady laminar flames. In order to achieve temporally resolved measurements the full spectral information must be gathered within a single laser shot. One possibility is to perform multiplex spectroscopy in which many transitions are recorded simultaneously using a broadband laser source. The resulting PS signal is dispersed and recorded using a high-resolution spectrometer. This technique was demonstrated by New et al. [257] for OH

thermometry using a broadband modeless dye laser [113]. Another interesting approach was developed by Nyholm et al. using a dual-wavelength laser [258]. In the beam of a broadband dye laser two separate birefringent crystals were placed achieving phase-matching for the second harmonic generation for two different wavelengths. The resulting ultraviolet radiation was used to do two-dimensional temperature measurements by simultaneously probing the $Q_1(2)$ and $Q_1(9)$ lines of OH. In order to separate the individual signals from each other a diffraction grating was employed projecting both wavelengths onto separate regions of a camera chip.

8 Other techniques

The previous chapters have described the four-wave mixing techniques which have been most often used for combustion diagnostics. These techniques have typically used a resonant enhancement of the nonlinear susceptibility by tuning the frequency of the incident laser fields to a molecular transition. A further FWM approach which is also suited for minor species detection in flames employs non-resonant pump beams in combination with a probe laser that is tuned to a resonance in the species of interest (see fig. 8.1). This method is similar to the resonant two-colour FWM described in chapter 4, but in this case the pumping process induces electrostrictive gratings instead of a population grating. As a consequence this technique suffers less from saturation effects than fully resonant methods. This approach has been demonstrated firstly by Lee et al. [259] who utilized a broadband probe laser for multiplex C_2 spectroscopy allowing single-shot thermometry in a premixed acetylene/oxygen flame. The spectrum recorded using the C_2 Swan band spectrum around 512 nm is shown in fig 8.2 together with the saturation curves of the line at 510.5 nm. The individual lines are well resolved which is advantageous for thermometry. Sun et al. [260] used the same technique with a tunable narrowband laser to scan the spectrum of OH with high resolution. They studied saturation and coherence effects using the second-harmonic radiation of a conventional multimode Nd:YAG laser as pump source.

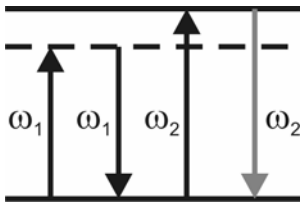

Figure 8.1: Energy level diagram of the non-resonant pump four-wave mixing technique.

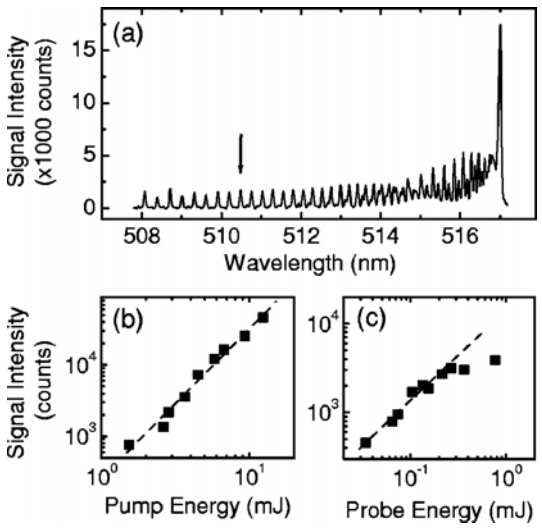

Figure 8.2: (a) NRP-FWM spectrum for the Swan band of the C_2 molecules in an oxy–acetylene flame. (b) Quadratic dependence of the signal on the pump pulse energy at 510.5 nm (dashed line: Logarithmic plot of slop 2.1). (c) The signal dependence on the probe pulse energy at 510.5 nm (dashed line: Logarithmic plot of slope 1.04). (Figure reproduced with permission from reference [259].)

In most cases four-wave mixing experiments are conducted using nanosecond pulsed lasers. Nanosecond time resolution is usually sufficient for studying macroscopic aspects of combusting flows. Molecular behaviour can also be investigated in the frequency domain when for instance line broadening delivers information about collisions. The molecular dynamics involved in collision broadening however occur on picosecond timescales or shorter. Therefore in order to either study molecular relaxation or dephasing in the time domain or to avoid influences from collisional processes ultra-short laser pulses in the pico- or femto-second range are required. In a typical time-resolved four-wave mixing experiment the molecules are pumped into a certain state and its evolution is probed as a function of time delay. Such "pump-probe experiments" are capable of resolving the temporal evolution of the coherences induced by the pump fields. This principle is illustrated in Fig. 8.3 taking the CARS process as an example. The simultaneous pump and Stokes laser pulses ω_1 respectively ω_2 excite the Raman coherence as a first step ($\tau = 0$). As a function of the time-delay $\Delta\tau$ between the pump process and probe laser pulse the temporal evolution of the Raman coherence can be observed. One particular advantage of delaying the probe pulse in four-

wave mixing is that the non-resonant background which complicates the interpretation of CARS signals is suppressed. The main reason for this is that the lifetime of the "virtual" states involved in non-resonant FWM decay on a timescale of $1/\Delta\omega$, where $\Delta\omega$ is the detuning of the pump laser from the nearest resonance. This is a consequence of Heisenberg's uncertainty principle. Therefore non-resonant signals are observed only when all input beam are coincident. The resonant signal however is detectable within the lifetime of the resonantly excited coherence which typically exceeds the duration of ultra-short pulses.

Another consequence of the Uncertainty Principle is that as pulse durations are decreased the spectral bandwidth increases. As a result the spectral width required to produce femtosecond pulses is much broader than the linewidth of atomic or molecular transitions leading to a loss of spectral resolution and the ability to selectively excite particular quantum states. It is possible however to use pulses of 10 – 100 picosecond duration which have a sufficiently narrow bandwidth to allow spectral plus time resolution of vibrational and even pure rotational CARS [166, 261]. Very recently, a hybrid approach employed for dual-broadband vibrational CARS utilized femtosecond pulses for the pump and Stokes beams and a picosecond probe beam [262]. This method takes advantage of the broad bandwidth of the fs pulses for multiplex spectroscopy, and at the same time it overcomes the problem of mode fluctuations that are typically associated with conventional broadband sources such as dye lasers. As mentioned above, the picosecond probe pulse is relatively narrow to allow signal detection in the frequency domain. Alternatively experiments in the growing field of coherent control have shown that using femtosecond pulses appropriately shaped in spectral intensity and phase can be used to selectively excite particular rotation-vibration modes in molecules [263, 264].

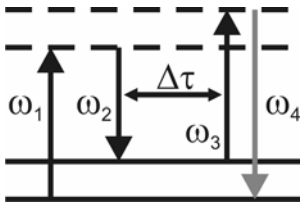

Figure 8.3: Energy level diagram of time-resolved CARS.

Nitrogen CARS thermometry is nowadays often realized using pico- or femtosecond lasers to take advantage of the non-resonant background suppression. Details can be found in the recent reviews by Gord et al. [265] and Roy et al. [266]. An interesting development that exploits the coherence excited by ultra-short pulses is the ability to isolate individual Raman modes by temporal/spectral shaping of the laser pulses. Motzkus and others have shown that such quantum coherence control may be used to identify particular species by means of their Raman signature using femtosecond CARS for the study of reaction dynamics [267]. Of particular interest to combustion diagnostics is the possibility of using the temperature effects on the coherent dynamics for thermometry [268]. Coherent states induced by femtosecond pulses in Raman induced polarization spectroscopy may lead to transient alignments of molecules that can be probed by time-delayed pulses. These alignments are observed as recurrences having a time period determined by the moments of inertia of the rotating molecules and are very sensitive to temperature.

The application of short-pulse lasers to resonant four-wave mixing has taken various forms. Dreizler et al. [269] studied orientational relaxation of OH radicals in an atmospheric pressure flame using picosecond polarization spectroscopy in the A-X (0,0) band. Their measurements allowed the simultaneous determination of different line broadening parameters which are required for accurate modelling of the molecular physics. Suvernev et al. [270] conducted picosecond time-resolved DFWM and PS experiments of OH in premixed methane/air and hydrogen/oxygen flames in order to study the dependence of the signal intensities on the polarization configurations of the incident laser beams. A comparison of the experimental

results with theoretically calculated data showed good agreement. The investigation of collisional effects and a theoretical treatment of picosecond polarization spectroscopy was reported by Lucht et al. [271, 272]. They showed that, when the laser pulse duration is significantly shorter than collisional time-scales, the PS signal is in principle relatively unaffected by collisions in the saturated regime in particular. OH radicals were also studied using a two-colour double-resonance FWM approach using picosecond pulses by Chen and Settersten [273]. After pumping rovibrational transitions in the mid-infrared spectral range the molecules were probed through electronic transitions in the ultraviolet spectrum. Measuring the temporal decay of laser-induced population, alignment and orientation allowed a detailed investigation of collisional effects on the electronic ground state.

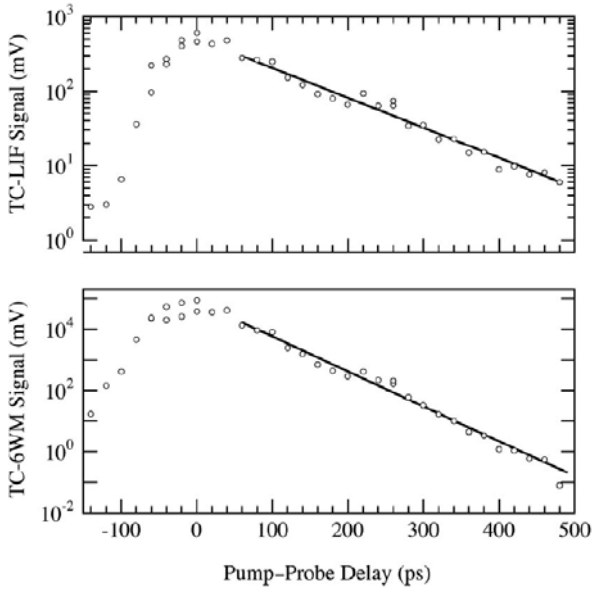

Figure 8.4: TC-6WM and TC-LIF signals as a function of the delay between pump and probe pulses. Single-exponential fits to the data in the tails of the decay are shown as solid lines. (Figure reproduced with permission from reference [237].)

A two-colour approach for PS and two-dimensional applications has already been mentioned for detecting atomic hydrogen [236, 238]. In this method two-photon excitation of hydrogen atoms from the ground state to the first excited state was followed by the four-wave mixing process of PS to access different higher excited states. As six photons are involved this

method can also be considered as six-wave mixing. Kulatilaka et al. [237] employed picosecond lasers to perform time-resolved 6WM and fluorescence measurements of H atoms for studying collisional effects. Figure 8.4 shows the recorded signals as a function of pump-probe delay. A delay of 0 ps means a temporal overlap of the pump and probe pulses as described above for CARS. The measured LIF decay time yields the upper state population lifetime while the nonlinear PS technique delivers information about the coherence life time.

9 Practical considerations, applications and fields under development

In the previous sections the underlying physics of resonant four-wave mixing and the most important techniques based on these processes have been presented. Applications of these methods have been described that focus mostly on molecular physics and the measurement of combustion relevant parameters of temperature and species concentration at a single point in either laminar laboratory flames or static gas cells. In this section extension of these techniques to multiple dimensions and multiple species measurements is outlined together with a discussion of applications in practical combustors such as engines.

9.1 Multidimensional applications

A typical four-wave mixing interaction involves the intersection of three laser beams at a point and at the appropriate angles to satisfy phase matching conditions. The “intersection point” is more exactly a finite volume which may be considered as a cylinder that can be determined precisely by focal-plane imaging techniques [274] in combination with a computational data analysis [275]. Such point-wise measurements however limit the applications to either stationary systems such as laminar flames and gas cells or to the determination of local statistics in turbulent environments. When practical combustion systems are investigated the measurement of spatially and temporally correlated data is usually required.

Initial attempts to extend CARS measurements to 1-dimension i.e. along a line met with limited success. The measurement line was defined by the intersection of co-planar pumps one of which was formed into a sheet. The Stokes beam then intersected this line at a small angle to the plane of the pumps resulting in a weak sheet-like signal beam emitted out of the plane [276].

More typically four-wave mixing measurements along a one-dimensional line require the three exciting laser beams to be formed into parallel light sheets and overlapped by a

cylindrical lens as illustrated in fig. 9.1. In the figure the signal is generated along the x-axis and imaged onto a camera chip or the entrance slit of a spectrograph. Jonuscheit et al. [277] demonstrated this approach for nitrogen thermometry using vibrational CARS. In their experiments however the spatial resolution was limited since imaging optics were not employed to direct the signal onto the spectrograph entrance slit. In general even when phase matching imposes a directional property on the signal beam imaging optics are required to form a spatially resolved image as described by Smith and Ewart [105].

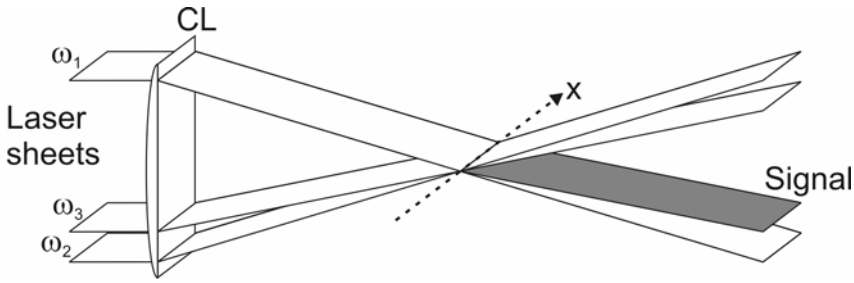

Figure 9.1: Four-wave mixing scheme for one-dimensional applications along the x-axis by overlapping laser sheets through a cylindrical lens, CL.

1-D measurements of temperature and pressure along a line in NO_2/N_2 mixtures over a range of pressures in a cell were achieved by Stevens and Ewart using time-resolved laser-induced thermal gratings [278]. The signal was produced using ns-duration pump pulses from a frequency-doubled Nd:YAG laser and a 1μs probe pulse from a flashlamp-pumped dye laser. A line like interaction region was achieved by intersecting two sheet-like pump beams in the manner shown in figure 9.1. The probe light scattered off this line was recorded on a streak camera which provided a space-resolved measurement of the temporal oscillations of the signal from each point on the line as shown in figure 9.2. Temperatures and pressures were obtained with precisions of the order of 0.5% and 20% respectively with time resolution of ~1μs and spatial resolution of 150μm along the line. The reduced precision in the pressure measurement arose in this case from the limited time range that could be measured using the

available streak camera and so the full exponential decay of the signals could not be recorded on a single shot.

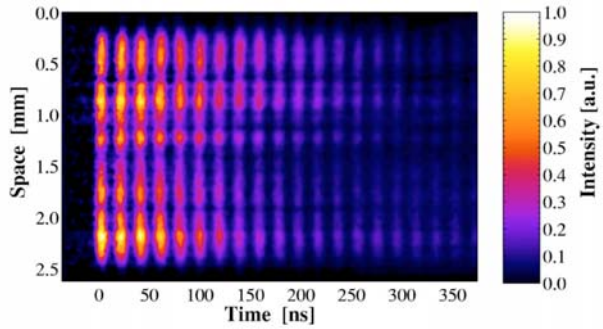

Figure 9.2: Spatially resolved LIGS signal from a line in a NO_2/N_2 mixture recorded on a streak camera with a time-base of 100 ns. The image is a composite of five single-shot LIGS signals obtained from five separate images at increasing delay. (Figure reproduced with permission from reference [278].)

The realisation of two-dimensional four-wave mixing is in principle more complicated as instantaneous phase-matching is required in an entire plane. This can be a problem when multi-colour techniques like CARS are used since up to three lasers must interact with the molecules of interest. For degenerate methods such as PS and DFWM this is not the case as multiple photons for the four-wave mixing process can be taken from one laser beam. Figure 9.3 illustrates a possibility for 2D experiments using PS and DFWM. The pump beam is formed to a thin laser sheet while the probe beam is a collimated beam extended in diameter. The measurement plane is defined by the pump sheet and the area by the cross-section of the probe beam. In the case of DFWM the pump photons may be provided by counter-propagating laser sheets.

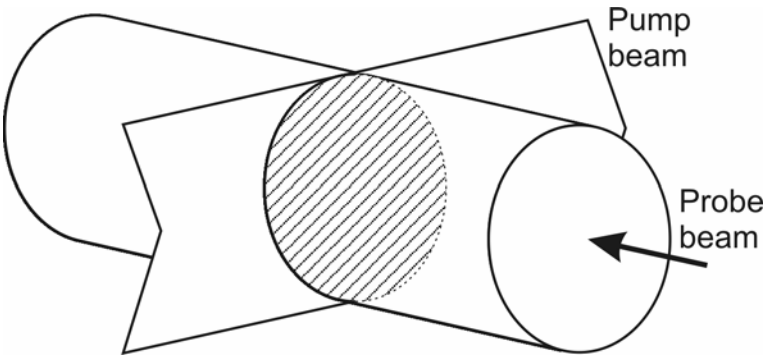

Figure 9.3: Scheme for orthogonal planar PS and DFWM. The measurement plane is indicated.

Two-dimensional imaging using DFWM was performed for the first time by Ewart et al. [103]. The principle was demonstrated by seeding NaCl to a laminar slot burner flame in order to image the resulting Na atom distribution. Rakestraw et al. [104] extended this technique to the natural flame species OH. Mann et al. [89] detected NO_2 in both flames and non-reacting environments in cold flows and inside a static glass cell. Under flame conditions they reported detection of NO_2 at concentrations as low as 7000 ppm with a spatial resolution of 150 μm in a single-shot measurement. As mentioned above the imaging process was discussed by Ewart et al. [105] to account for diffraction effects and spatial resolution. Imaging of OH and NO in flows was reported together with an image referencing method to compensate for structure on the images arising from beam and laser sheet inhomogeneities. Similar to the DFWM approach Hemmerling and Stampanoni-Panariello employed 2D electrostrictive LIGS to image a helium flow in ambient air as well as a sooting flame [279].

In 1993 imaging using PS was demonstrated for the first time by Nyholm et al. [252] who recorded 2D images of flame OH. Löfstedt and Aldén [230] also demonstrated 2D detection of OH and NO. In both works the pump laser sheet and the probe beam were overlapped at relatively small angles which leads to foreshortening of the image and limited spatial resolution. The optimal spatial resolution is obtained when pump and probe laser intercept orthogonally as described by Reppel [251]. Further planar PS studies were conducted for OH [253] and C_2 [229] by Walewski et al. More recently Linvin et al. [238] demonstrated imaging

of ground-state hydrogen atoms by PS after two-photon pumping into the 2s state. The single-shot H distribution obtained by the latter method in a hydrogen/oxygen welding torch flame is illustrated in Fig 9.4.

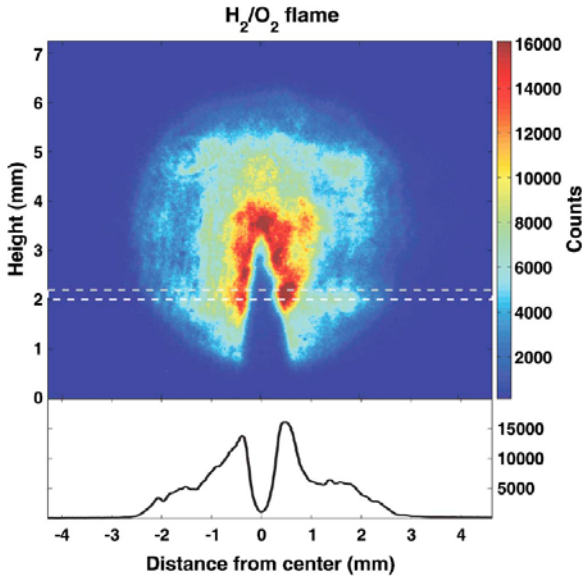

Figure 9.4: Single-shot image of ground-state hydrogen atoms recorded in a hydrogen/oxygen welding torch flame using two-photon planar polarization spectroscopy. (Figure reproduced with permission from reference [238].)

Extension of 2D imaging of concentration distributions to two-dimensional flame thermometry was demonstrated by Ewart and Kaczmarek [280]. 2D DFWM images of OH in a laminar premixed methane/air flame were recorded using two different rotational transitions. The intensity of the images at each position reflects the Boltzmann distribution of population from which the temperature was derived. Since the laser had to be tuned between recording the two images, single-shot measurement was not possible. To overcome this limitation Nyholm et al. [258] employed a dual-wavelength laser source where each of the wavelengths was tuned to a different rotational line of OH. The two UV wavelengths were generated by second harmonic generation in two separate crystals each adjusted to frequency double a different spectral component of the beam from a Nd:YAG pumped dye laser. The output thus consisted of a single beam containing two separately tunable frequency components. With this

laser 2D DFWM and 2D PS signals were generated at each of the two wavelengths. Since the signals at the two wavelengths are also collinear a grating was employed to spatially separate the images. Both images were then recorded on a single CCD chip allowing single-shot temperature measurements.

9.2 Multi-species and multiplex measurements

In most resonant four-wave mixing experiments spectra are recorded by scanning a narrowband laser over a certain spectral range. In many practical situations, however, it is desirable to record the entire spectrum in a single laser pulse in order to achieve temporal resolution. This requires a laser source with a bandwidth covering the relevant spectral region and allows single-shot thermometry since multiple lines of a single species are recorded simultaneously. Alternatively such broadband spectroscopy allows detection of multiple species when their transitions are in close spectral vicinity. Dispersion of the signal is required to measure the separate spectral components and this is usually provided by a spectrograph or interferometer. The most common four-wave mixing technique where at least one broadband laser is used for realizing multiplex measurements is CARS for single-shot nitrogen thermometry [266]. So far there have been relatively few studies using multiplex methods with other four-wave mixing processes.

The use of broadband lasers violates one of the basic assumptions of the theoretical models of four-wave mixing viz. the interacting beams are considered monochromatic. Theoretical treatments of the effects of finite bandwidth on the signal intensity of resonant FWM were developed using a density matrix formalism assuming that the bandwidth exceeded all other relaxation rates in the interaction [71, 72]. This approach was extended to calculate the spectral lineshape of the resonant FWM signal by Smith and Ewart [74]. Measurements of the signal linewidth obtained from flame OH showed good agreement with the theory. In a follow-up study Walker et al. [73] measured the dependence of the spectral lineshape on

pressure by recording signals from nitric oxide in nitrogen buffer gas. The variation of the signal generated by broadband lasers with the length of the interaction region was modelled theoretically by Bratfalean and Ewart [281, 282].

Another effect of finite bandwidths in FWM experiments is the reduction in the coherence length of the radiation i.e. the distance over which the electromagnetic waves retain a consistent phase. Since the magnitude of the FWM signal depends on the atomic or molecular coherence induced over a finite spatial extent the signal intensity will be affected by the temporal correlation of the incident waves. In practice this means that optimum signal generation is found when all three input beams are temporally coincident. The optical paths for each beam to the interaction volume therefore need to be controlled accurately. An extreme example of this problem is represented by the work of Kozlov et al. [205] who employed two beams from a broadband (~400 cm^{-1}) dye laser to generate thermal laser-induced gratings through two-photon excitation of pure rotational Raman transitions. They reported that the difference between the path lengths for the two beams had to be less than 33 μm, which was approximately the coherence length.

The first multiplex DFWM experiments were carried out by Ewart and Snowdon [110] using the broadband output of a Nd:YAG-pumped modeless dye laser. The laser pulse having a bandwidth of ~2 nm FWHM centred on 590 nm was used to record single-shot spectra showing the two D-lines (separated by ~0.6 nm) of atomic sodium that had been seeded into a flame. Kaminski et al. [112] employed a similar laser source to generate multiplex DFWM spectra of C_2 radicals for single-shot thermometry in an acetylene/oxygen flame stabilized on a welding torch. The multiplex FWM signal was directed to the slit of a spectrograph and the spectrum recorded on a CCD camera. A small fraction of the dye laser beam was delivered directly to the spectrograph slit at a lower position to record the spectral excitation profile for online referencing. A typical multiplex DFWM spectrum of the C_2 Swan bands is displayed in figure 9.5(a) together with the simultaneously recorded spectral profile of the incident beam.

This figure also shows a theoretically calculated spectrum fitted to the experimental data using temperature as the fitting parameter. The temperatures derived from such data had a single-shot precision of ~10% as indicated by the histogram in figure 9.5(b). The precision of measurement is improved by averaging over several laser shots. Optical dephasing effects that occur when broadband excitation allows coupled transitions to be pumped simultaneously were studied theoretically and experimentally by Lloyd and Ewart [116]. This work identified the conditions where such effects affect the accuracy of the temperature derived from multiplex FWM. Multiplex FWM spectroscopy of OH for flame thermometry has also been reported by Lloyd et al. [76]. Latzel et al. [209] recorded broadband DFWM spectra in methane/air flames at elevated pressure (atmospheric to 30 bar) concluding that thermometry is possible at pressures as high as 6 bar. Beyond this pressure the experimental DFWM signals did not provide sufficient intensity levels.

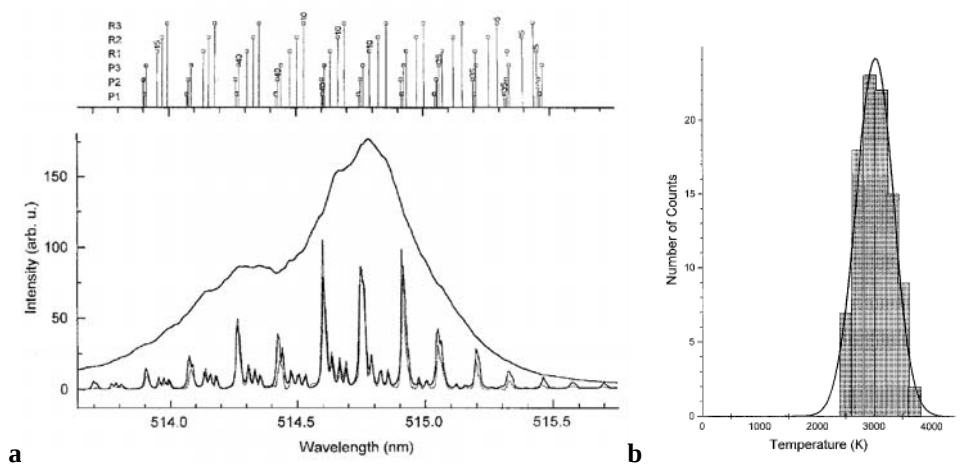

Figure 9.5: (a) Multiplex DFWM spectrum of C_2 recorded from an oxy-acetylene welding torch. The solid line shows a least-square best fit calculated spectrum to the experimental spectrum (dashed line). The stick spectra in the upper part of the diagram indicate the spectral assignments. The spectrum includes more than 60 lines in the R and P branches of the $d^3\Pi_g - a^3\Pi_u$ (0,0) band. The upper curve peaking at 514.8 nm is the simultaneously recorded laser intensity spectrum. (b)Typical histogram of temperatures obtained from 100 single-shot multiplex DFWM spectra. The *solid line* indicates the Gaussian distribution of this data giving a mean temperature of 2993 K with a standard deviation of 325 K. (Figure reproduced with permission from reference [112].)

New et al. [257] performed OH polarization spectroscopy measurements using both a broadband laser and a tunable narrowband laser for comparison. They report strong interference from absorption effects leading to systematic errors in the temperature determination. After correcting for these effects a precision of 4% in the single-shot multiplex data could be achieved.

Multi-species measurements have been demonstrated by Löfstedt and Aldén [230] using simultaneous polarization spectroscopy of OH and NO in a hydrogen/N_2O flame. They utilized a Nd:YAG pumped dye laser which was tuned to 570 nm. The beam was frequency-doubled to provide 285 nm radiation for OH detection in the A-X(1,0) band. Frequency mixing the 285 nm beam with the residual fundamental Nd:YAG output at 1064 nm delivered additional radiation at 225 nm suited for NO detection. Both wavelengths were combined in a single laser beam and scanning this dual-wavelength laser facilitated simultaneous detection of OH and NO at the spectral coincidences of the OH $Q_1(11.5)$ / NO $Q_2(35.5)$ lines and the OH $P_1(9.5)$ / NO $R_2(20.5)$ lines.

9.3 Applications to technical systems

Combustion in technical systems often presents complex challenges for diagnostics. Flames may be unsteady or highly turbulent and are often confined within chambers with limited optical access. Important examples are turbine combustors, industrial furnaces and internal combustion (IC) engines. As described in section 2 conventional optical techniques either are line-of-sight methods or require large numerical apertures for signal collection. For example application of Raman spectroscopy or laser-induced fluorescence to a technical combustion system requires large access windows in order to obtain sufficient signal levels. Large areas of glass however may significantly alter the important thermodynamic properties of the device, e.g. heat transfer characteristics. In contrast, four-wave mixing techniques require only small optical access and for this reason are well suited for measurements in such environments.

Owing to the complications and poor optical access the internal operations of technical combustion systems have proved difficult to study. Measurements of parameters involving minor species therefore have not had high priority in such studies and so resonant four-wave mixing studies in technical combustion are rare in the literature. In contrast, temperature is a key parameter in combustion and its determination is certainly desirable in technical systems. Conventional N_2 CARS has been the most widely used technique in such systems and the basics of these applications have been extensively reviewed [16, 283].

Internal combustion engines are of utmost importance in modern society, particularly for individual transport. They provide a typical example of a highly complex system involving a repetitive combustion process in a confined and temporally varying volume. In the past few decades there has been increasing application of non-intrusive methods for in-cylinder, cycle-resolved measurements [284]. Four-wave mixing techniques, particularly CARS, have proven to be of value. More recently other resonant four-wave mixing processes have begun to find applications in engine diagnostics as supplementary or complementary techniques to CARS.
Modern engine designs employing direct injection of fuel depend critically on the mixture formation process. The gaseous or liquid fuel must be rapidly intermixed with air to obtain an ignitable mixture typically within a few milliseconds. The specific volume of air mixed may be affected by cooling induced by evaporation of the injected liquid fuel. Beyrau et al. [137, 285] used pure-rotational CARS thermometry of nitrogen to measure the temporally resolved local cooling when a liquid iso-octane spray evaporated in a constant volume chamber. By additionally applying Raman spectroscopy Weikl et al. [286] simultaneously determined mixture composition and gas temperature in gaseous and liquid propane injection systems. In the same propane gas injection process Seeger et al. [212, 213] used laser-induced gratings to measure the local equivalence ratio as a function of time after the start of injection. At high fuel concentration the grating oscillation period was utilized while at low propane

concentration the ratio between electrostrictive and thermal gratings yielded results with good accuracy. A similar approach has previously been reported by Schlamp and Sobota who measured iodine concentration in nitrogen [287].

Although vibrational CARS is the most commonly used form of CARS, rotational CARS offers some advantages particularly at lower temperature regimes. Prior to combustion the in-cylinder temperature is in the range where the "hot bands" of N_2 are not sufficiently prominent to provide precise measurements. In this regime rotational CARS, in spite of the difficulties with scattered light from the spectrally adjacent pump light provides improved temperature sensitivity. Pure rotational CARS has been used by Bengtsson and co-workers [288] to measure the temperature and relative oxygen/nitrogen concentrations during the compression stroke. They demonstrated the first rotational CARS experiments in a natural gas fired spark-ignited IC engine. In their follow-up work they studied also the influences of mixture composition and exhaust gas recirculation (EGR) on the knock behaviour [289]. A summary of these activities has been given by Brackmann et al. [290]. Weikl et al. [18] obtained simultaneous information about local temperature and EGR rate from the compression stroke in a homogeneous charge compression ignition (HCCI) engine.

At high temperatures vibrational CARS is preferred owing to its relative freedom from scattering interference and therefore has been used to study the engine combustion process. The first thermometry applications have been demonstrated some 30 years ago by Stenhouse [291] and Klick [292]. More recently Ewart et al. [293] studied the influence of the fuel on the burnt gas temperature and compared their experimental results with predictions from a multi-zone computer simulation.

As mentioned above, resonant FWM processes have so far found fewer applications in technical combustors. The reason seems to have been the perception that aligning the input pump and probe beams is difficult and the supposed effects of turbulence on the induced grating. In practice however the alignment of the three beams for a DFWM experiment is no

more difficult than for CARS. In addition, as explained above, CARS involves a laser induced grating in exactly the same way as DFWM and so the latter will be no more or less sensitive to turbulence than CARS which has been shown to work in many applications. The first use of DFWM to detect a minor species in a firing IC engine was reported by Grant et al. [294]. Stable and reliable beam alignment in the forward phase matching geometry, and freedom from scattered light interference, was achieved by using a simple beam splitter arrangement consisting of parallel sided quartz blocks and a simple two-lens focussing system. Spectra of combustion generated NO were obtained with excellent signal-to-noise ratio. (See figure 9.6(a).) The application of DFWM in IC engines has recently been extended to quantitative measurements of NO concentrations in a firing methane-fuelled engine by Stevens et al. who recorded the DFWM signal intensity on a temperature-insensitive line [295]. A comparison of the quantitative results with reference data from absorption measurements and a conventional exhaust analyzer showed good agreement as depicted in Figure 9.6(b). As the formation of NO_x is strongly dependent on the combustion temperature the results of NO concentration as a function of the mixture stoichiometry reveal a similar behaviour as expected for the adiabatic flame temperature [296].

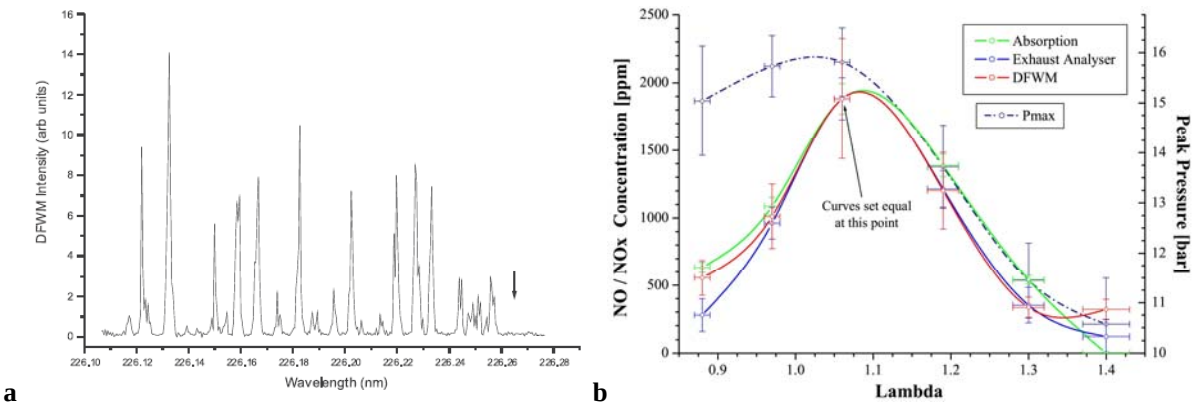

Figure 9.6: (a) DFWM spectrum of NO in a firing methane-fuelled engine. The noise level is indicated by the region to the right of the arrow. (Figure reproduced with permission from reference [294].) (b) NO concentrations measured using DFWM on a temperature insensitive line. The data agrees with measurements on NO measured by absorption and on NO_x measured by an exhaust gas analyser. (Figure reproduced with permission from reference [295].)

Apart from IC engines four-wave mixing measurements have been demonstrated in several other technical systems. Hemmerling et al. [297] utilized electrostrictive laser-induced gratings to determine flow velocity close to the exit of a rocket nozzle. Lucas et al. employed polarization spectroscopy for studying Na atoms in a welding plasma [298]. Bédué et al. [299] performed temperature and oxygen concentration measurements with vibrational CARS in a model turbomachine combustor. The same method was used by Eckbreth et al. [300] in jet engine exhaust gases for N_2 thermometry and detection of oxygen, water and carbon monoxide. Kampmann et al. [301] applied pointwise vibrational CARS and planar laser Rayleigh scattering simultaneously in a highly turbulent swirl flame. While the Rayleigh measurement was used to obtain a relative temperature distribution, the CARS data could be used to determine the absolute temperature in one point of the plane hence potentially providing a calibration of the planar technique. Thermometry in laminar high-pressure combustion environments has been demonstrated, e.g., by Vestin et al. [302] using pure rotational CARS and Brown and Roberts [215] using laser-induced gratings. Industrial coal and oil furnaces have been investigated with CARS by Aldén and Wallin [303] and by Ferrario et al. [304]. Besides large scale systems like gas turbines, furnaces and jet engines technical combustion is often realized in compact devices. In such environments it is important to make measurements close to surfaces as heat transfer may influence the combustion process. Brübach et al. [305] combined thermographic phosphors and vibrational nitrogen CARS to study the normal temperature gradients close to surfaces where gas jets and flames impinged. Braeuer et al. [306] performed temperature and oxygen concentration measurements employing dual-pump CARS in an automotive auxiliary heating combustor operated with dodecane and diesel fuels. Kiefer et al. [19] determined temperature and hydrogen concentration in the ceramic foam matrix of a porous burner. In their experiments a single hole with 1.5 mm diameter provided sufficient optical access for the three CARS laser

beams to enter the combustion zone. Their results revealed the strong heat recuperation effects on the gas phase temperature profile inside the porous material.

10 Summary, conclusion and outlook

In this article we have reviewed the development and use of resonant four-wave mixing techniques for the detection and measurement of minor combustion species. A brief overview of conventional methods for trace species detection has been given together with a discussion of their limitations and the possibility of addressing these by nonlinear methods. The fundamentals of nonlinear optical processes, in particular four-wave mixing, have been introduced to show how their advantageous properties arise. These properties such as coherent (laser-like) signal and high sensitivity were shown to have useful implications for experimental combustion diagnostics. The commonly employed techniques of degenerate four-wave mixing (DFWM), coherent anti-Stokes Raman scattering (CARS), laser-induced thermal grating spectroscopy (LITGS) and polarization spectroscopy (PS) have been reviewed in detail. Other related methods have been outlined together with a brief review of practical considerations and fields currently under development.

The standing of combustion diagnostics based on four-wave mixing techniques has significantly changed over the past decades. This is shown by considering the number of related publications per annum. In the late 1970s the first proof-of-principle studies were published along with the first attempts to describe the complicated physics behind resonant FWM in gases. During the 80s the annual amount of published work remained almost constant at a relatively low level. In the 1990s, however, resonant FWM methods become broadly accepted diagnostic tools resulting in a steep increase in the number of publications forming a plateau over the entire decade. In this period nonlinear techniques have been pushed forward in terms of experimental arrangements as well as theoretical understanding. The interest dropped rather abruptly in the beginning of the current decade, but has experienced a renaissance during the past five years. This revival of resonant four-wave mixing techniques in combustion can be correlated with the recent developments in

experimental equipment and computational power. Novel laser systems and detectors have opened the field to new spectral regions and time scales.

Powerful pulsed near- and mid-infrared lasers facilitate four-wave mixing of so-called “dark species”. These are species that do not absorb by electronic transitions in the ultraviolet and visible spectral region or that do not fluoresce and so are not amenable to the usual absorption or fluorescence detection methods. In the context of combustion diagnostics a large number of combustion-relevant hydrocarbons as well as water and carbon dioxide fall into this category. These species previously have been mainly detected using sampling methods like molecular beam mass spectrometry which involves low pressure detection. FWM in the IR provides the possibility of probing these species *in situ* and non-intrusively with high temporal and spatial resolution. One of the severe problems in using DFWM in the infrared is setting up and maintaining alignment of three input beams and directing the signal beam to the detector. This problem has been solved using a robust beam splitter arrangement developed for DFWM in firing engines using UV lasers [294]. This simple and stable system has recently been successfully applied in the mid-infrared demonstrating the potential for *in situ* sensing of important trace molecular species [95]. Furthermore these optical detection schemes are not limited to low-pressure environments. This is a potentially important field for future developments and may contribute significantly to the understanding of hydrocarbon decomposition and the formation of soot precursors and particles.

Reliable and easy-to-use ultra-short pulse lasers have become commercially available allowing spectroscopy in the time-domain. Amongst other advantages the use of such ultra-short pulses allows the effects of collisions to be avoided. In addition, by suitable choices of time-delays interferences from non-resonant FWM can be suppressed. Furthermore the short pulses provide the high intensity needed for the nonlinear interaction whilst having low energy and so this minimizes interference from elastically scattered light and reduces the risk of damaging optics. The signals are sometimes strong enough to be observed by the naked eye

which means that intensified detectors with their limitations are no longer required. Recent progress in quantitative measurements and single-shot applications using these techniques has sparked new interest within the combustion diagnostics community and is expected to lead to a continuing effort to further development. Another feature of ultra-short pulse lasers is their usually high repetition rate in the order of kHz or even MHz. As a consequence transient phenomena including flame ignition and extinction as well as knocking in engines can be studied in real-time if single-shot measurements are feasible.
Last, but not least, the applicability of FWM in technically relevant combustion systems exploiting the coherent, laser-like signal properties will be another driving force in the future. FWM techniques have finally disproved the prejudice that they are inherently complicated and of limited use. By contrast, it can be expected that they become common tools for measurements of species concentration, temperature and other combustion parameters in environments and situations that are beyond the limits of other more conventional methods.

Acknowledgement

The authors are grateful to our colleagues with whom we have worked and collaborated over the years and to members of the combustion diagnostics community with whom we have interacted in fruitful and enjoyable discussions. In particular, we would like to thank the anonymous referees of the present article who provided many helpful comments and thereby contributed to the final manuscript.

References

[1] Demirbas A. Progress and recent trends in biofuels. Progress in Energy and Combustion Science 2007; 33:1-18.

[2] Haile SM. Fuel cell materials and components. Acta Materialia 2003; 51:5981-6000.

[3] Lindstedt P. Modeling of the chemical complexities of flames. Proceedings of the Combustion Institute 1998; 27:269-85.

[4] Miller JA, Pilling MJ and Troe J. Unravelling combustion mechanisms through a quantitative understanding of elementary reactions. Proceedings of the Combustion Institute 2005; 30:43-88.

[5] Böckle S, Kazenwadel J, Kunzelmann T, Shin D-I and Schulz C. Single-shot laser-induced fluorescence imaging of formaldehyde with XeF excimer excitation. Applied Physics B 2000; 70:733-5.

[6] Medwell PR, Kalt PAM and Dally BB. Simultaneous imaging of OH, formaldehyde, and temperature of turbulent nonpremixed jet flames in a heated and diluted coflow. Combustion and Flame 2007; 148:48-61.

[7] Najm HN, Paul PH, Mueller CJ and Wyckoff PS. On the adequacy of certain experimental observables as measurements of flame burning rate. Combustion and Flame 1998; 113:312-32.

[8] Kiefer J, Li ZS, Seeger T, Leipertz A and Aldén M. Planar laser-induced fluorescence of HCO for instantaneous flame front imaging in hydrocarbon flames. Proceedings of the Combustion Institute 2009; 32:921-8.

[9] Najm HN, Knio OM, Paul PH and Wyckoff PS. A study of flame observables in premixed methane-air flames. Combustion Science and Technology 1998; 140:369-403.

[10] Barlow RS, Dibble RW, Chen J-Y and Lucht RP. Effect of Damköhler number on superequilibrium OH concentration in turbulent nonpremixed jet flames. Combustion and Flame 1990; 82:235-51.

[11] Kiefer J, Li ZS, Zetterberg J, Bai XS and Aldén M. Investigation of local flame structures and statistics in partially premixed turbulent jet flames using simultaneous single-shot CH and OH planar laser-induced fluorescence imaging. Combustion and Flame 2008; 154:802-18 .

[12] Li ZS, Kiefer J, Zetterberg J, Linvin M, Leipertz A, Bai XS and Aldén M. Development of improved PLIF CH detection using an Alexandrite laser for single-shot investigation of turbulent and lean flames. Proceedings of the Combustion Institute 2007; 31:727-35.

[13] Nogenmyr KJ, Kiefer J, Li ZS, Bai XS and Aldén M. Numerical computations and optical diagnostics of unsteady partially premixed methane/air flames. Combustion and Flame 2010; 157:915-25.

[14] Miller JA and Bowman CT. Mechanism and modeling of nitrogen chemistry in combustion. Progress in Energy and Combustion Science 1989; 15:287-338.

[15] Richter H and Howard JB. Formation of polycyclic aromatic hydrocarbons and their growth to soot - a review of chemical reaction pathways. Progress in Energy and Combustion Science 2000; 26:565 - 608.

[16] Eckbreth AC. Laser Diagnostics for Combustion Temperature and Species. Gordon and Breach; 1996.

[17] Kaiser SA, Frank JH and Long MB. Use of Rayleigh imaging and ray tracing to correct for beam-steering effects in turbulent flames. Applied Optics 2005; 44:6557-64.

[18] Weikl MC, Beyrau F and Leipertz A. Simultaneous temperature and exhaust-gas recirculation-measurements in a homogeneous charge-compression ignition engine by use of pure rotational coherent anti-Stokes Raman spectroscopy. Applied Optics 2006; 45:3646-51.
[19] Kiefer J, Weikl MC, Seeger T, von Issendorff F, Beyrau F and Leipertz A. Non-intrusive gas-phase temperature measurements inside a porous burner using dual-pump CARS. Proceedings of the Combustion Institute 2009; 32:3123–9.
[20] Shea JD. The structure of the Swan bands. Physical Review 1927; 30:825-43.
[21] Hardalupas Y and Orain M. Local measurements of the time-dependent heat release rate and euivalence ratio using chemiluminescent emission from a flame Combustion and Flame 2004; 139:188-207.
[22] Hertz HM and Faris GW. Emission tomography of flame radicals. Optics Letters 1988; 13:351-3.
[23] Pauwels J-F, Carlier M and Sochet L-R. Analysis by gas-phase electron spin resonance of H, O, OH, and halogen atoms in flames. Journal of Physical Chemistry 1982; 86:4330-5.
[24] Biordi JC. Molecular beam mass spectrometry for studying the fundamental chemistry in flames. Progress in Energy and Combustion Science 1977; 3:151-73.
[25] Hansen N, Cool TA, Westmoreland PR and Kohse-Höinghaus K. Recent contributions of flame-sampling molecular-beam mass spectrometry to a fundamental understanding of combustion chemistry. Progress in Energy and Combustion Science 2009; 35:168-91.
[26] Gore JP and Zhan NJ. NOx emission and major species concentrations in partially premixed laminar methane / air co-flow jet flames. Combustion and Flame 1996; 105:414-27.
[27] Daniel RG, McNesby KL and Miziolek AW. Application of tunable diode laser diagnostics for temperature and species concentratiuon profiles of inhibited low-pressure flames. Applied Optics 1996; 35:4018-25.
[28] Allen MG, Furlong ER and Hanson RK. Tunable diode laser sensing and combustion control. in Kohse-Höinghaus K and Jeffries JB (ed.) *Applied Combustion Diagnostics* New York: Taylor and Francis, 2002.
[29] Kraetschmer T, Dagel D and Sanders ST. Simple multiwavelength time-division multiplexed light source for sensing applications. Optics Letters 2008; 33:738-40.
[30] Ma L, Cai WW, Caswell AW, Kraetschmer T, Sanders ST, Roy S and Gord JR. Tomographic imaging of temperature and chemical species based on hyperspectral absorption spectroscopy. Optics Express 2009; 17:8602-13.
[31] Kranendonk LA, An X, Caswell AW, Herold RE, Sanders ST, Huber R, Fujimoto JG, Okura Y and Urata Y. High speed engine gas thermometry by Fourier-domain mode-locked laser absorption spectroscopy. Optics Express 2007; 15:15115-28.
[32] Cheskis S. Quantitative measurements of absolute concentrations of intermediate species in flames. Progress in Energy and Combustion Science 1999; 25:233-52.
[33] Cheskis S and Goldman A. Laser diagnostics of trace species in low-pressure flat flame. Progress in Energy and Combustion Science 2009; 35:365-82.
[34] McIlroy A and Jeffries JB. Cavity ringdown spectroscopy for concentration measurements. in Kohse-Höinghaus K and Jeffries JB (ed.) *Applied Combustion Diagnostics* New York: Taylor and Francis, 2002.
[35] Bialkowski SE. Pulsed laser photothermal spectroscopy. Spectroscopy 1986; 1:26.
[36] Kohse-Höinghaus K. Laser techniques for the quantitative detection of reactive intermediates in combustion systems. Progress in Energy and Combustion Science 1994; 20:203-79.

[37] Smyth KC and Crosley DR. Detection of minor species with laser techniques. in Kohse-Höinghaus K and Jeffries JB (ed.) *Applied Combustion Diagnostics* New York: Taylor and Francis, 2002.
[38] Daily JW. Laser induced fluorescence spectroscopy in flames. Progress in Energy and Combustion Science 1997; 23:133-99.
[39] Schrader B (eds.), Infrared and Raman Spectroscopy, VCH Verlagsgesellschaft, Weinheim, 1995.
[40] Getty JD, Burmeister MJ, Westre SG and Kelly PB. Examination of allyl radical excited-state dynamics and ground-state vibrational frequencies by ultraviolet resonance Raman spectroscopy. Journal of the American Chemical Society 1991; 113:801-5.
[41] Geier M, Dreyer CB and Parker TE. Laser-induced emission spectrum from high-temperature silica-generating flames Journal of Quantitative Spectroscopy and Radiative Tranfer 2008; 109:822-30.
[42] Getty JD, Westre SG, Bezabeh DZ, Barrall GA, Burmeister MJ and Kelly PB. Detection of benzene and trichloroethylene in sooting flames. Applied Spectroscopy 1992; 46:620-5.
[43] Ashfold MNR, Clement SG, Howe JD and Western CM. Multiphoton ionisation spectroscopy of free radical species. Journal of the Chemical Society Faraday Transactions 1993; 89:1153-72.
[44] Boyd RW. Nonlinear Optics. Academic Press; 1992.
[45] Shen YR. The Principles of Nonlinear Optics. John Wiley; 2003.
[46] Bratfalean RT, Lloyd GM and Ewart P. Degenerate four-wave mixing for arbitrary pump and probe intensities. Journal of the Optical Society of America B 1999; 16:952-60.
[47] Lloyd GM, Four Wave Mixing Techniques and Applications in Combustion Diagnostics, Ph.D. thesis, University of Oxford, 1997.
[48] Ewart P and O'Leary SV. Comparisons of sodium: rare-gas potentials by measurements of excited-state degenerate four-wave mixing. Journal of Physics B 1982; 15:3669-77.
[49] Pender J and Hesselink L. Phase conjugation in a flame. Optics Letters 1985; 10:264-6.
[50] Ewart P and O'Leary SV. Detection of OH in a flame by degenerate four-wave mixing. Optics Letters 1986; 11:279-81.
[51] Yariv A. Quantum Electronics. Wiley; 1989.
[52] Allen L and Eberly JH. Optical resonance and two level atoms. Dover: 1987.
[53] Abrams RL and Lind RC. Degenerate four-wave mixing in absorbing media. Optics Letters 1978; 2:94-6.
[54] Abrams RL and Lind RC. Degenerate four-wave mixing in absorbing media: errata. Optics Letters 1978; 3:205.
[55] Lucht RP, Farrow RL and Rakestraw DJ. Saturation effects in gas-phase degenerate four-wave mixing spectroscopy: nonpertubative calculations. Journal of the Optical Society of America B 1993; 10:1508-20.
[56] Fisher RA (eds.), Optical Phase Conjugation, Academic Press, Inc., 1983.
[57] Ducloy M and Bloch D. Theory of degenerate four-wave mixing in resonant Doppler-broadened systems - I. Angular dependence of intensity and lineshape of phase-conjugate emission. Journal de Physique France 1981; 42:711-21.
[58] Nilsen J and Yariv A. Nondegenerate four-wave mixing in a Doppler-broadened resonant medium. Journal of the Optical Society of America 1981; 71:180-3.
[59] Steel DG and Remillard JT. Resonant nearly degenerate backward four-wave mixing in open and closed systems. Physical Review A 1987; 36:4330-7.

[60] Bervas H, Attal-Tretout B, LeBoiteux S and Taran JP-E. OH detection and spectroscopy by DFWM in flames; comparison with CARS. Journal of Physics B 1992; 25:949-69.
[61] Attal-Trétout B, Bervas H, Taran JP, Le Boiteux S, Kelley P and Gustafson TK. Saturated FDFWM lineshapes and intensities: theory an application to quantitative measurements in flames. Journal of Physics B 1997; 30:497-522.
[62] Reichardt TA and Lucht RP. Effect of Doppler broadening on quantitative concentration measurements with degenerate four-wave mixing spectroscopy. Journal of the Optical Society of America B 1996; 13:1107 - 19.
[63] Danehy PM, Friedman-Hill EJ, Lucht RP and Farrow RL. The effects of collisional quenching on degenerate four-wave mixing. Applied Physics B 1993; 57:243-8.
[64] Reichardt TA and Lucht RP. Interaction of closely spaced resonances in degenerate four-wave-mixing spectroscopy. Journal of the Optical Society of America B 1997; 14:2449 - 58.
[65] Reichardt TA and Lucht RP. Resonant degenerate four-wave mixing spectroscopy of transitions with degernate energy levels: Saturation and polarization effects Journal of Chemical Physics 1999; 111:10008-20.
[66] Reichardt TA, Lucht RP, Danehy PM and Farrow RL. Theoretical investigation of the forward phase-matched geometry for degenerate four-wave mixing spectroscopy. Journal of the Optical Society of America B 1998; 15:2566-72.
[67] Ai B and Knize RJ. Degenerate four-wave mixing in two-level saturable absorbers. Journal of the Optical Society of America B 1996; 13:2408-19.
[68] Yu D-H, Lee J-H, Chang J-S and Hahn JW. Theory of forward degenerate four-wave mixing in two-level saturable absorbers. Journal of the Optical Society of America B 1999; 16:1261-8.
[69] Lloyd GM and Ewart P. High resolution spectroscopy and spectral simulation of C_2 using degenerate four-wave mixing Journal of Chemical Physics 1999; 110:385-92.
[70] Bultitude K, Bratfalean R and Ewart P. Saturation effects in molecular spectroscopy using degenerate four-wave mixing. Journal of Raman Spectroscopy 2003; 34:1030-6.
[71] Cooper J, Charlton A, Meacher DR, Ewart P and Alber G. Revised theory of resonant degenerate four-wave mixing with broad bandwidth lasers Physical Review A 1989; 40:5705-15.
[72] Meacher DR, Smith PGR, Ewart P and Cooper J. Frequency spectrum of the signal wave in resonant four-wave mixing induced by broad-bandwidth lasers. Physical Review A 1992; 46:2718-25.
[73] Walker DJW, Lloyd GM, Williams RB, Bratfalean R and Ewart P. Pressure effects on the spectral line shape of broad-band degenerate four-wave mixing. Journal of Modern Optics 1998; 45:2541-9.
[74] Smith PGR and Ewart P. Spectral line shape of resonant four-wave mixing induced by broad-bandwidth lasers. Physical Review A 1996; 54:2347-55.
[75] Wasserman TAW, Vaccaro PH and Johnson BR. The influence of finite bandwidth excitation sources in degenerate four-wave mixing spectroscopy. Journal of Chemical Physics 2002; 116:10099-121.
[76] Lloyd GM, Hughes IG, Bratfalean R and Ewart P. Broadband degenerate four-wave mixing of OH for flame thermometry. Applied Physics B 1998; 67:107-13.
[77] Williams S, Zare RN and Rahn LA. Reduction of degenerate four-wave mixing spectra to relative populations I. Weak-field limit. Journal of Chemical Physics 1994; 101:1072-92.
[78] Williams S, Zare RN and Rahn LA. Reduction of degenerate four-wave mixing spectra to relative populations II. Strong-field limit. Journal of Chemical Physics 1994; 101:1093-107.

[79] Jefferies IP, Yates AJ and Ewart P. Broadband DFWM of OH for thermometry. in: Advances in Coherent Raman Spectroscopy, IX European CARS Workshop, Righni et al (eds.) World Scientific 1992; .
[80] Smith AP and Astill AG. Temperature measurement using degenerate four-wave mixing with non-saturating laser powers. Applied Physics B 1994; 58:459-66.
[81] Reichardt TA, Giancola WC, Shappert CM and Lucht RP. Experimental investigation of saturated degenerate four-wave mixing for quantitative concentration measurements. Applied Optics 1999; 38:6951-61.
[82] Rakestraw DJ, Thorne LR and Dreier T. Detection of NH radicals in flames using degenerate four-wave mixing. Proceedings of the Combustion Institute 1991; 23:1901-7.
[83] Dreier T and Rakestraw DJ. Degenerate four-wave mixing diagnostics on OH and NH radicals in flames. Applied Physics B 1990; 50:479-85.
[84] Williams S, Green DS, Sethuraman S and Zare RN. Detection of trace species in hostile environments using degenerate four-wave mixing: CH in an atmospheric-pressure flame. Journal of the American Chemical Society 1992; 114:9122-30.
[85] Tsay SJ, Owens KG, Aniolek KW, Miller DL and Cernansky NP. Detection of CN by degenerate four-wave mixing. Optics Letters 1995; 20:1725-7.
[86] Nyholm K, Kaivola M and Aminoff CG. Detection of C2 and temperature measurement in a flame by using degenerate four-wave mixing in a forward geometry. Optics Communications 1994; 107:406-10.
[87] Kaminski CF, Hughes IG and Ewart P. Degenerate four-wave mixing spectroscopy and spectral simulation of C_2 in an atmospheric pressure oxy-acetylene flame Journal of Chemical Physics 1997; 106:5324-32.
[88] Vander Wal RL, Farrow RL and Rakestraw DJ. High-resolution investigation of degenerate four-wave mixing in the $\gamma(0, 0)$ band of nitric oxide. Proceedings of the Combustion Institute 1992; 24:1653-9.
[89] Mann BA, O'Leary SV, Astill AG and Greenhalgh DA. Degenerate four-wave mixing in nitrogen dioxide: Applicatio to combustion diagnostics. Applied Physics B 1992; 54:271-7.
[90] Sick V, Bui-Pham MN and Farrow RL. Detection of methyl radicals in a flat flame by degenerate four-wave mixing. Optics Letters 1995; 20:2036-8.
[91] Farrow RL, Bui-Pham MN and Sick V. Degenerate four-wave mixing measurements of methyl radical distributions in hydrocarbon flames: Comparison with model predictions. Proceedings of the Combustion Institute 1996; 26:975-83.
[92] Richard K and Ewart P. High-resolution infrared polarization spectroscopy and degenerate four wave mixing spectroscopy of methane. Applied Physics B 2009; 94:715-23.
[93] Germann GJ, Farrow RL and Rakestraw DJ. Infrared degenerate four-wave mixing spectrsocopy of polyatomic molecules: CH_4 and C_2H_2. Journal of the Optical Society of America B 1995; 12:25-32.
[94] Germann GJ, McIlroy A, Dreier T, Farrow RL and Rakestraw DJ. Detection of polyatomic molecules using infrared degenerate four-wave mixing. Berichte der Bunsengesellschaft für Physikalische Chemie 1993; 97:1630-4.
[95] Sun ZW, Li ZS, Li B, Aldén M and Ewart P. Detection of C_2H_2 and HCl using mid-infrared degenerate four-wave mixing with stable beam alignment: towards practical in situ sensing of trace molecular species. Applied Physics B 2010; 98:593-600.
[96] Farrow RL and Rakestraw DJ. Analysis of degenerate for-wave mixing spectra of NO in a $CH_4/N_2/O_2$ flame. Applied Physics B 1999; 68:741-7.
[97] Georgiev N and Aldén M. Two-photon degenerate four-wave mixing (DFWM) for the detection of ammonia: Applications to flames. Applied Physics B 1993; 56:281-6.

[98] Gray JA and Trebino R. Two-photon-resonant four-wave mixing spectroscopy of atomic hydrogen in flames. Chemical Physics Letters 1993; 216:519-24.
[99] Krüger V, Le Boiteux S, Picard YJ and Attal-Tretout B. Atomic oxygen detection in flames using two-photon degenerate four-wave mixing. Journal of Physics B 2000; 33:2887-905.
[100] Germann GJ and Rakestraw DJ. Multiplex spectroscopy: determining the transition moments and absolute concentrations of molecular species. Science 1994; 264:1750-3.
[101] Mischler B, Beaud P, Gerber T, Tzannis A-P and Radi PP. Degenerate four-wave mixing of S_2 and OH in fuel-rich propane/air/SO_2 flames. Combustion Science and Technology 1996; 119:375-93.
[102] Radi PP, Mischler B, Schlegel A, Tzannis A-P, Beaud P and Gerber T. Absolute concentration measurements using DFWM and modeling of OH and S_2 in a fuel-rich H_2/air/SO_2 flame. Combustion and Flame 1999; 118:301-7.
[103] Ewart P, Snowdon P and Magnusson I. Two-dimensional phase-conjugate imaging of atomic distributions in flames by degenerate four-wave mixing. Optics Letters 1989; 14:563-5.
[104] Rakestraw DJ, Farrow RL and Dreier T. Two-dimensional imaging of OH in flames by degenerate four-wave mixing. Optics Letters 1990; 15:709-11.
[105] Ewart P, Smith PGR and Williams RB. Imaging of trace species distributions by degenerate four-wave mixing: diffraction effects, spatial resolution, and image referencing. Applied Optics 1997; 36:5959-68.
[106] Dreier T and Rakestraw DJ. Measurement of OH rotational temperatures in a flame using degenerate four-wave mixing. Optics Letters 1990; 15:72-4.
[107] Winter M and Radi PP. Nearly degenerate 4-wave-mixing using phase-conjugate pump beams. Optics Letters 1992; 17:320-2.
[108] Winter M, Radi PP and Stampanoni A. Double phase-conjugate four-wave mixing of OH in flames. Proceedings of the Combustion Institute 1992; 24:1645-52.
[109] Feikema DA, Domingues E and Cottereau M-J. OH rotational temperature and number density measurements in high-pressure laminar flames using double phase-conjugate four-wave mixing. Applied Physics B 1992; 55:424-9.
[110] Ewart P and Snowdon P. Multiplex degenerate four-wave mixing in a flame. Optics Letters 1990; 15:1403-5.
[111] Yip B, Danehy PM and Hanson RK. Degenerate four-wave mixing temperature measurements in a flame. Optics Letters 1992; 17:751-3.
[112] Kaminski CF, Hughes IG, Lloyd GM and Ewart P. Thermometry of an oxy-acetylene flame using multiplex degenerate four-wave mixing of C_2. Applied Physics B 1996; 62:39-44.
[113] Ewart P. A modeless, variable bandwidth, tunable laser. Optics Communications 1985; 55:124-6.
[114] Snowdon P, Skippon SM and Ewart P. Improved precision of single-shot temperature measurements by broadband CARS by use of a modeless laser. Applied Optics 1991; 30:1008-10.
[115] Snelling DR, Sawchuk RA and Parameswaran T. Noise in single-shot broadband coherent anti-Stokes Raman spectroscopy that employs a modeless dye laser. Applied Optics 1994; 33:8295 - 301.
[116] Lloyd GM and Ewart P. Optical dephasing effects in broadband four-wave mixing in C_2: Implications for broadband FWM thermometry. Journal of Chemical Physics 2002; 116:1370-9.
[117] Butenhoff TJ and Rohlfing EA. Resonant four-wave mixing spectroscopy of transient molecules in free jets. Journal of Chemical Physics 1992; 97:1595-8.

[118] McCormack EF, Pratt ST, Dehmer PM and Dehmer JL. Double-resonance laser-induced grating spectroscopy of nitric oxide. Chemical Physics Letters 1993; 211:147-55.
[119] Buntine MA, Chandler DW and Hayden CC. Detection of vibrational-overtone excitation in water via laser-induced grating spectroscopy. Journal of Chemical Physics 1995; 102:2718-26.
[120] Radi PP, Frey HM, Mischler B, Tzannis A-P, Beaud P and Gerber T. Stimulated emission pumping of OH and NH in flames by using two-color resonant four-wave mixing. Chemical Physics Letters 1997; 265:271-6.
[121] Kouzov AP and Radi PP. Collision-induced resonances in two-color resonant four-wave mixing spectra. Physical Review A 2001; 63:010701.
[122] Hung WC, Huang ML, Lee YC and Lee YP. Detection of CH in an oxyacetylene flame using 2-color resonant 4-wave-mixing technique. Journal of Chemical Physics 1995; 103:9941-6.
[123] Hemmerling B and Stampanoni-Panariello A. Investigation of soot by two-colour four-wave mixing. Chemosphere 2001; 42:647-53.
[124] Ashfold MNR, Chandler DW, Hayden CC, McKay RI and Heck AJR. Two-color resonant four-wave mixing spectroscopy of ammonia. Chemical Physics 1995; 201:237-44.
[125] Maker PD and Terhune RW. Study of optical effects due to an induced polarization third order in the electric field strength. Physical Review 1965; 137:A801-A18.
[126] Lucht RP. Three-laser coherent anti-Stokes Raman scattering measurements of two species. Optics Letters 1987; 12:78-80.
[127] Boyack KW and Hedman PO. Dual-Stokes CARS system for simultaneous measurement of temperature and multi species in turbulent flames. Proceedings of the Combustion Institute 1990; 23:1893-9.
[128] Roy S, Meyer TR, Lucht RP, Belovich VM, Corporan E and Gord JR. Temperature and CO2 concentration measurements in the exhaust stream of a liquid-fueled combustor using dual-pump coherent anti-Stokes Raman scattering (CARS) spectroscopy. Combustion and Flame 2004; 138:273-84.
[129] Weikl MC, Seeger T, Hierold R and Leipertz A. Dual-pump CARS measurements of N_2, H_2 and CO in a partially premixed flame. Journal of Raman Spectroscopy 2007; 38:983-8.
[130] Eckbreth AC, Anderson TJ and Dobbs GM. Multi-color CARS for hydrogen-fueled scramjet applications. Applied Physics B 1988; 45:215-23.
[131] Buldyreva J, Bonamy J, Weikl MC, Beyrau F, Seeger T, Leipertz A, Vestin F, Afzelius M, Bood J and Bengtsson P-E. Linewidth modelling of C_2H_2-N_2 mixtures tested by rotational CARS measurements. Journal of Raman Spectroscopy 2006; 37:647-54.
[132] Kuehner JP, Naik SV, Kulatilaka WD, Chai N, Laurendeau NM, Lucht RP, Scully MO, Roy S, Patnaik AK and Gord JR. Perturbative theory and modeling of electronic-resonance-enhanced coherent anti-Stokes Raman scattering spectroscopy of nitric oxide. Journal of Chemical Physics 2008; 128:174308.
[133] Boquillon JP, Pealat M, Bouchardy P, Collin G, Magre P and Taran JP. Spatial averaging and multiplex coherent anti-Stokes Raman scattering temperature-measurement error Optics Letters 1988; 13:722-4.
[134] Parameswaran T and Snelling DR. Estimation of spatial averaging of temperatures from coherent anti-Stokes Raman spectroscopy. Applied Optics 1996; 35:5461-4.
[135] Seeger T, Weikl MC, Beyrau F and Leipertz A. Identification of spatial averaging effects in vibrational CARS spectra. Journal of Raman Spectroscopy 2006; 37:641-6.

[136] Owyoung A, The origin of the nonlinear refractive indices of liquids and gases, Dissertation, California Institute of Technology, 1971.
[137] Beyrau F, Bräuer A, Seeger T and Leipertz A. Gas-phase temperature measurement in the vaporizing spray of a gasoline direct-injection injector by use of pure rotational coherent anti-Stokes Raman scattering. Optics Letters 2004; 29:247-9.
[138] Vestin F, Afzelius M and Bengtsson P-E. Development of rotational CARS for combustion diagnostics using a polarization approach. Proceedings of the Combustion Institute 2007; 31:833-40.
[139] Druet SAJ, Attal B, Gustafson TK and Taran JP-E. Electronic resonance enhancement of coherent anti-Stokes Raman scattering. Physical Review A 1978; 18:1529-57.
[140] Oudar JL and Shen YR. Nonlinear spectroscopy by multiresonant four-wave mixing. Physical Review A 1980; 22:1141-58.
[141] Attal-Tretout B, Berlemont P and Taran JP-E. Three-colour CARS spectroscopy of the OH radical at triple resonance. Molecular Physics 1990; 70:1-51.
[142] Attal B, Schnepp OO and Taran JP-E. Resonant CARS in I_2 vapor. Optics Communications 1978; 24:77-82.
[143] Verdieck JF, Hall RJ and Eckbreth AC. Electronically resonant CARS detection of OH. in Raux JA and McCay TD (ed.) *Combustion diagnostics by nonintrusive methods* New York: AIAA, 1984.
[144] Attal-Tretout B, Schmidt SC, Crete E, Dumas P and Taran JP-E. Resonance CARS of OH in high pressure flames. Journal of Quantitative Spectroscopy and Radiative Transfer 1990; 43:351-64.
[145] Bervas H, Attal-Tretout B, Labrunie L and LeBoiteux S. Four-wave mixing in OH: Comparison between CARS and DFWM. Il Nuovo Cimento D 1992; 14:1043-50.
[146] Kohse-Höinghaus K, Meier U and Attal-Tretout B. Laser-induced fluorescence in flames study of OH in flat flames of 1-10 bar compared with resonance CARS experiments Applied Optics 1990; 29:1560-9.
[147] Gross KP, Guthals DM and Nibler JW. Electronic three wave mixing spectra of transient species produced by UV laser photolysis of benzene Journal of Chemical Physics 1979; 70:4673-80.
[148] Attal B, Debarre D, Kuller-Dethlefs K and Taran JP-E. Resonance enhanced coherent anti-Stokes Raman scattering in C_2. Revue de Physique Appliquée (Paris) 1983; 18:39-50.
[149] Chen PC and Joyner CC. Peak separation and soring by coherent 2D resonance Raman spectroscopy. Analytical Chemistry 2005; 77:5467-73.
[150] Doerk T, Jauernik P, Hädrich S, Pfelzer B and Uhlenbusch J. Resonance enhanced CARS applied to the CH radical. Optics Communications 1995; 118:637-47.
[151] Doerk T, Ehlbeck J, Jedamzik R, Uhlenbusch J, Höschele J and Steinwandel J. Application of coherent anti-Stokes Raman scattering (CARS) technique to the detection of NO. Applied Spectroscopy 1997; 51:1360-8.
[152] Pott A, Doerk T, Uhlenbusch J, Ehlbeck J, Höschele J and Steinwandel J. Polarization-sensitive coherent anti-Stokes Raman scattering applied to the detection of NO in a microwave discharge for reduction of NO. Journal of Physics D 1998; 31:2485-98.
[153] Guthals DM, Gross KP and Nibler JW. Resonant CARS spectra of NO_2. Journal of Chemical Physics 1979; 70:2393-8.
[154] Dreier T and Wolfrum J. Detection of free NH_2 (X^2B_1) radicals by CARS spectroscopy. Applied Physics B 1984; 33:213-8.
[155] Farrow RL, Lucht RP, Flower WL and Palmer RE. Coherent anti-Stokes Raman spectroscopic measurements of temperature and acetylene spectra in a sooting diffusion flame. Proceedings of the Combustion Institute 1984; 20:1307-12.

[156] Hanna SF, Kulatilaka WD, Arp Z, Opatrny T, Scully MO, Kuehner JP and Lucht RP. Electronic-resonance-enhanced coherent anti-Stokes Raman spectroscopy of nitric oxide. Applied Physics Letters 2003; 83:1887-9.
[157] Kulatilaka WD, Chai N, Naik SV, Laurendeau NM, Lucht RP, Kuehner JP, Roy S and Gord JR. Measurement of nitric oxide concentrations in flames by using electronic-resonance-enhanced coherent anti-Stokes Raman scattering Optics Letters 2006; 31:3357-9.
[158] Chai N, Kulatilaka WD, Naik SV, Laurendeau NM, Lucht RP, Kuehner JP, Roy S, Katta VR and Gord JR. Nitric oxide concentration measurements in atmospheric pressure flames using electronic-resonance-enhanced coherent anti-Stokes Raman scattering. Applied Physics B 2007; 88:141-50.
[159] Chai N, Naik SV, Laurendeau NM, Lucht RP, Roy S and Gord JR. Single-laser-shot detection of nitric oxide in reacting flows using electronic resonance enhanced coherent anti-Stokes Raman scattering Applied Physics Letters 2008; 93:091115.
[160] Chai N, Naik SV, Kulatilaka WD, Laurendeau NM, Lucht RP, Roy S and Gord JR. Detection of acetylene by electronic resonance-enhanced coherent anti-Stokes Raman scattering Applied Physics B 2007; 87:731-7.
[161] Patnaik AK, Roy S, Lucht RP and Gord JR. Collisional effects on molecular dynamics in electronic-resonance-enhanced CARS. Journal of Modern Optics 2008; 55:3263-72.
[162] Roy S, Kulatilaka WD, Naik SV, Laurendeau NM, Lucht RP and Gord JR. Effects of quenching on electronic-resonance-enhanced coherent anti-Stokes Raman scattering of nitric oxide. Applied Physics Letters 2006; 89:104105.
[163] Rahn LA, Zych LJ and Mattern PL. Background-free CARS studies of carbon monoxide in a flame. Optics Communications 1979; 30:249-52.
[164] Weikl MC, Seeger T, Wendler M, Sommer R, Beyrau F and Leipertz A. Validation experiments for spatially resolved one-dimensional emission spectroscopy temperature measurements by dual-pump CARS in a sooting flame. Proceedings of the Combustion Institute 2009; 32:745-52.
[165] Meyer TR, Roy S and Gord JR. Improving signal-to-interference ratio in rich hydrocarbon-air flames using picosecond coherent anti-Stokes Raman scattering. Applied Spectroscopy 2007; 61:1135-40.
[166] Roy S, Meyer TR and Gord JR. Time-resolved dynamics of resonant and nonresonant broadband picosecond coherent anti-Stokes Raman scattering signals. Applied Physics Letters 2005; 87:264103.
[167] Seeger T, Kiefer J, Leipertz A, Patterson BD, Kliewer CJ and Settersten TB. Picosecond time-resolved pure-rotational coherent anti-Stokes Raman spectroscopy for N_2 thermometry. Optics Letters 2009; 34:3755-7.
[168] Kliewer CJ, Gao Y, Seeger T, Kiefer J, Patterson BD and Settersten TB. Picosecond time-resolved pure-rotational coherent anti-Stokes Raman spectroscopy in sooting flames. Proceedings of the Combustion Institute 2010; 33:accepted for publication.
[169] Eckbreth AC and Hall RJ. CARS concentration sensitivity with and without nonresonant background suppression. Combustion Science and Technology 1981; 25:175-92.
[170] Beyrau F, Datta A, Seeger T and Leipertz A. Dual-pump CARS for the simultaneous detection of N_2,O_2 and CO in CH_4 flames. Journal of Raman Spectroscopy 2002; 33:919-24.
[171] Hahn JW, Park SN, Lee ES, Rhee C, Kang KT, Chung SH, Choi CY and Huh YD. Measuring the concentration of minor species from the modulation dip of the nonresonant background of broad-band CARS spectra. Applied Spectroscopy 1993; 47:710-4.

[172] Roh WB and Schreiber PW. Pressure-dependence of integrated CARS power. Applied Optics 1978; 17:1418-24.
[173] Roy S, Wrzesinski P, Pestov D, Gunaratne T, Dantus M and Gord JR. Single-beam coherent anti-Stokes Raman scattering spectroscopy of N_2 using a shaped 7 fs laser pulse. Applied Physics Letters 2009; 95:074102.
[174] Dreizler A, Dreier T and Wolfrum J. Thermal grating effects in infrared degenerate four-wave mixing for trace gas detection. Chemical Physics Letters 1995; 233:525-32.
[175] Paul PH, Farrow RL and Danehy PM. Gas-phase thermal-grating contributions to four-wave mixing. Journal of the Optical Society of America B 1995; 12:384-92.
[176] Dreizler A, Latzel H, Dreier T, Koch A and Wolfrum J. Berichte der Bunsengesellschaft für Physikalische Chemie 1996; 100:1678-83.
[177] Nelson KA, Lutz DR, Fayer MD and Madison L. Laser-induced phonon spectroscopy - optical generation of ultrasonic waves and investigation of electronic excited-state intercations in solids. Physical Review B 1981; 24:3261-75.
[178] Stampanoni-Panariello A. Laser-induced Gratings in the Gas Phase: Formation Mechanisms and Applications for Diagnostics. Konstanz: Hartung-Gorre Verlag; 2003.
[179] Stampanoni-Panariello A, Kozlov DN, Radi PP and Hemmerling B. Gas phase diagnostics by laser-induced gratings: I. Theory. Applied Physics B 2005; 81:101-11.
[180] Trebino R, Siegman AE and Ladera CL. Suppression of thermal gratings in polarization spectroscopy. Journal of the Optical Society of America B 1984; 1:549-50.
[181] Cummings EB. Laser-induced thermal acoustics: simple accurate gas measurements. Optics Letters 1994; 19:1361-3.
[182] Cummings EB, Leyva IA and Hornung HG. Laser-induced thermal acoustics (LITA) signals from finite beams. Applied Optics 1995; 34:3290-302.
[183] Hubschmid W, Hemmerling B and Stampanoni-Panariello A. Rayleigh and Brillouin modes in electrostrictive gratings. Journal of the Optical Society of America B 1995; 12:1850-4.
[184] Eichler HJ, Gunter P and Pohl DW. Laser-induced dynamic gratings. Berlin: Springer; 1986.
[185] Hart RC, Balla RJ and Herring GC. Nonresonant referenced laser-induced thrmal acoustics thermometry in air. Applied Optics 1999; 38:577-84.
[186] Hemmerling B and Kozlov DN. Collisional relaxation of singlet $O_2(b^1\Sigma_g^+)$ in neat gas investigated by laser-induced grating technique. Chemical Physics 2003; 291:213-42.
[187] Stevens R and Ewart P. Single-shot measurement of temperature and pressure using laser-induced thermal gratings with a long probe pulse. Applied Physics B 2004; 78:111-7.
[188] Stevens RE, Laser induced grating techniques for combustion diagnostics, D.Phil thesis, Oxford University, 2004.
[189] Hemmerling B, Kozlov DN and Stampanoni-Panariello A. Temperature and flow-velocity measurements by use of laser-induced electrostrictive gratings. Optics Letters 2000; 18:1340-2.
[190] Chu RS and Tamir T. Bragg-diffraction of Gaussian beams by periodically modulated media. Journal of the Optical Society of America 1976; 66:220-6.
[191] Siegman AE. Bragg diffraction of a Gaussian beam by a crossed-Gaussian volume grating. Journal of the Optical Society of America 1977; 67:545-50.
[192] Wang J, Fiebig M and Wu G. Numerical simulation and error analysis for thermal diffusivity measurements using a thermal laser-induced grating technique. International Journal of Thermophysics 1996; 17:329-45.
[193] Hemmerling B, Bombach R and Hubschmid W. Laser-induced gratings in oxygen excited via the b $^1\Sigma_g^+$(v'=0) state. Chemical Physics Letters 1996; 256:71-6.

[194] Hubschmid W and Hemmerling B. Relaxation processes in singlet O_2 analyzed by laser-induced gratings Chemical Physics 2000; 259:109-20.
[195] Stampanoni-Panariello A, Kozlov DN, Radi PP and Hemmerling B. Gas-phase diagnostics by laser-induced gratings: II. Experiments. Applied Physics B 2005; 81:113-29.
[196] Hubschmid W. Molecular relaxation in mixtures of O_2 and CO_2 observed on laser-induced gratings. Applied Physics B 2009; 94:345-54.
[197] Gutfleisch M, Shin DI, Dreier T and Danehy PM. Mid-infrared laser-induced grating experiments of C_2H_4 and NH_3 from 0.1-2 MPa and 300-800 K. Applied Physics B 2000; 71:673-80.
[198] Fantoni R, Giorgi M, De Dominicis L and Kozlov DN. Collisional relaxation and internal energy redistribution in NO_2 investigated by means of laser-induced thermal grating technique Chemical Physics Letters 2000; 332:375-80.
[199] Butenhoff TJ and Rohlfing EA. Laser-induced gratings in free jets. II. Photodissociation dynamics via photofragment transient gratings Journal of Chemical Physics 1993; 98:5469-76.
[200] Gray JA, Goldsmith JEM and Trebino R. Detection of atomic hydrogen by two-color laser-induced grating spectroscopy. Optics Letters 1993; 18:444-6.
[201] Booze JA, Govoni DE and Crim FF. Diffraction mechanisms in gas-phase laser induced grating spectroscopy of vibrational overtone transitions. Journal of Chemical Physics 1995; 103:10484-91.
[202] Kozlov DN and Radi PP. Detection of vibrational overtone excitation in methane by laser-induced grating spectroscopy. Journal of Raman Spectroscopy 2008; 39:730-8.
[203] Kozlov DN, Bombach R, Hemmerling B and Hubschmid W. Laser-induced gratings in the gas phase excited by Raman-active transitions. Optics Letters 1997; 22:46-8.
[204] Kozlov DN, Bombach R, Hemmerling B and Hubschmid W. Excitation of laser-induced thermal gratings in the gas phase via Raman-active transitions. Optics Communications 1999; 166:245-54.
[205] Kozlov DN, Weikl MC, Kiefer J, Seeger T and Leipertz A. Two-photon stimulated Raman excitation of thermal laser-induced gratings in molecular gases using broadband radiation of a single laser Optics Express 2008; 16:18379-89.
[206] Butenhoff TJ and Rohlfing EA. Laser-induced gratings in free jets. I. Spectroscopy of predissociating NO_2. Journal of Chemical Physics 1993; 98:5460-8.
[207] Loubignac E, Attal-Tretout B, Le Boiteux S and Kozlov DN. Two-color non-linear spectroscopy: application to NO_2. C.R. Acad. Sci. Paris 2001; Serie IV:1013-27.
[208] Williams S, Rahn LA, Paul PH, Forsman JW and Zare RN. Laser-induced thermal grating effects in flames. Optics Letters 1994; 19:1681-3.
[209] Latzel H, Dreizler A, Dreier T, Heinze J, Dillmann M, Stricker W, Lloyd GM and Ewart P. Thermal grating and broadband degenerate four-wave mixing spectroscopy of OH in high-pressure flames. Applied Physics B 1998; 67:667-73.
[210] Hart RC, Balla RJ and Herring GC. Observation of H_2O in a flame by two-colour laser-induced-grating spectroscopy. Measurement Science and Technology 1997; 8:917-20.
[211] Hemmerling B, Kozlov DN, Stel'makh OM and Attal-Trétout B. Diagnostics of water-containing gas mixtures using thermal laser-induced gratings. Chemical Physics 2006; 320:103-17.
[212] Seeger T, Kiefer J, Weikl MC, Leipertz A and Kozlov DN. Time-resolved measurement of the local equivalence ratio in a gaseous propane injection process using laser-induced gratings. Optics Express 2006; 14:12994-3000.
[213] Kiefer J, Kozlov DN, Seeger T and Leipertz A. Local fuel concentration measurements for mixture formation diagnostics using diffraction by laser-induced

gratings in comparison to spontaneous Raman scattering. Journal of Raman Spectroscopy 2008; 39:711-21.
[214] Brewer TR, Fourkas JT and Fayer MD. Flame temperature measurement using picosecond transient grating experiments. Chemical Physics Letters 1993; 203:344-8.
[215] Brown MS and Roberts WL. Single-point thermometry in high-pressure, sooting, premixed combustion environments. Journal of Propulsion and Power 1999; 15:119-27.
[216] Hart RC, Herring GC and Balla RJ. Pressure measurement in supersonic air flow by differential absorptive laser-induced thermal acoustics. Optics Letters 2007; 32:1689-91.
[217] Wieman C and Hänsch TW. Doppler-free Laser Polarization spectroscopy. Physical Review Letters 1976; 36:1170-3.
[218] Feinberg R, Hänsch TW, Schawlow AL, Teets RE and Wieman C. Laser polarization spectroscopy of atoms and molecules. Optics Communications 1976; 18:227-8.
[219] Teets RE, Kowalski FV, Hill WT, Carlson N and Hänsch TW. Laser polarization spectroscopy. Proceedings of the SPIE 1977; 113:80-7.
[220] Ernst WE. Doppler-free polarization spectroscopy of diatomic molecules in flame reactions. Optics Communications 1983; 44:159-64.
[221] Reichardt TA and Lucht RP. Theoretical calculation of line shapes and saturation effects in polarization spectroscopy. Journal of Chemical Physics 1998; 109:5830 - 43.
[222] Demtröder W. Laser Spectroscopy. Berlin, New York: Springer Verlag; 1996.
[223] Zizak G, Lanauze J and Winefordner JD. Cross-beam polarization in flames with a pulsed dye laser. Applied Optics 1986; 25:3242-6.
[224] Nyholm K, Maier R, Aminoff CG and Kaivola M. Detection of OH in flames by using polarisation spectroscopy. Applied Optics 1993; 32:919-24.
[225] Reichardt TA, Giancola WC and Lucht RP. Experimental investigation of saturated polarization spectroscopy for quantitative concentration measurements. Applied Optics 2000; 39:2002 - 8.
[226] Walewski J, Kaminski CF, Hanna SF and Lucht RP. Dependence of partially saturated polarization spectroscopy signals on the pump intensity and collision rate. Physical Review A 2001; 64:063816.
[227] Suvernev AA, Dreizler A, Dreier T and Wolfrum J. Polarization-spectroscopic measurement and spectral simulation of OH($A^2\Sigma$-$X^2\Pi$) and NH($A^3\Pi$-$X^3\Sigma$) transitions in atmospheric pressure flames. Applied Physics B 1995; 61:421-7.
[228] Nyholm K, Kaivola M and Aminoff CG. Polarization spectroscopy applied to C_2 detection in a flame. Applied Physics B 1995; 60:5-10.
[229] Walewski J, Rupinski M, Bladh H, Li ZS, Bengtsson P-E and Aldén M. Soot visualisation by use of laser-induced soot vapourisation in combination with polarisation spectroscopy. Applied Physics B 2003; 77:447-54.
[230] Löfstedt B and Aldén M. Simultaneous detection of OH and NO in a flame using polarization spectroscopy. Optics Communications 1996; 124:251-7.
[231] Löfstedt B, Fritzon R and Aldén M. Investigation of NO detection in flames by use of polarization spectroscopy. Applied Optics 1996; 35:2140-6.
[232] Kiefer J, Li ZS, Zetterberg J, Linvin M and Aldén M. Simultaneous laser-induced fluorescence and sub-Doppler polarization spectroscopy of the CH radical. Optics Communications 2007; 270:347-52.
[233] Nyholm K, Fritzon R, Georgiev N and Aldén M. Two photon induced polarization spectroscopy applied to the detection on NH_3 and CO molecules in cold flows and flames. Optics Communications 1995; 114:76-82.

[234] Kaminski CF, Löfstedt B, Fritzon R and Aldén M. Two-photon polarization spectroscopy and (2 + 3) -photon laser induced fluorescence of N_2. Optics Communications 1996; 129:38-43.
[235] Grützmacher K, De La Rosa MI, Gonzalo AB, Steiger M and Steiger A. Two-photon polarization spectroscopy applied for quantitative measurements of atomic hydrogen in atmospheric pressure flames. Applied Physics B 2003; 76:775-85.
[236] Kulatilaka WD, Lucht RP, Hanna SF and Katta VR. Two-color, two-photon laser-induced polarization spectroscopy (LIPS) measurements of atomic hydrogen in near-adiabatic, atmospheric pressure hydrogen/air flames. Combustion and Flame 2004; 137:523-37.
[237] Kulatilaka WD, Lucht RP, Roy S, Gord JR and Settersten TB. Detection of atomic hydrogen in flames using picosecond two-color two-photon-resonant six-wave-mixing spectroscopy. Applied Optics 2007; 49:3921-7.
[238] Linvin M, Li ZS, Zetterberg J and Aldén M. Single-shot imaging of ground-state hydrogen atoms with a nonlinear laser spectroscopic technique. Optics Letters 2007; 32:1569-71.
[239] Roy S, Lucht RP and McIlroy A. Mid-infrared polarization spectroscopy af carbon dioxide. Applied Physics B 2002; 75:875 - 82.
[240] Alwahabi ZT, Li ZS, Zetterberg J and Aldén M. Infrared polarization spectroscopy of CO_2 at atmospheric pressure. Optics Communications 2004; 233:373-81.
[241] Alwahabi ZT, Zetterberg J, Li ZS and Aldén M. High resolution polarization spectroscopy and laser induced fluorescence of CO2 around 2 μm. European Physical Journal D 2007; 42:41-7.
[242] Alwahabi ZT, Zetterberg J, Li ZS and Aldén M. Measurements of collisional broadening coefficients by infrared polarization spectroscopy Applied Spectroscopy 2007; 61:424-7.
[243] Alwahabi ZT, Zetterberg J, Li ZS and Aldén M. Vibrational relaxation of CO_2 ($12^0 1$) by argon. Chemical Physics 2009; 359:71-6.
[244] Li ZS, Rupinski M, Zetterberg J, Alwahabi ZT and Aldén M. Mid-infrared polarization spectroscopy of polyatomic molecules: detection of nascent CO_2 and H_2O in atmospheric pressure flames. Chemical Physics Letters 2005; 407:243-8.
[245] Li ZS, Hu CH, Zetterberg J, Linvin M and Aldén M. Midinfrared polarization spectroscopy of OH and hot water in low pressure lean premixed flames. Journal of Chemical Physics 2007; 127:084310.
[246] Li ZS, Rupinski M, Zetterberg J, Alwahabi ZT and Aldén M. Detection of methane with mid-infrared polarization spectroscopy. Applied Physics B 2004; 79:135-8.
[247] Li ZS, Rupinski M, Zetterberg J and Aldén M. Mid-infrared PS and LIF detection of CH_4 and C_2H_6 in cold flows and flames at atmospheric pressure. Proceedings of the Combustion Institute 2005; 30:1629-36.
[248] Li ZS, Linvin M, Zetterberg J, Kiefer J and Aldén M. Mid-infrared polarization spectroscopy of C2H2: non-intrusive spatial-resolved measurements of polyatomic hydrocarbon molecules for combustion diagnostics. Proceedings of the Combustion Institute 2007; 31:817-24.
[249] Li ZS, Sun ZW, Li B, Aldén M and Försth M. Spatially resolved trace detection of HCl in flames with mid-infrared polarization spectroscopy. Optics Letters 2008; 33:1836-8.
[250] Sun ZW, Li ZS, Li B, Alwahabi ZT and Aldén M. Quantitative C_2H_2 measurements in sooty flames using mid-infrared polarization spectroscopy. Applied Physics B 2010; in print:DOI: 10.1007/s00340-010-4057-z.
[251] Reppel J and Alwahabi ZT. Orthogonal planar laser polarization spectroscopy. Applied Optics 2002; 41:4267-72.

[252] Nyholm K, Fritzon R and Aldén M. Two-dimensional imaging of OH in flames by use of polarization spectroscopy. Optics Letters 1993; 18:1672-4.
[253] Walewski JW, Nyholm K, Dreizler A and Aldén M. Polarization Spectroscopy applied to the detection of trace constituents in sooting combustion. Applied Spectroscopy 2004; 58:238-42.
[254] Nyholm K. Measurements of OH rotational temperatures in flames by using polarization spectroscopy. Optics Communications 1994; 111:66-70.
[255] Kiefer J, Meyerhoefer A, Seeger T, Leipertz A, Li ZS and Aldén M. OH-Thermometry using laser-induced fluorescence spectroscopy and polarization spectroscopy in the A-X (1,0) band. Journal of Raman Spectroscopy 2009; 40:828-35.
[256] Luque J and Crosley DR. LIFBASE: Database and spectral simulation program (version 1.5). 1999; .
[257] New MJ, Ewart P, Dreizler A and Dreier T. Multiplex polarization spectroscopy of OH for flame thermometry. Applied Physics B 1997; 65:633-7.
[258] Nyholm K, Fritzon R and Aldén M. Single-pulse two-dimensional temperature imaging in flames by degenerate four-wave mixing and polarization spectroscopy. Applied Physics B 1994; 59:37-43.
[259] Lee ES, Choi DS, Lee JY and Hahn JW. Multiplex nonresonant pump four-wave mixing. Applied Physics Letters 2004; 85:546-8.
[260] Sun ZW, Kiefer J, Li ZS, Li B and Aldén M. Four-wave mixing with non-resonant pump and resonant probe for OH detection in flames. Applied Physics B 2008; 92:287-93.
[261] Seeger T, Kiefer J, Gao Y, Patterson BD, Kliewer CJ and Settersten TB. Suppression of Raman-resonant interferences in rotational coherent anti-Stokes Raman spectroscopy using time-delayed picosecond probe pulses. Optics Letters 2009; 35:2040-2.
[262] Miller JD, Slipchenko MN, Meyer TR, Stauffer HU and Gord JR. Hybrid fs/ps coherent anti-Stokes Raman scattering for high-speed gas-phase thermometry. Optics Letters 2010; accepted for publication, Doc. ID: 128362.
[263] Lang T, Motzkus M, Frey HM and Beaud P. High resolution femtosecond coherent anti-Stokes Raman scattering: Determination of rotational constants, molecular anharmonicity, collisional line shifts, and temperature. Journal of Chemical Physics 2001; 115:5418-26.
[264] Lang T and Motzkus M. Determination of line shift coefficients with femtosecond time resolved CARS. Journal of Raman Spectroscopy 2000; 31:65-70.
[265] Gord JR, Meyer TR and Roy S. Applications of ultrafast lasers for optical measurements in combusting flows. Annual Review of Analytical Chemistry 2008; 1:663-87.
[266] Roy S, Gord JR and Patnaik AK. Recent advances in coherent anti-Stokes Raman scattering spectroscopy: Fundamental developments and applications in reacting flows. Progress in Energy and Combustion Science 2010; 36:280-306.
[267] Buckup T, Hauer J and Motzkus M. Coherent control for molecular ultrafast spectroscopy. in Hall TJ, Gaponenko S, Corkum P and Stolow A (ed.) *Extreme Photonics: Applications to Ultra-fast Science, Biomedicine and Security* Heidelberg: Springer, 2010.
[268] Hornung T, Skenderovic H, Kompa K-L and Motzkus M. Prospect of temperature determination using degenerate four-wave-mixing with sub-20fs pulses. Journal of Raman Spectroscopy 2005; 35:934.
[269] Dreizler A, Tadday R, Suvernev AA, Himmelhaus M, Dreier T and Foggi P. Measurement of orientational relaxation time of OH in a flame using picosecond time-resolved polarization spectroscopy. Chemical Physics Letters 1995; 240:315-23.

[270] Suvernev AA, Tadday R and Dreier T. Measurement and theoretical modeling of quantum beats in picosecond time-resolved degenerate four-wave mixing and polarization spectroscopy of OH in atmospheric pressure flames. Physical Review A 1998; 58:4102-15.
[271] Reichardt TA, Di Teodoro F, Farrow RL, Roy S and Lucht RP. Collisional dependence of polarization spectroscopy with a picosecond laser Journal of Chemical Physics 2000; 113:2263-9.
[272] Roy S, Lucht RP and Reichardt TA. Polarization spectroscopy using short-pulse lasers: Theoretical analysis. Journal of Chemical Physics 2002; 116:571-80.
[273] Chen X and Settersten TB. Investigation of OH $X^2\Pi$ collsional kinetics in a flame using picosecond two-color resonant four-wave mixing spectroscopy. Applied Optics 2007; 46:3911-20.
[274] Bivolaru D and Herring GC. Focal-plane imaging of crossed beams in nonlinear optics experiments. Review of Scientific Instruments 2007; 78:056102.
[275] Tedder SA, Weikl MC, Seeger T and Leipertz A. Determination of probe volume dimensions in coherent measurement techniques. Applied Optics 2008; 47:6601-5.
[276] Snow JB, Zheng J-B and Chang RK. Spatially and spectrally resolved multi-point coherent anti-Stokes Raman scattering from N_2 and O_2 flows. Optics Letters 1983; 8:599-601.
[277] Jonuscheit J, Thumann A, Schenk M, Seeger T and Leipertz A. One-dimensional vibrational coherent anti-Stokes Raman-scattering thermometry. Optics Letters 1996; 21:1532-4.
[278] Stevens R and Ewart P. Simultaneous single-shot measurement of temperature and pressure along a one-dimensional line by use of laser-induced thermal grating spectroscopy. Optics Letters 2006; 31:1055-7.
[279] Hemmerling B and Stampanoni-Panariello A. Imaging of flames and cold flows in air by diffraction from a laser-induced grating. Applied Physics B 1993; 57:281-5.
[280] Ewart P and Kaczmarek M. Two-dimensional mapping of temperature in a flame by degenerate four-wave mixing in OH. Applied Optics 1991; 30:3996-9.
[281] Bratfalean R and Ewart P. The dependence of broadband four-wave mixing signal intensity on the length of the interaction region. Journal of Modern Optics 1996; 43:2523-31.
[282] Bratfalean R and Ewart P. Erratum: The dependence of broadband four-wave mixing signal intensity on the length of the interaction region. Journal of Modern Optics 1999; 46:1051-2.
[283] Kohse-Höinghaus K and Jeffries JB (eds.), Applied Combustion Diagnostics, Taylor and Francis, New York, 2002.
[284] Drake MC and Haworth DC. Advanced gasoline engine development using optical diagnostics and numerical modeling. Proceedings of the Combustion Institute 2007; 31:99-124.
[285] Beyrau F, Weikl MC, Schmitz I, Seeger T and Leipertz A. Locally resolved investigation of the vaporization of GDI sprays applying different laser techniques. Atomization and Sprays 2006; 16:319-30.
[286] Weikl MC, Beyrau F, Kiefer J, Seeger T and Leipertz A. Combined coherent anti-Stokes Raman spectroscopy and linear Raman spectroscopy for simultaneous temperature and multiple species measurements. Optics Letters 2006; 31:1908-10.
[287] Schlamp S and Sobota TH. Measuring concentrations with laser-induced thermalization and electrostrictive gratings. Experiments in Fluids 2002; 32:683-8.
[288] Bengtsson P-E, Martinsson L, Aldén M, Johansson B, Lassesson B, Marforio K and Lundholm G. Dual-broadband rotational CARS measurements in an IC engine. Proceedings of the Combustion Institute 1994; 25:1735-42.

[289] Grandin B, Denbratt I, Bood J, Brackmann C and Bengtsson P-E. A study of the influence of exhaust gas recirculation and stoichiometry on the heat release in the end-gas prior to knock using rotational coherent anti-Stokes-Raman spectroscopy thermometry. International Journal of Engine Research 2002; 3:209-21.
[290] Brackmann C, Bood J, Afzelius M and Bengtsson P-E. Thermometry in internal combustion engines via dual-broadband rotational coherent anti-Stokes Raman spectroscopy. Measurement Science and Technology 2004; 15:R13-R25.
[291] Stenhouse IA, Williams DR, Cole JB and Swords MD. CARS measurements in an internal combustion engine. Applied Optics 1979; 18:3819-25.
[292] Klick D, Marko KA and Rimai L. Braodband single-pulse CARS spectra in a fired internal combustion engine. Applied Optics 1981; 20:1178-81.
[293] Ewart P, Williams RB, Lim EP and Stone CR. Comparison of-incylinder coherent anti-Stokes-Raman scattering temperature measurements with predictions from an engine simulation. International Journal of Engine Research 2001; 2:149-62.
[294] Grant AJ, Ewart P and Stone CR. Detection of NO in a spark-ignition research engine using degenerate four-wave mixing. Applied Physics B 2002; 74:105-10.
[295] Stevens R, Ewart P, Ma H and Stone CR. Measurement of nitric oxide concentration in a spark-ignition engine using degenerate four-wave mixing. Combustion and Flame 2007; 148:223-33.
[296] Law CK, Makino A and Lu TF. On the off-stoichiometric peaking of adiabatic flame temperature. Combustion and Flame 2006; 145:808-19.
[297] Hemmerling B, Neracher M, Kozlov DN, Kwan W, Stark R, Klimenko D, Clauss W and Oschwald M. Rocket nozzle cold-gas flow velocity measurements using laser-induced gratings. Journal of Raman Spectroscopy 2002; 33:912-8.
[298] Lucas O, Alwahabi ZT, Linton V and Meeuwissen K. Laser diagnostics of welding plasma by polarization spectroscopy. Applied Spectroscopy 2007; 61:565-9.
[299] Bédué R, Gastebois P, Bailly R, Péalat M and Taran JP. CARS measurements in a simulated turbomachine combustor. Combustion and Flame 1984; 57:141-53.
[300] Eckbreth AC, Dobbs GM, Stufflebeam JH and Tellex PA. CARS temperature and species measurements in augmented jet engine exhausts. Applied Optics 1984; 23:1328-39.
[301] Kampmann S, Seeger T and Leipertz A. Simultaneous coherent anti-Stokes Raman scattering and two-dimensional laser Rayleigh thermometry in a contained technical swirl combustor. Applied Optics 1995; 34:2780-6.
[302] Vestin F, Sedarsky D, Collin R, Aldén M, Linne M and Bengtsson P-E. Rotational coherent anti-Stokes Raman spectroscopy (CARS) applied to thermometry in high-pressure hydrocarbon flames. Combustion and Flame 2008; 154:143-52.
[303] Aldén M and Wallin S. CARS experiments in a full-scale (10x10 m) industrial coal furnace. Applied Optics 1985; 24:3434-7.
[304] Ferrario A, Garbi M and Malvicini C. Real-time CARS spectroscopy in a semi-industrial furnace. Technical Digest, Conference on Lasers and Electro-Optics (Optical Society of America) 1983; Paper WD2.
[305] Brübach J, Van Veen E and Dreizler A. Combined phosphor and CARS thermometry at the wall-gas interface of impinging flame and jet systems. Experiments in Fluids 2008; 44:897-904.
[306] Braeuer A, Beyrau F, Weikl MC, Seeger T, Kiefer J, Leipertz A, Holzwarth A and Soika A. Investigation of the combustion process in an auxiliary heating system using dual-pump CARS. Journal of Raman Spectroscopy 2006; 37:633-40.